Summer 2018

Synthesis, Characterization, and Applications of Ammonium/ Phosphonium Chitosan Derivatives for Investigative DNA Interactions

Quinton Kirk Wyatt
Missouri State University, Wyatt116374@live.missouristate.edu

SYNTHESIS, CHARACTERIZATION, AND APPLICATIONS OF AMMONIUM/PHOSPHONIUM CHITOSAN DERIVATIVES FOR INVESTIGATIVE DNA INTERACTIONS

A Masters Thesis

Presented to

The Graduate College of

Missouri State University

In Partial Fulfillment

Of the Requirements for the Degree

Master of Science, Chemistry

By

Quinton K. Wyatt

August 2018

SYNTHESIS, CHARACTERIZATION, AND APPLICATIONS OF AMMONIUM/PHOSPHONIUM CHITOSAN DERIVATIVES FOR INVESTIGATIVE DNA INTERACTIONS

Chemistry

Missouri State University, August 2018

Master of Science

Quinton K. Wyatt

ABSTRACT

Chitosan is examined as a non-viral vector capable of efficient gene delivery due to its favorable properties such as biodegradability, biocompatibility, and is non-toxic to mammalian cells. Cell modifications and vector permeability are enhanced in non-viral vectors that incorporate electrostatic interactions. This work synthesizes cationic (N^+, P^+) chitosan derivatives, to enhance electrostatic interactions towards nucleotides, using amide coupling agents EDC and HOBt. The final chitosan derivatives will bear cationic functional groups (N^+, P^+) with various alkyl groups (Me, Et, Pr, Ph) to examine their affinities to nucleotides and antifungal properties. mPEG grafted cationic chitosan derivatives were also synthesized to examine enhanced cell permeability. ^{1}H NMR and FT-IR analysis are implemented to observe coupling of cationic ligands to chitosan and examine electron withdrawing effects of changing cationic groups. Turbidity studies were conducted to test chitosan derivatives for pH-dependent solubility. Changes in chitosans stability through loss of intramolecular interactions after ligand coupling was analyzed using TGA-DTG. CD and agarose gel electrophoreses were used to observe cationic chitosan derivatives affinity to nucleotides. Fluorescence Microscopy and Yeast Growth Assays examined anti-fungal properties of cationic derivatives. This work aims to investigate ammonium and phosphonium chitosan derivatives as a viable gene therapy candidate capable of enhanced affinity toward nucleotides.

KEYWORDS: Chitosan, Ammonium, Phosphonium, mPEG, Gene Therapy.

This abstract is approved as to form and content.

_____

Dr. Reza Sedaghat-Herati
Chairperson, Advisory Committee
Missouri State University

SYNTHESIS, CHARACTERIZATION, AND APPLICATIONS OF AMMONIUM/PHOSPHONIUM CHITOSAN DERIVATIVES FOR INVESTIGATIVE DNA INTERACTIONS

By

Quinton K. Wyatt

A Master's Thesis
Submitted to the Graduate College
Of Missouri State University
In Partial Fulfillment of the Requirements
For the Degree of Master of Science, Chemistry

August 2018

Approved:

_____
Reza Sedaghat-Herati, Ph.D., Chair

_____
Richard N. Biagioni, Ph.D.

_____
Gautam Bhattacharyya, Ph.D.

_____
Matthew S. DeVore, Ph.D.

_____
Julie Masterson, PhD: Dean, Graduate College

ACKNOWLEDGEMENTS

I am thankful for my research advisor, Dr. Herati, for his support over the past two years. I am also thankful to the members of my committee, Dr. Biagioni, Dr. Bhattacgaryya, and Dr. Devore for their guidance, and encouragement through my writing process. I am very thankful for Dr. Kim's help with all confocal studies and yeast growth assays. I thank all the Missouri State professors who contributed to my project with their gifts such as, Dr. Meints gifting NMR solvents and DNA, Dr. Gerasimchuk for NMR solvents and use of instrumentation, Dr. Yoshimatsu for plasmid and agarose gel electrophoresis equipment, and Dr. Richter for gifting tripropylamine. I am thankful to my thesis editors Michelle Wyatt and Tom Lancaster for reviewing and editing in the completion process of my thesis writing project. My eternal gratitude goes out to my wife, Katie Wyatt, for her support throughout my graduate career.

TABLE OF CONTENTS

LIST OF TABLES

LIST OF FIGURES

CHAPTER 1. INTRODUCTION

1.1. Chitin and Chitosan

Chitin is the most abundant nitrogen-bearing organic compound and second most abundant polysaccharide found in nature.[1,2] Its polymer chain is comprised of linear β-(1,4)-linked N-acetyl glucosamine units, as seen in Figure1.[3,4] The most common sources of chitin are crustaceans, shrimp, and crab shells, through demineralization and deproteinization.[1,5] By the late 1950's, professor C. Rought discovered chitosan by boiling chitin in concentrated alkaline solution, removing the N-acetyl groups (Figure 1), a process known as deacetylation.[6,7] The deacetylation of chitin decreases this hydrogen bonding affect which decreases the molecular stability of the polymer chain compared to other polysaccharides such as cellulose.[8,9] Chitin and chitosan are very similar polymers with various degrees of N-acetylated glucosamine units. The primary distinction between chitin and chitosan is the percent of acetyl groups remaining along the polymer chain. These two polymers, chitin, and chitosan, are a polymer blend where both N-deacetylated, and N-acetyl glucosamine units are arranged throughout the length of the polymer.[9] Unlike chitosan, chitin exhibits intramolecular hydrogen bonding through its acetyl and hydroxyl groups giving it a three-dimensional α-helices structure.[3,10] When more than 50% of N-glucosamine units have an acetyl group present, then the polymer is chitin. When 50% or more of acetyl groups have been removed, the polymer is named chitosan. The degree of acetylation (DA) is the determining factor that distinguishes their names and properties.

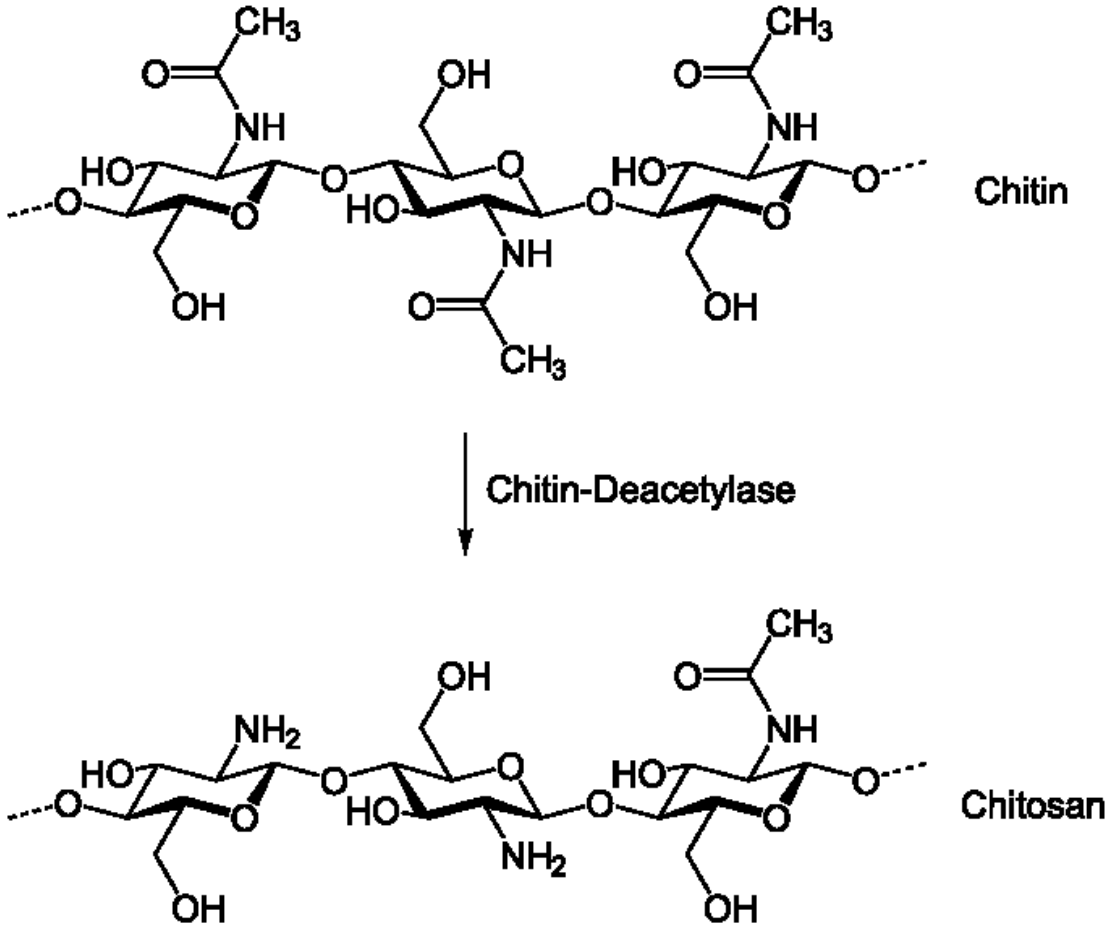

Figure 1. Displays chitin being deacetylated by a deacetylase into chitosan.

Although chitosan's structure is similar to that of other polysaccharides such as cellulose, it does not share many of its properties. Chitosan is insoluble in both organic and neutral to basic aqueous solvents. It was discovered that chitin with a DA less than sixty percent is soluble in dilute, acid solutions.[1] At pH 6, the free amino groups found on chitosan's N-deacetylated units begin to protonate, which slowly increases solubility. The increased solubility at lower pH's allows for synthetic modifications to take place in solution. The protonation of free amino groups at lower pH's allows for the formation of ionic cross-linking with multivalent ions.[1] Like cellulose, chitosan has secondary and primary hydroxyl groups, which, once in solution, can be synthetically modified. The ability to synthetically alter chitosan's amino and hydroxyl groups gives rise to a variety of applications ranging from soaps, cosmetics, water treatment, protein separation, gene delivery, and cancer treatments.[1,4,11-20]

The applications of chitosan can be dictated by two main factors, DA and its molecular weight (MW). The DA and MW allow for specific physicochemical interactions making chitosan a suitable non-viral vector.[1] DA can determine many of chitosan's physical and chemical characteristics. The lower percentage of DA, the more available amino groups are present for modifications and protonation.

The stability of chitin's α-helix structure is disrupted by a lower percentage of DA and an increase in protonation of free amino groups. The disruption of intramolecular interactions allows for greater solvation and cationic interactions. When DA is greater than sixty percent, intramolecular hydrogen bonding and hydrophobic methyl groups make chitin insoluble in water.[1,5,21] As DA decreases, the solubility of chitin increases

with decreasing pH. With lower DA, chitin is less sterically hindered and has less intramolecular interactions.[5,21,22]

The microbial degradation of chitosan is correlated to two main factors: the DA and distribution of N-acetylated glucosamine units throughout the polymer chain. Lee et al.[13] observed that chitosan's degradation process rapidly declines after DA reaches lower than 30%. Similarly, the work of Aiba et al.[12] concluded that chitosan with homogenous distribution of N-acetylated glucosamine units was less susceptible to degradation within lysosomal space.[13] Controlling DA and distribution of N-acetylated glucosamine units affects chitosan's ability to degrade within biological systems.[13]

Like DA, MW significantly affects chitosan's function in a variety of applications including burn healing, coagulation of pollutants, lowering blood cholesterol levels, enhancing drug dissolution, control of viscosity and improving crop yields.[1,23] The MW has been reported to influence the growth of *E. coli.* Higher MW prevented *E. coli.* growth, while lower MW promoted it.[24] Sodium nitrite ($NaNO_2$) can be used to depolymerize chitosan controllably, allowing for a wide variety of different MW chitosan.[24]

The MW of chitosan can determine the strength of interaction between DNA and chitosan. When electrostatic attraction occurs between protonated chitosan and DNA in acidic solution, higher MW chitosan can wrap around short double-stranded DNA and create a stronger interaction through entanglement.[25] Low MW chitosan has been proven to be less effective at condensing short double-stranded DNA due to lack of this entanglement effect.[1,26] These electrostatic interactions between DNA and chitosan are

generated by the protonation of chitosan's free amino groups. However, this interaction is reversed at increasing the pH.

Chitosan may be chemically modified to bear pH-independent cationic groups that can provide sustained interactions with short double-stranded DNA through a broad pH range.[24] Controlling the positive to negative charge ratio (+/-) determines the degree of complexation of short double-stranded DNA when utilizing modified chitosan (of any MW). Modifying chitosan to contain cationic functional groups that are not dependent on pH can provide a means for chitosan to become a viable non-viral vector suitable for gene therapy.

1.2. Chitosan Modification

Modifications to chitosan to improve solubility in neutral conditions were previously investigated.[1] Chitosan derivatives that bear various functional groups were prepared for a wide variety of applications which can be seen in Figure 2.[1,27-33] Chitosan's amino and primary hydroxyl groups allow chemical modification that can lead to an increase in solubility and affinity to nucleotides. Although chitosan is non-toxic to mammalian cells on its own, the addition of cationic functional groups to its polymer chain can increase toxicity.[34] Chitosan derivatives incorporating cationic triphenyl groups into their structure have been shown to be toxic to mammalian cells.[35]

The coupling of carboxylic acids to amino groups to form a more stabilized amide was subjected to rigorous research, and many new methods have been developed in recent years.[36] The coupling of carboxylic acids to amino groups requires a preliminary activation step to create a stable intermediate that is more reactive toward amino groups.

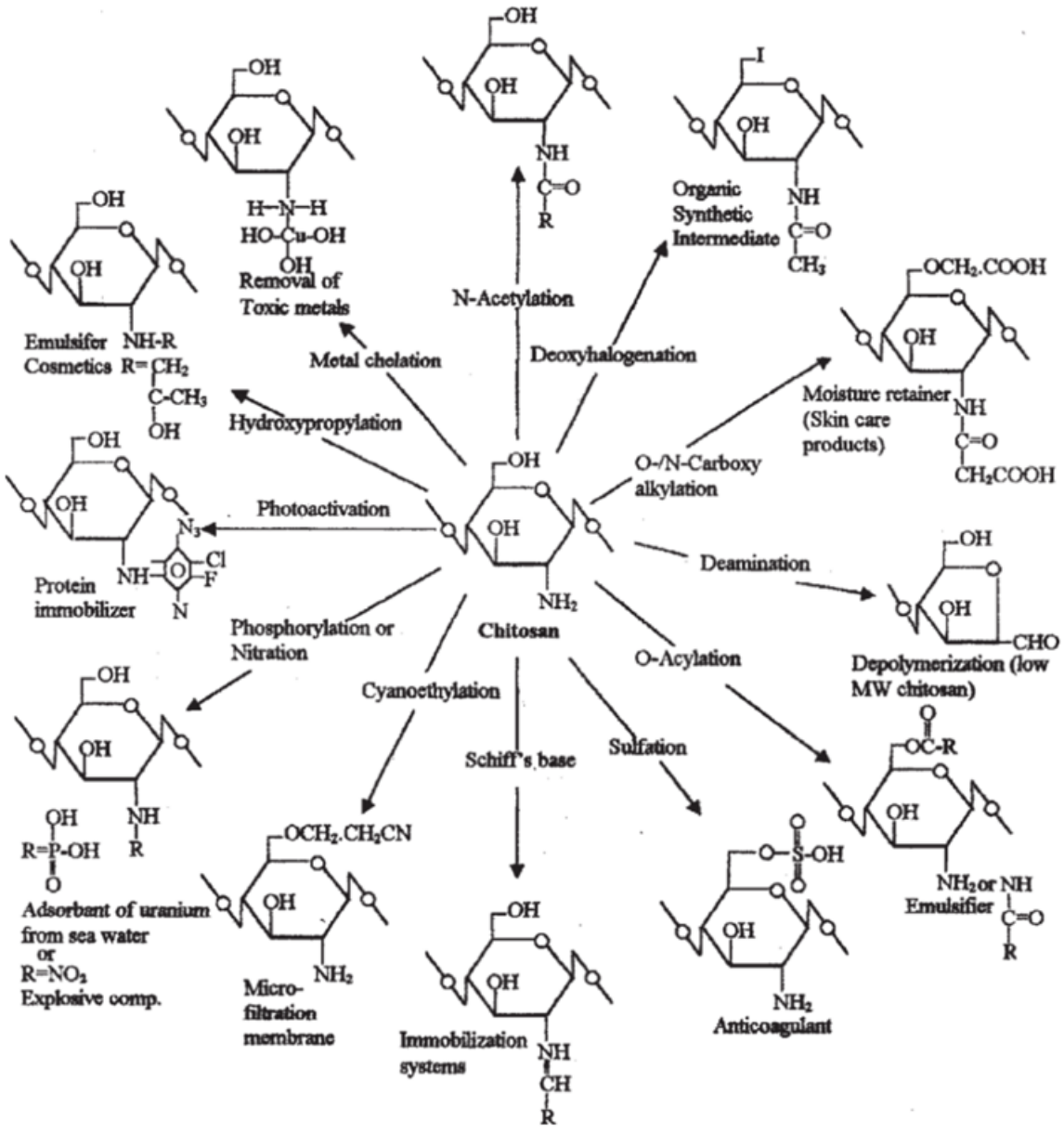

Figure 2. Various chemical modifications of chitosan and their applications. Modifications have been made to the amino and primary hydroxyl groups.

In 1995, Nakajima et al.[37] conducted experiments where altered carbodiimides were used to observe the effects on coupling efficiency. N,N'-dicyclohexylcarbodiimide (DCC) and 1-ethyl-3-(3-dimethylaminopropyl)carbodiimide (EDC) were reacted with various nucleophiles to observe the reaction mechanism. In both cases (EDC and DCC), the rate-limiting step was the formation of O-acylisourea, where the fully-protonated carbodiimide and the carboxylate ligand react to form a reactive intermediate. The O-acylisourea complex is very reactive and short-lived in solution.[36] At a pH lower than six, the intermediate hydrolizes reforming the carboxylic acid ligand and a deactivated EDC-urea. At pH's between 6-8, the intermediate remains in solution long enough to encounter amino groups and undergo successful coupling. Although coupling with EDC and DCC has proven successful, many new additives have been studied to improve coupling efficiency. Hydroxybenzotriazole (HOBt) has been used in carbodiimide reaction schemes to stabilize the O-acylisourea intermediate, as seen in Figure 3. HOBt attacks the activated EDC-carboxy intermediate and forms a more stable intermediate that can remain in solution for an extended period of time, increasing the overall efficiency of the EDC/HOBt coupling scheme.[36] The linking of functionalized carboxylic acids to chitosan's primary amines has been investigated using EDC and HOBt.[31,34] Using water-soluble EDC, these modifications to chitosan can take place at room temperature under open air conditions. Using EDC followed by NHS or HOBt allows for cationic modification to chitosan making it more efficient for short double-stranded DNA interactions.[37, 38]

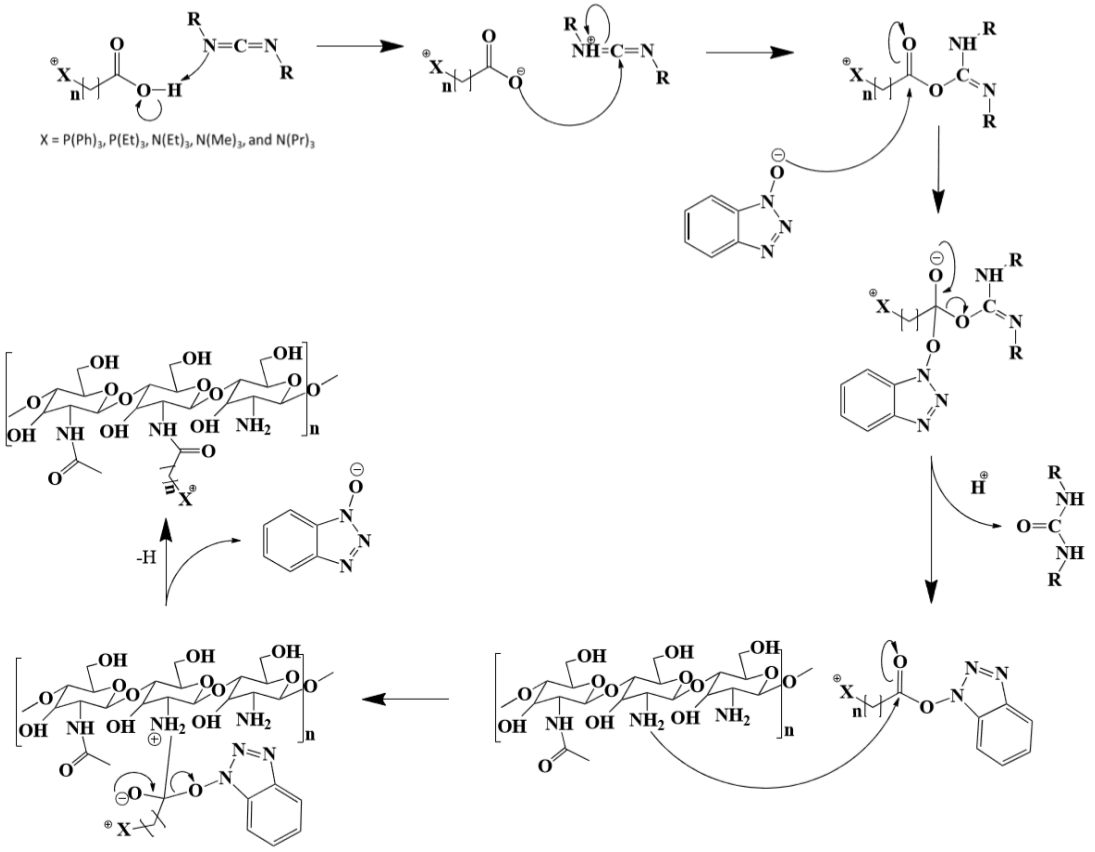

Figure 3. Reaction mechanism of EDC and HOBt coupling carboxylic acid ligand to chitosan.

1.3. PEGylation

PEGylation can be referred to as the coupling of polyethylene glycol (PEG) to other materials such as proteins or therapeutic vectors. Chitosan's ability to interact with DNA has been improved through several modifications including PEGylation.[38] Coupling of PEG to chitosan produces conjugates with reduced toxicity, and increased stability in aqueous media.[39] The incorporation of PEG into many pharmaceutical applications, including gene therapy, is not surprising and is often encouraged.[40]

PEG-grafted chitosan has been prepared to lower toxicity of certain cationic chitosan derivatives and increase water solubility.[39] Jiang et al.[34] synthesized PEG-grafted

chitosan using methoxy PEG-nitro phenol carbonate and chitosan.[40] PEG-grafted non-viral vectors have been shown to stabilize complexation of short double-stranded DNA through shielding of the positive charges present on modified vectors. These vectors displayed higher solubility and complexation with short double-stranded DNA compared to non-PEG-grafted vectors.[40]

PEG is one of the few hydrophilic polymers approved by the Food Drug Association (FDA) and has proven to play a vital role in biomedical and biotechnical fields. PEG has been used in a variety of applications ranging from cosmetics to polymer-based drug delivery systems.[39] PEGs are classified as linear or branched polyether compounds that are often found in a variety of molecular weights ranging from 3 to 40,000 g/mol.[39] Low molecular weight PEGs have lower melting points and are liquids at room temperature, while higher molecular weight PEGs have high melting points and are crystalline at room temperature. The most commonly used PEG is methoxy polyethylene glycol (mPEG), where one hydroxyl group has been converted into a methoxy group.[39] PEGs have been shown to be soluble in many organic solvents including, but not limited to, benzene, acetone, acetonitrile, methanol, and methylene chloride.[39] The addition of PEG to medication and gene delivery vectors increases solubility which, in turn, increases their overall efficiency.

1.4. Gene Therapy

Chitin and chitosan were investigated for their applications in gene therapy since the early 1990's when their structures were identified through infrared spectroscopy (IR). Chitin and chitosan are among the non-viral vectors heavily researched for gene delivery

due to their low toxicity in mammalian cells and naturally high abundance.[1] Therapeutic fields have extensively researched gene therapy for over twenty years.[1,31] Restored function to diseased genes by the addition of new genetic material has been previously reported.[1,29] These methods have also been used as a research tool to investigate inherited single gene disorders.[29] Gene delivery vectors, or vehicles, are needed to transfer new genetic materials into or near the desired therapeutic sites. The transfer of new genetic material can occur through techniques such as *ex vivo*, *in vivo*, or *in situ.*[1]

Gene therapy's main approaches utilize viral and non-viral vectors.[3] Viral gene delivery utilizes viruses to infect cells with the modified genetic material. Viruses can be modified to stop their reproductive cycle by removing genetic sequencing needed for reproduction. However, they still require sequences for binding and gene delivery to be useful.[33] Commonly used viral vectors include retrovirus[1,41,42] adenovirus,[1,4] adeno-associated viruses,[43] herpes virus[44] and vaccinia virus[1,45]. Each viral vector listed above has been incorporated into its own unique application. A few of these viruses listed above can produce sustained gene expression, but only in cells that divide. Others are just as effective against non-dividing cells without integrating into their host cell chromosome.[35] Mutations in the cell can occur through the integration of viral DNA into the genomes of the cell while using viral gene delivery systems, which can lead to safety concerns.[33]

The safety concerns of viral gene delivery began to grow after the accidental death of a patient using gene therapy for immune deficiency.[34] The fear of using viral vectors resulted in increased interest in non-viral vectors. Non-viral vectors can deliver large fragments of genetic material to mammalian cells comparable to that of viral

vectors.[34] Non-viral vectors have proven successful, but are far less effective than viral vectors in transfecting mammalian cells.[46]

Many approaches have been investigated for improving non-viral vectors for gene therapy. Amongst cationic polymers investigated, dendrimers and short chain, oligomers have been found to meet the pharmaceutical standard for human use.[47,48] Dendrimers have shown to form complexes with pDNA (polyplexes), and are regarded as one of the most effective non-viral vectors.[49] Although dendrimers seem to have been the research standard for DNA interaction, there have been recent studies that have raised concern over their toxicity within biological systems.[50,51] Decreasing the molecular weight and lowering the degree of branching of these dendrimers have been shown to only slightly lower the toxicity in biological systems.[52-54] Cationic polymers that can be formed in long-chain fashion or polycationic-spherical balls have shown to have increased interaction with pDNA.[52-55] Short-chain polymers, such as chitosan oligomers 14 units or shorter, have been shown to have weaker interactions and lower overall stability.[50,51] Chitosan and its family of linear polysaccharides have been proposed as biocompatible gene delivery vectors that can be tailored for electrostatic interactions. Studies have shown that chitosan exhibits low cytotoxicity within mammalian cells and displays viability in gene therapy.[52-56] In the research so far conducted on chitosan's interaction with DNA with cationic derivatives, high molecular weight chitosan has been shown to exhibit the highest complexation and stability and delays the release of pDNA.[57-61]

1.5. Anti-Yeast and Anti-Microbial

There has been increasing concern regarding resistance of microbial pathogens to drug treatments. Although drug-resistant microbial pathogens have mostly been controlled for the latter half of the 20th century, they can cause infections or diseases in animals, plants, or humans.[62] Microbial pathogens that have increased resistance to drug treatments can ultimately threaten human health and social development.[62] Bacteria, viruses, and fungi have contributed to more than one-fourth of global deaths annually, due to outbreaks of infectious diseases.[63-65] Microbial pathogens have many ways to spread, and controlling them is increasingly difficult. The widespread overuse of antibiotics and disinfectants has led to development of new strains of antimicrobial-resistant microbial pathogens.[66-68] There has been an urgent demand for researching new techniques of increasing the effectiveness of anti-yeast and anti-microbial agents on microbial pathogens.

Antimicrobials have mainly consisted of natural or low molecular weight compounds that are susceptible to resistance, which can often lead to toxicity in the human body due to biological diffusion.[69,70] Polymeric antimicrobials have been used for their compatibility within biological systems and lower susceptibility to resistance. These polymers are self-stabilizing and can be used for long-term while remaining viable antimicrobials.[66-68] Polymer materials used for antimicrobials characteristically inherently have long lasting durability and are environmentally friendly.[65-70] The moieties that were extensively researched are those bearing quaternary ammonium salts and quaternary phosphonium salts. The cationic species have been shown to create complexations with cell membranes and DNA to inhibit cell growth.[71] These cationic groups have been

investigated previously as disinfectant products and have displayed that ammonium salt were more effective and used more often than their phosphonium analogs.[68] One research group is conducting polymeric anti-yeast studies modified chitosan polymers to bear three different cationic functional groups.[71] Ammonium and phosphonium groups were the only two of the three groups that displayed antimicrobial properties. The antimicrobial activities of these cationic species of chitosan were evaluated through the cut plug method of treating bacteria and fungi.[71] Phosphonium cationic derivatives displayed a higher activity against the microbes than did the ammonium derivatives. More research is necessary to synthesis cationic chitosan derivatives that can successfully inhibit microbe growth and reproduction.

1.6. Previous Work

Previous research has shown the use of ammonium, phosphonium, and mPEG to increase solubility and electrostatic interactions with DNA in aqueous solutions. Integrating these properties into our work could potentially lead to a viable non-viral vector suitable for gene therapy. Shi et al.[66] research group developed pH dependent chitosan derivatives that revealed strong binding abilities between carboxymethyl chitosan derivatives and plasmid DNA.[72] Imidazole carboxymethyl chitosan derivatives were synthesized to increase transfection efficiency within HEK293T cells. Chitosan derivatives bearing pH-dependent functional groups which maintained water solubility were the precursors to formally charged chitosan derivatives. Research conducted by Tan et al.[60] used chitosan phosphonium derivatives to analyze their viability as antifungal agents.[73] Their work concluded that phosphonium derivatives could enhance anti-fungal

activity compared to ammonium analogs, however, their work was not reproducible in our lab. Their procedure used chloroacetic chloride that was added dropwise into an aqueous solution that contained deacetylated chitosan and reacted for 12 hours. After conducting this experiment ourselves several times, it was clear that these results were not reproducible. Qian et al.[37] also utilized phosphonium derivatives, but in conjunction with HeLa cells instead of fungal cells used by Tan et al.[60] Phosphonium compounds were observed interacting with DNA while maintaining cell viability up to 200 μg/ml. Qian et al.[37] research protocol established a successful synthesis route for coupling carboxylic acids to primary amines without using 1% acetic acid to solubilize the reactants. Their procedure used hydroxybenzotriazole (HOBt) and 1-ethyl-3-(3-dimethylaminopropyl) carbodiimide (EDC) rather than the more commonly used N-hydroxysuccinimide (NHS), as the coupling agent. Wang et al.[68] modifications to chitosan were similar to that of Qian et al.[37], but with slight changes to the carbon linker between chitosan and phosphonium functional groups. This work is among many others that show a strong interaction between phosphonium derivatives and short double-stranded DNA while maintaining mammalian cell viability. Layek et al.[69] synthesized cationic chitosan derivatives containing hydrophobic regions that self-assemble into micelles upon interaction with DNA. This work created increased interest for its viable application as a gene carrier capable of efficient gene therapy. A series of work done by Lin et al.[70] and Casettari et al.[71] incorporated mPEG into chitosan derivatives and observed lower toxicity, and increased permeability, in mammalian cells. Research conducted by Fréchet et al.[72] observed that the alkyl groups on phosphonium cations play an essential role in the overall interaction with DNA and toxicity in HeLa cells.[73,74]

Among the phosphonium groups tested, triethylphosphonium was found to be less toxic in HeLa cells up to 350 μg/ml compared to trimethylphosphonium, which was found to be toxic at 100 μg/ml. This work also revealed a distinction between ammonium and phosphonium interactions with siRNA. Phosphonium complexed siRNA at much lower concentrations than ammonium, which required up to ten times the concertation.

1.7. Purpose of Work

This research aims to synthesize ammonium and phosphonium chitosan derivatives, seen in Figure 4, to observe and characterize their antimicrobial properties and interaction with short double-stranded DNA and yeast cells.

In this work, ammonium and phosphonium chitosan derivatives, seen in Figure 4, were prepared by modifying previously reported methods, to enhance complexation of short double-stranded DNA. Tri(methyl, ethyl, and propyl)ammonium and tri(ethyl, and phenyl)phosphonium carboxy ligands were prepared form halogenated propionic acid or ethyl esters. The prepared ammonium and phosphonium ligands were coupled to 95% DA chitosan using EDC and HOBt. The final cationic chitosan derivatives were examined for their antifungal properties, and affinity towards nucleotides, using NMR, FT-IR, CD, TGA, degree of substitution, agarose gel electrophoresis, turbidity, yeast growth assay, florescense microscopy studies. The cationic derivatives with the most enhanced interactions compared to unmodified chitosan were subjected to PEGylations to observe changes in the interactions between nucleotides and yeast cells.

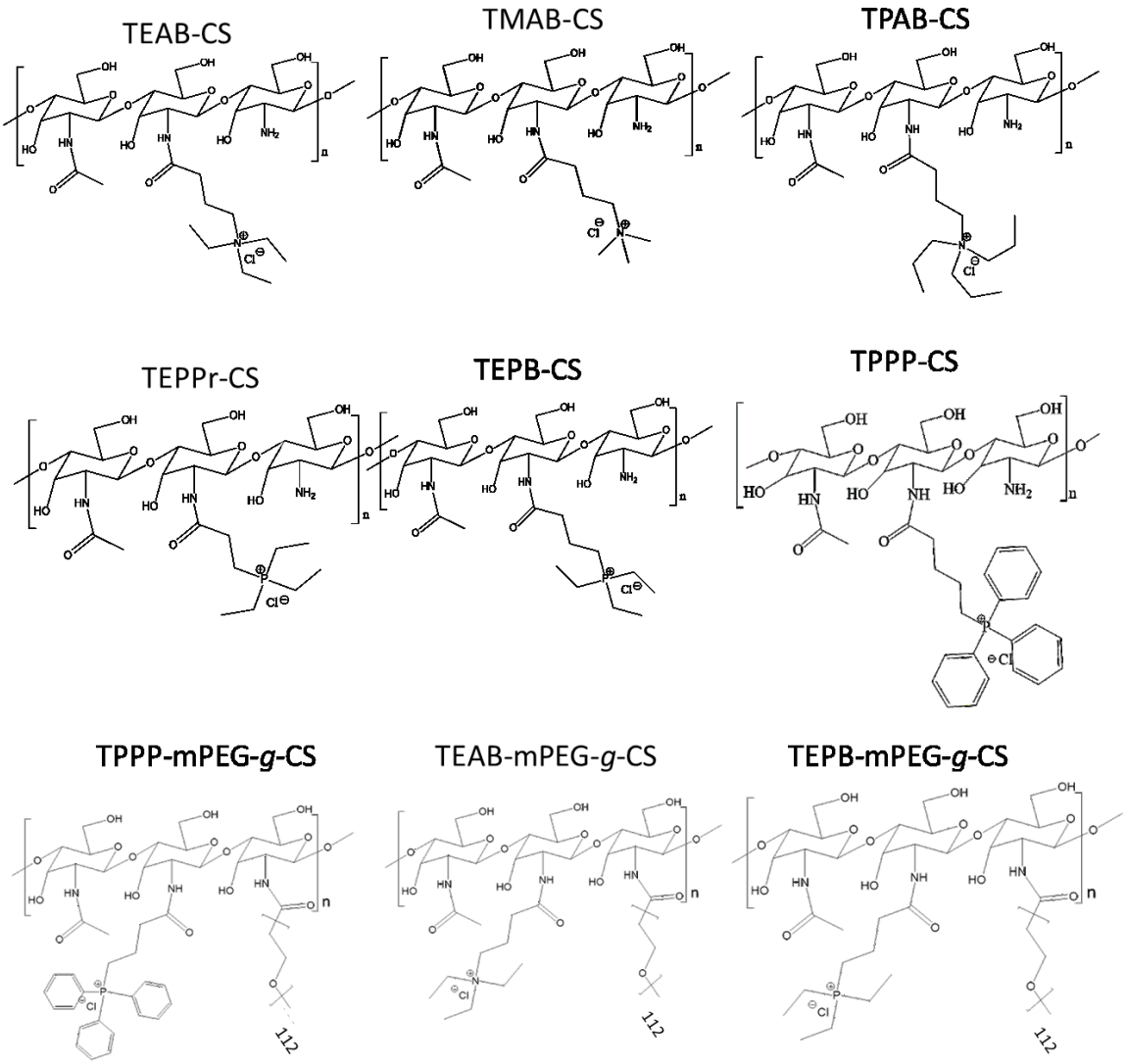

Figure 4. Ammonium, phosphonium, and PEGylated chitosan derivatives prepared in this work.

CHAPTER 2. EXPERIMENTAL METHODS

2.1. Materials and Instrumentation

2.1.1. Materials. Chitosan 95% deacetylated (medical grade) was purchased from Bonding Chemical Co.. Ethyl-4-bromobutyrate, ethyl bromoacetate, chloroacetyl chloride, 3-chloropropionyl chloride, trimethylamine, triethylamine, tripropylamine, were purchased from Sigma-Aldrich. 1-Ethyl-3-(3-dimethylaminopropyl) carbodiimide (EDC) was purchased from Chem Empex. DMSO, DMSO-d_6, D_2O, hydroxybenzotriazole (HOBt), N-hydroxysuccinimide (NHS), methoxy polyethylene glycol 5000 were purchased from Alfa Aesar. 24-mer Dickerson DNA was a gift from Dr. Gary Meints. Dr. Kyoungtae Kim provided yeast cells. Sam Kasson, from Dr. Keiichi Yoshimatsu's lab, supplied fluorescein isothiocyanate.

2.1.2. Nuclear magnetic resonance (NMR). Ammonium/phosphonium carboxylic acid ligands and chitosan derivatives were subjected to ^{1}H NMR spectroscopy studies using a Varian 400 MHz NMR spectrometer for data collection and third-party ACD Labs 1D NMR processor software for data analysis. All ^{1}H NMR studies were conducted at 25° C in D_2O or DMSO. D_2O was used for all chitosan derivatives, while DMSO was used for all ammonium/phosphonium carboxylic acid ligands. All samples prepared for ^{1}H NMR analysis contained 1 mg of chitosan derivative and 700 µL of solvent. The solution was then placed into Branson 2510 ultrasonic bath for one hour to ensure the samples were completely dissolved in the solvent, and then analyzed. The parameters of each study were held constant with the solvent volume of 700 µL, 5 second acquisition time, 5-second relaxation, 90° pulse angle, and auto gain control. Correction

values were based on literature values of each solvent's chemical shift rather than TMS. The results of these studies can be seen in Appendix A.

2.1.3. Fourier-transform infrared spectroscopy (FT-IR). Chitosan and its derivatives were subjected to Fourier-transform infrared spectroscopy studies to confirm coupling of functionalized carboxylic acid ligands to N-glucosamine units. A Bruker Vertex 70 FT-IR was used for data collection, using Bruker OPUS 7.5. software for instrument control and data analysis. All FT-IR experiments where conducted using KBr pellets in which 1 mg of a sample was added to 30 mg of KBr. The parameters of each study were held constant with a wavenumber range of 4000-400 cm^{-1}, 2 cm^{-1} resolution, 100 scans, and automatic atmospheric correction. The results of these studies can be seen in Appendix B.

2.1.4. Agarose Gel Electrophoresis. Agarose gel electrophoresis was carried out in pH 7.4 tris acetate EDTG (TAE) buffer using 2% agarose gels, 2 μL of 80 μM Dickerson 24-mer DNA, 5 μL of concentrated ethidium bromide, 2 μL of loading dye, and 10 μL of chitosan derivatives. The molar cationic charge of chitosan derivatives was obtained by comparing degree of substitution (DS) to the average N-glucosamine unit molecular weight after carboxy ligand coupling. Molar electrostatic ratios were determined to compare moles of cationic chitosan derivative to 24-mer Dickerson DNA in each well, resulting in (+/-) ratios. The (+/-) ratio solutions used ranged from 16x-0.25x. 2 μL of 80 μM 24-mer Dickerson DNA was added to each well, followed by a series of solutions containing increased charge ratios using cationic chitosan derivatives. Visualization was done using a short-range UV lamp, ethidium bromide filter camera

lens, and Microsoft digital image capturing software. The results of these studies can be seen in Appendix D.

2.1.5. Yeast Growth Assay. Yeast cells with an initial optical density (OD) of 0.06 were placed into a 96 well plate with increasing concertation of chitosan derivatives ranging from 0.1 to 1000 μg/mL. The prepared samples were incubated for 24 hours at 25 °C while shaking at 600 rpm. The OD of each well was read at 490 nm every ten minutes over the duration of the experiment using a BioTek ELx808 microplate reader. The data of each chitosan derivative was collected and compared using Microsoft Excel. The results of these studies can be seen in appendix G.

2.1.6. Circular Dichroism (CD). CD Analysis was conducted using a Jasco J-815 spectrometer coupled with a PFD-425s single position peltier. The samples were loaded into a cuvette with a path length of 1mm and max volume of 400 μL. 100 μL of 10 mM phosphate-buffered saline (PBS) (pH: 7.4) was loaded into the cuvette and used as background measurement. After the background scan was complete, 2 μL of 80 μM Dickerson Drew Dodecamer (DDD) was added to the previous 100 μL of 10 mM PBS sample and scanned. When both background and DDD measurements were collected, a series of 10 μL of increasing charge ratios using cationic chitosan derivatives were added to 100 μL of 10 mM PBS and 2 μL of 80 μM DDD. The charge ratios used ranged from 1 to 48 (+/-) and were prepared as previously established in agarose gel electrophoresis analysis. Each sample was scanned 6 times at a speed of 50 nm/min at room temperature. Data points were collected every 0.025 nm. The results were then analyzed using the Jasco Data Analysis tool and overlaid in Microsoft Excel 2016. Further analysis and final results can be found in Results and Discussion section, and Appendix E.

2.1.7. Turbidity. Turbidity data were collected using a Varian Cary 50 UV-Vis spectrophotometer with fiber optic probe. Turbidity instrument was unavailable for true measurement. 1.00 mg of chitosan and its derivatives were dissolved in 5.00 mL of 1% aqueous acetic acid. The pH was gradually increased using 0.1 M NaOH until a pH of 13 was obtained. Data was collected at various pH ranges between 3.0 and 13.0 using a Fischer Science 810 series pH meter. The wavelength of 600 nm was used in %T evaluation after running all samples through full range scan from 190 nm to 800 nm to verify no conflicting signals. Turbidity results can be seen in Figure 26.

2.1.8. Thermogravimetric analysis (TGA). Thermogravimetric analysis was conducted using a TA Instrument Q600 Thermogravimetric Analyzer. The TGA scale was tared using two empty crucibles: one as a reference, and the second for the sample. The sample crucible was torched with a flame and cooled before taring the instrument. After taring, the sample crucible was then loaded with a chitosan derivative, and the starting mass was recorded. The procedure for TGA used a ramp temperature of 20 ^{o}C/min with an initial temperature of 25 ^{o}C and the final temperature of 600 ^{o}C. Nitrogen was used as a purge gas flowing at 200 mL/s. Further analysis of TGA data was conducted using TA Universal software, and the results can be found in Results and Discussion section, and in Appendix C.

2.1.9. Fluorescence Microscopy Studies. Yeast cells were incubated overnight, and their OD measured before analyzing with FITC tagged chitosan derivatives. 10.0 µL of 10.0 mM FITC solution was added to 1.0 µL of 100.0 mM chitosan derivative and shaken for one hour. The solution was then centrifuged into a pellet, and the solvent was removed. The pellet was resuspended using acetone, vortexed for 1 minute, and then

centrifuged down again. The FITC tagged derivatives were washed in this manner 3 times. Yeast cells (250 µL, OD 0.30) were placed in 1.0 µg/1.00 mL concentrations of FITC tagged chitosan derivatives and incubated for 4 hours. The resulting solution after 4 hours was centrifuged down into a pellet and washed three times with glucose media to remove free FITC tagged polymer. The final pellet was suspended in 100 µL and vortexed for 1 min. Soon after, 2 µL of the suspended cells were removed, placed on a glass slide, and put under a microscope. The final images were obtained using a 3i lambda XL GFP 488 lamp for excitation, an Orca R2 wide-lens microscope for visualization, and Slidebook Image Capturing software for digitally capturing the images. These images can be found in the Results and Discussion, and in Appendix F.

2.2. Synthesis of Ammonium Ligands

The procedure was carried out following the protocol established by Yousuke Ono et al.[73] 5.0 mL of 95% ethanol and 10.5 mmol of ethyl bromoacetate, or ethyl 4-bromobutyrate, was added to a 25 mL round bottom flask. While stirring, 11.4 mmol of trialkylamine ($N(R)_3$) was addetable d dropwise to the ethanol solution. The reaction was stirred vigorously and refluxed using a heating mantle for 15 hours.[73] The solution was then cooled to room temperature before ethanol was evaporated using a Heidolph model 036000820 rotary evaporator, yielding a clear oily residue. Without purification, the oily residue was dissolved in 100 mL of 2M HCl solution and refluxed for 24 hours. The reaction was allowed to cool to room temperature before the solvent was removed at 70 ^{o}C using the rotary evaporator.[73] This resulted in an orange oily residue. The oily residue was dissolved in 1 mL of 95 % ethanol and added dropwise into 50 mL of ethyl acetate

then cooled in an ice bath for 1 hour. This solution was placed on the rotary evaporator and crystallization of cationic carboxylic acids occurred. The solvent was filtered off using vacuum filtration, and the crystals were washed with three portions of ethyl acetate. The final trialkyl carboxylic acid ligands were placed in a vacuum desiccator and allowed to dry for three days. The final products were then examined using ^{1}H NMR spectroscopy. The reaction scheme for the synthesis of ammonium carboxylic acid and TEPB ligands is shown in Figure 5.

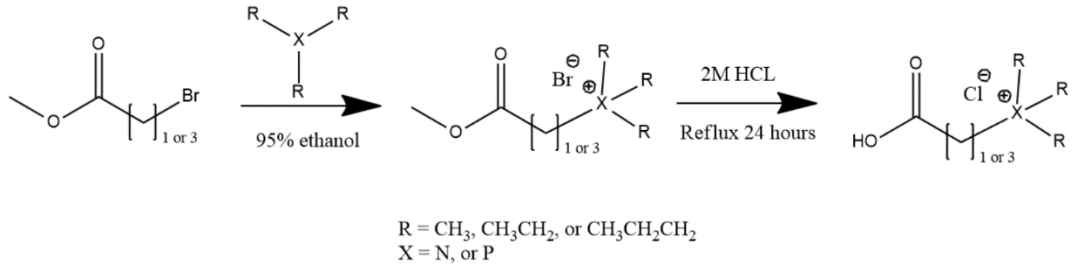

Figure 5. Reaction scheme for synthesizing ammonium/phosphonium carboxylic acid ligands

2.3. Synthesis of Phosphonium Ligands

Freshly recrystallized chloroacetic acid, or iodopropionic acid, (5.3 mmol) was dissolved in triethlyphosphine (5.3 mmol) and placed into a 15 mL microwave tube.[73] Once fully dissolved, the tube was placed into a CEM Discover SP microwave reactor and subjected to 35 Watts for 30 minutes under nitrogen. The reaction was then washed with diethyl ether and dried for three days. The final products were (1-carboxymethyl) triethylphosphonium chloride (TEPA) or (2-carboxyethyl) triethylphosphonium chloride (TEPPr). The reaction scheme for TEPA and TEPPr can be seen in Figure 6. Synthesis of (3-carboxypropyl)triethylphosphonium chloride (TEPB) was conducted using the

previously established procedure for the synthesis of ammonium carboxylic acid ligands.[73]

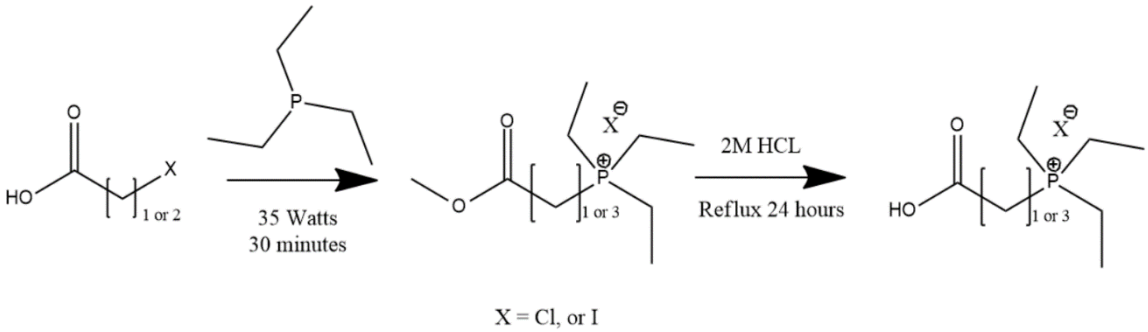

Figure 6. Reaction scheme using microwave reactor to synthesize phosphonium acetic, or propionic, carboxylic acid ligands

2.4. Synthesis of Ammonium/Phosphonium Chitosan Derivatives

The procedure was carried out following the protocol established by Qian et al.[37] 1.24 mmol of ammonium/phosphonium carboxylic acid ligand was added to 0.350 g (1.83 mmol) of EDC, and 0.350 g (2.30mmol) of HOBt in 15 mL of DMSO, and alotted one hour to dissolve. Once completely dissolved, 0.200 g (1.24 mmol) of 95% deacetylated chitosan was placed into the reaction mixture along with 15 mL of DI water, stirred till homogenous, and reacted for 24 hours. After 24 hours, an additional 0.350 g of EDC was added to the reaction mixture and stirred for 12 more hours. After 12 hours, the reaction mixture (30 mL) was precipitated, dropwise, in 300 mL of acetone and was shaken for 15 minutes. The acetone wash solution was then filtered using vacuum filtration. The resulting filter cake was then returned to the original acetone wash flask then washed with 300 mL of 95% ethanol for 15 minutes and filtered again. After washing the product three times with ethanol, the filter cake was submerged in diethyl ether and stirred for 15 minutes and then allowed to gravity filter for one hour followed

by 30 minutes of air drying under vacuum filtration. The final products were ammonium/phosphonium carboxylic acid substituted chitosan derivatives.

2.5. PEGylation of Ammonium/Phosphonium Chitosan Derivatives

Following a slightly modified protocol established in section 2.2. (shown in Figure 7), 1.00 mmol of freshly synthesized ammonium/phosphonium chitosan derivative (as prepared on page 25-26) was dissolved in 15 mL of DI water. In a separate 50 mL flask, 1.0 g (0.2 mmol) of mPEG-5000 acetic acid (prepared by other graduate students within our lab) was dissolved in 15 mL DMSO. 0.350 g (1.83 mmol) of EDC and 0.350 g (2.30mmol) of HOBt was added to the DMSO reaction vessel and stirred for one hour (or until completely dissolved). The two solutions were combined and stirred vigorously for 24 hours. The DMSO/water reaction mixture was placed in a 14Kda-16Kda dialysis membrane tube and dialyzed for three days. The dialyzed product was then lyophilized for three days, until dry. The dry product was then crushed into fine powder and soaked in methylene chloride for one hour to remove all un-grafted mPEG-5000 acetic acid. The methylene chloride solution was filtered off using vacuum filtration and then washed

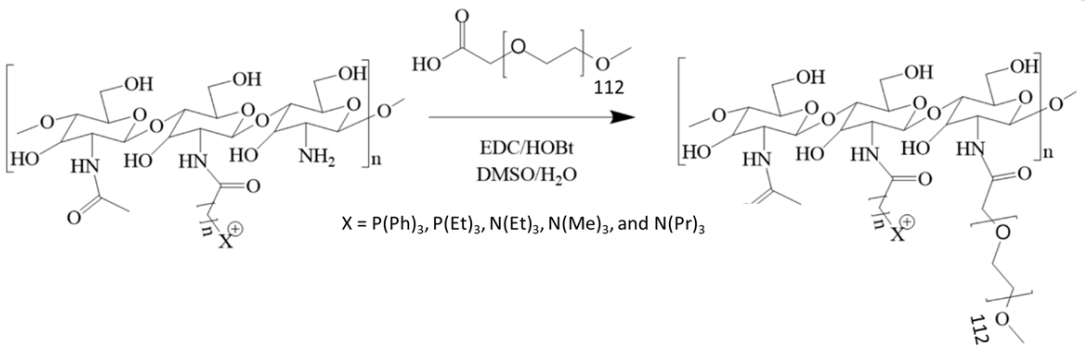

Figure 7. Reaction scheme using EDC and HOBt to graft mPEG-acid to chitosan.

three more times. Then the mPEG-*g*-chitosan derivatives were dried at 50 °C using a vacuum oven. The final products were PEGylated ammonium/phosphonium chitosan derivatives.

CHAPTER 3. RESULTS AND DISCUSSION

3.1. ^{1}H NMR Analysis

3.1.1. Ammonium and Phosphonium Carboxylic Acid Ligands. Ammonium carboxylic acid ligands, phosphonium carboxylic acid ligands, and chitosan derivatives were analyzed using ^{1}H NMR spectroscopy. The results of each study can be viewed in Appendix A. The integral lines, and values, are indicated in red while the proton signals are labeled with numbers above the spectra. After each sample was dried at 50 ^{o}C in a vacuum oven for 12 hours, 1 mg of sample was dissolved in 700 μL of DMSO, or D_2O, and placed into an NMR tube. All chemical shift values for ammonium carboxylic acid ligands are compiled in Table 1.

The spectrum consisting of TMAA signals displays peaks at 4.33 ppm (2H) which is assigned to the two protons on signal labeled **1** in Figure 8, while the peak at 3.19 ppm (9H) corresponds to the nine protons located on the signal labeled **2**. The integration values, labeled in red, for signals **1** and **2** are proportional indicating that successful (1:1) substitution of bromide for trimethylamine occurred. There was no acetic carboxylic acid peak observed downfield for all acetic ligands.

The TEAA spectrum is similar to TMAA with one additional peak. The signal furthest downfield at 4.18 ppm (2H) is assigned to the protons located on signal labeled **1** in Figure 9. When comparing the alpha carbons chemical shift (labeled **1**) on TEAA and TMAA, their value shifts from 4.33 to 4.18 ppm, displaying a delocalization of an electron withdrawing effect brought on by increased carbon length of the triethylammonium group. The signal observed at 3.45 ppm (6H) is assigned to six protons located on the triethylammonium, ($N^+(C\mathbf{H_2}CH_3)_3$) and is labeled **2**. The signal

Table 1. Table of synthesized ammonium carboxylic acid ligands with their abbreviations, yield, and ^{1}H NMR ppm assignments using $DMSO_{d6}$

Ligand Name	Abbreviation	Yield	^{1}H NMR ppm DMSO-d_6
(1-Carboxymethyl) trimethylammonium chloride	TMAA	(73.8%)	4.33 (2H, -C**H**$_2$N$^+$(CH$_3$)$_3$), 3.19 (9H, -N$^+$(C**H**$_3$)$_3$)
(1-Carboxymethyl) triethylammonium chloride	TEAA	(62.8%)	4.18 (2H, -C**H**$_2$N$^+$(CH$_2$CH$_3$)$_3$), 3.44 (6H, -N$^+$(C**H**$_2$CH$_3$)$_3$), 1.16 (9H, -N$^+$(CH$_2$C**H**$_3$)$_3$
(1-Carboxymethyl) tripropylammonium chloride	TPAA	(70.3%)	3.29 (2H, HO$_2$CC**H**$_2$-), 2.96 (6H, -N$^+$(C**H**$_2$CH$_2$CH$_3$)$_3$), 1.62 (6H, -N$^+$(CH$_2$C**H**$_2$CH$_3$)$_3$), 0.85 (9H, -N$^+$(CH$_2$CH$_2$C**H**$_3$)$_3$
(3-Carboxypropyl) trimethylammonium chloride	TMAB	(88.9%)	12.31 (1H, **H**O$_2$CCH$_2$-), 3.01 (9H, -CH$_2$CH$_2$CH$_2$N(C**H**$_3$)$_3$), 2.71 (2H, -C**H**$_2$CH$_2$CH$_2$N$^+$(CH$_3$)$_3$), 2.26 (2H, -CH$_2$CH$_2$C**H**$_2$N$^+$(CH$_3$)$_3$), 1.88 (2H, -CH$_2$C**H**$_2$CH$_2$N$^+$(CH$_3$)$_3$
(3-Carboxypropyl) triethylammonium chloride	TEAB	(82.6%)	12.31 (1H, **H**O$_2$CCH$_2$-), 3.20 (9H, -N$^+$(C**H$_2$**CH$_3$)$_3$), 3.07 (2H, -C**H$_2$**N$^+$(CH$_2$CH$_3$)$_3$), 2.31 (2H, -C**H**$_2$CH$_2$CH$_2$N$^+$-), 1.75 (2H, -CH$_2$C**H**$_2$CH$_2$N$^+$-), 1.13 (2H, -N$^+$(CH$_2$C**H**$_2$)$_3$
(3-Carboxypropyl) tripropylammonium chloride	TPAB	(39.2%)	12.31 (1H, **H**O$_2$CCH$_2$-), 3.20 (6H, -N$^+$(C**H$_2$**CH$_2$CH$_3$)$_3$), 3.07 (2H, -C**H$_2$**N$^+$(CH$_2$CH$_2$CH$_3$)$_3$), 2.31 (2H, -C**H**$_2$CH$_2$CH$_2$N$^+$-), 1.75 (2H, -CH$_2$C**H**$_2$CH$_2$N$^+$-), 1.13 (9H, -N$^+$(CH$_2$CH$_2$C**H**$_3$)$_3$

observed at 1.16 ppm (9H) is assigned to the nine protons found on triethylammonium, ($N^+(CH_2C\mathbf{H_3})_3$) and is labeled **3**. The integration values for these signals are labeled in red in Figure 9. These values are (1:1) indicating proportional substitution of bromide for triethylamine.

The signals observed for TPAA in Figure 10, again, are similar to the other ammonium acetic acid ligands prepared. The signal at 3.29 ppm (2H) corresponds with the protons found on the alpha carbon, labeled **1**. This signal demonstrates a continued delocalization of electron withdrawing effect as the alkyl substituents lengthen. The signal observed at 2.96 ppm (6H) is assigned to the protons labeled **2,** followed by the signal at 1.62 (6H)ppm and is labeled **3**. The nine protons associated with the three methyl groups on signal **4** appear at 0.85 ppm (9H). The integration values for TPAB are shown in Figure 10, and again, these values are proportional (1:1) indicating no other impurities are present in the NMR sample.

The spectrum of TMAB is shown in Figure 11. The proton signal found at 12.31 ppm (1H) is assigned to the carboxylic acid grouped labeled **5.** The signal labeled **3** is located at 3.26 ppm (2H) and is the CH_2 closest to the carboxy group. The peak observed at 3.01 ppm (9H) is assigned to the nine protons located on the signal labeled **4**. The signals for protons **2** and **3** are located at 2.26-1.86 ppm (4H).

The spectrum of TEAB, shown in Figure 12, displays a carboxylic acid peak labeled **6** at 12.30 ppm (1H). The chemical shift values of the carbon chain found on TEAB, are similar to that of TMAB and can be assigned accordingly 3.09 ppm (2H label **3**), 2.31 ppm (2H label **1**), 1.75 ppm (2H label **2**). However, unlike that of TMAB, TEAB has one new peak emerge at 3.20 ppm (6H label **4**) that is assigned to the -CH_2- closest to

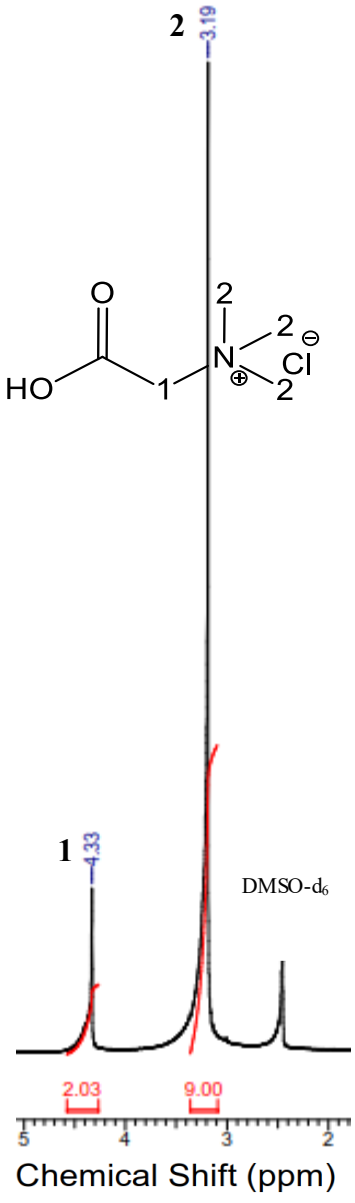

Figure 8. Integrated ^{1}H NMR of TMAA.

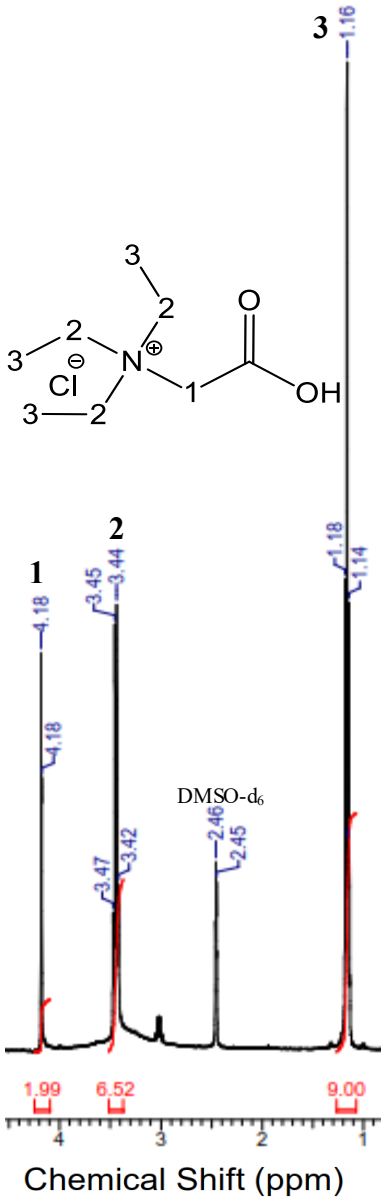

Figure 9. Integrated ^{1}H NMR of TEAA.

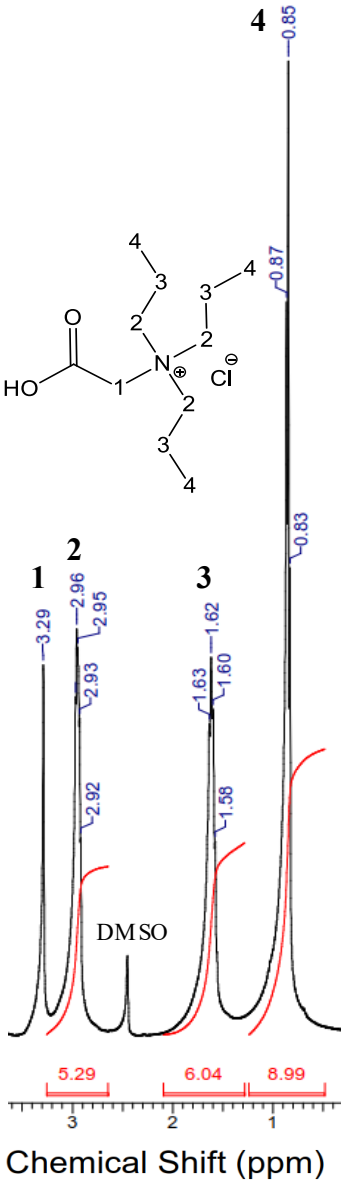

Figure 10. integrated ^{1}H NMR of TPAA

N^+. The nine protons assigned to the methyl groups are labeled **5** and are observed at 1.13 ppm (9H label **5**). The butanoic ligands display similar delocalization of the electron withdrawing effect like that of acetic acid ligands.

The proton signals for TPAB were similar to that of TEAB and TMAB except for the addition of one new peak. Like that of TEAB and TMAB, the butanoic carbon chain signals are located at 3.09 ppm, 2.29ppm, and 1.77 ppm corresponding to labels **3**, **1**, and **2**, shown in Figure 13. A clear carboxylic acid peak is present at 12.31 ppm (1H label **7**) indicating successful ester hydrolysis. The peak labeled **4**, **5**, and **6** are the ammonium tripropyl group and have chemicals shift values of 3.12 ppm (6H, label **4**), 1.60 ppm (6H, label **5**), and 0.85 ppm (9H, label **6**).

The phosphonium carboxylic acid ligands were examined in the same way and values are found in table 2. TEPA proton signals were examined and labeled **1**, **2**, and **3** shown in Figure 14. Label **1** is assigned to the protons located between the carboxyl and phosphonium groups and has a chemical shift value of 3.75 ppm (2H, *d*). The protonsignals for the triethyl group bound to P^+ have chemical shift values of (6H) and (9H) and are labeled **2** and **3**, respectively.

TEPPr proton signals were examined and labeled **1**, **2**, **3**, and **4,** shown in Figure 15. Labels **1** and **2** are assigned to the protons located between the carboxyl and phosphonium groups and have a chemical shift value of 2.59 ppm (2H) and 2.39 ppm (2H). The proton signals for the triethyl group bound to P^+ have chemical shift values of 2.23 ppm (6H) and 1.10 ppm(9H) and are labeled **3** and **4**, respectively. The signal located at 12.59 ppm (1H) is labeled **5** and is assigned to the carboxylic acid.

Table 2. Table of synthesized phosphonium carboxylic acid ligands with their abbreviations, yield, and 1H NMR ppm assignments using DMSOd6

Ligand Name	Abbreviation	Yield	^{1}H NMR ppm $DMSO_{d6}$
(1-Carboxymethyl) triethylphosphonium chloride	TEPA	90.0%	3.75 (2H, -$\mathbf{H}_2P^+(CH_2CH3)_3$), 2.30 (6H, HO_2CCH_2 $P^+(C\mathbf{H}_2CH3)_3$), 1.10 (9H, -$P^+(CH_2C\mathbf{H}3)_3$
(2-Carboxyethyl) triethylphosphonium chloride	TEPPr	75.3%	12.58 (1H, $\mathbf{H}O_2CCH_2$-), 2.55 (2H, -$C\mathbf{H}_2CH_2P^+$-), 2.39 (2H, -$C\mathbf{H_2}$ $P^+(CH_2CH_3)_3$), 2.23 (6H, -$P^+(C\mathbf{H}_2CH_3)_3$), 1.08 (9H, -$P^+(CH_2C\mathbf{H}_3)_3$
(3-Carboxypropyl) triethylphosphonium chloride	TEPB	76.1%	12.16 (1H, $\mathbf{H}O_2CCH_2CH_2$-), 2.36 (2H, $HO_2CC\mathbf{H}_2CH_2CH_2$-), 2.26 (2H, -$C\mathbf{H}_2$ $P^+(CH_2CH_3)_3$), 2.22 (6H, -$P^+(C\mathbf{H}_2CH_3)_3$), 1.67 (2H, -$C\mathbf{H}_2CH_2P^+(CH_2CH_3)_3$), 1.08 (9H, -$P^+(CH_2C\mathbf{H}_3)_3$

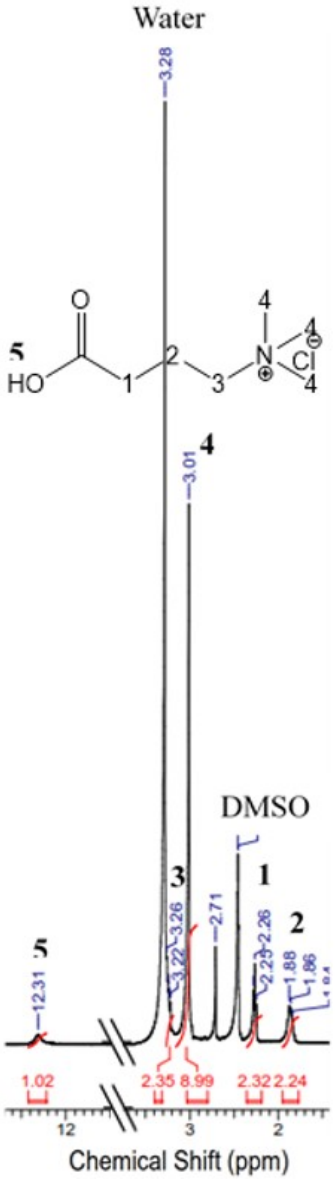

Figure 11. ^{1}H NMR spectrum of TMAB

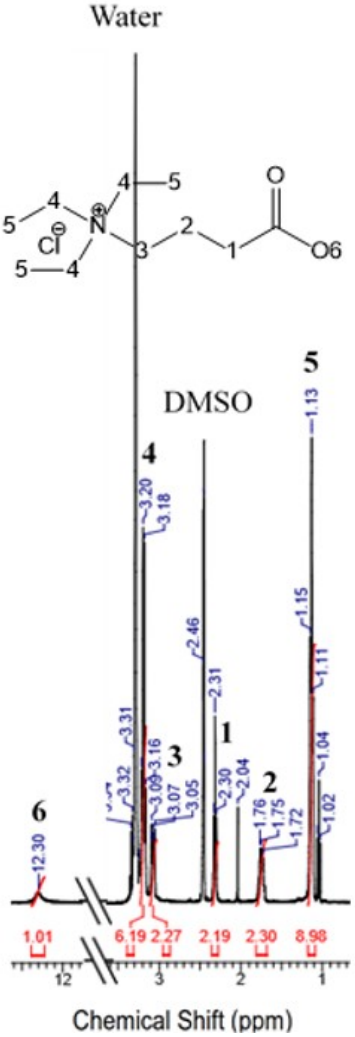

Figure 12. ^{1}H NMR spectrum of TEAB

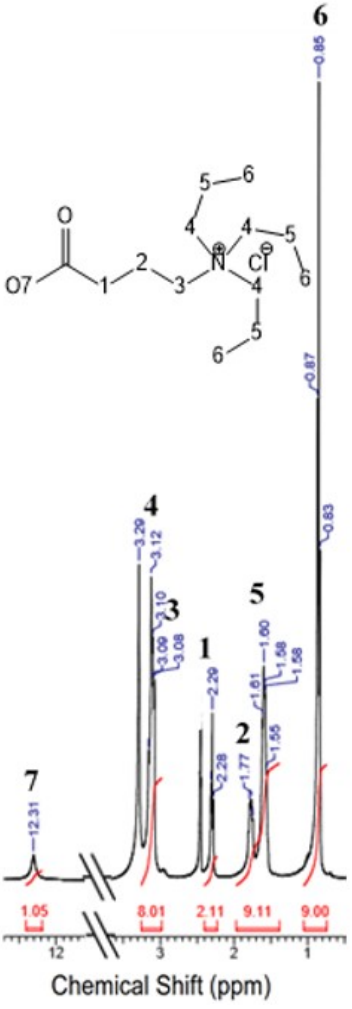

Figure 13. ^{1}H NMR spectrum of TPAB

The spectrum of TEPB, shown in Figure 16, was examined and labeled **1**, **2**, **3**, **4** and **5**. Labels **1**, **2**, and **3** are assigned to the protons located between the carboxyl and phosphonium groups and have a chemical shift value at 2.36 ppm (2H), 2.16 ppm (2H), and 1.67 ppm (2H). The proton signals for the triethyl group bound to P^+ have chemical shift values of 2.2 ppm (6H) and 1.10 ppm(9H) and are labeled **4** and **5**, respectively. The signal located at 12.31 ppm (1H) is labeled **6** and is assigned to the carboxylic acid.

3.1.2 Ammonium and Phosphonium Chitosan Derivatives. All synthesized derivatives displayed characteristic chitosan signals as evidenced by the broad peaks located from 4.00-3.30 ppm, shown in Figure 17, and they are assigned to the protons found on Chitosans glucosamine ring (labeled $\mathbf{C_2}$-$\mathbf{C_6}$). All ammonium and phosphonium chitosan derivatives ppm values are shown in Table 3 and 4.

TMAB-CS's -CH_2- signals labeled **b**, **c**, and **d** are found between the amide and ammonium group and have a chemical shift values of 2.29 ppm (2H), 1.96 ppm (2H), and 3.21 ppm (2H), as shown in Figure 17. The proton signals for the trimethyl group found on N^+ have a chemical shift value of 2.96 ppm (9H) and are labeled **e**.

For TEAB-CS, the -CH_2- signals, also labeled **b**, **c**, and **d,** are found between the amide and ammonium group and have a chemical shift values of 2.28 ppm (2H), 1.85 ppm (2H), and 3.04 ppm (2H)), as shown in Figure 17. The proton signals for the triethyl group found on N^+ have chemical shift values of 3.15 ppm (6H) and 1.11 ppm (9H) and are labeled **e** and **f.**

For TPAB-CS, the -CH_2- signals, once more labeled **b**, **c**, and **d,** are found between the amide and ammonium group and have a chemical shift values of 2.26 ppm (2H), 1.85 ppm (2H), and 2.74 ppm (2H)), as shown in Figure 17 The proton signals for

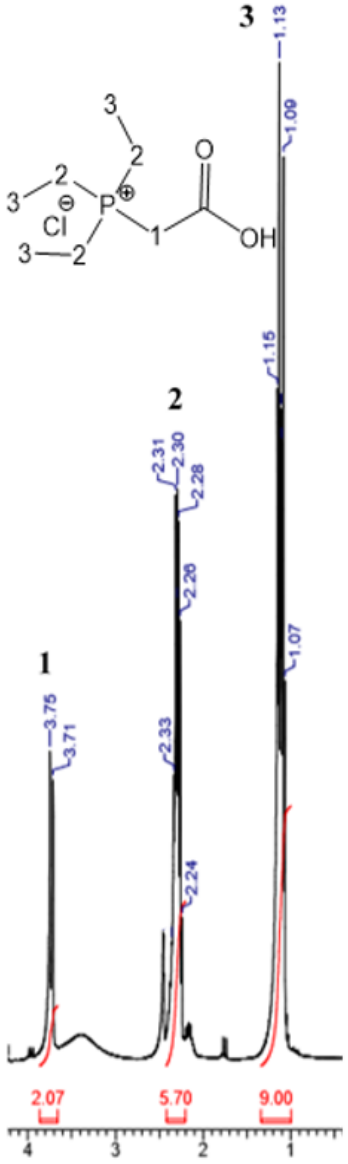

Figure 14. ^{1}H NMR spectrum of TEPA

Figure 15. ^{1}H NMR spectrum of TEPPr

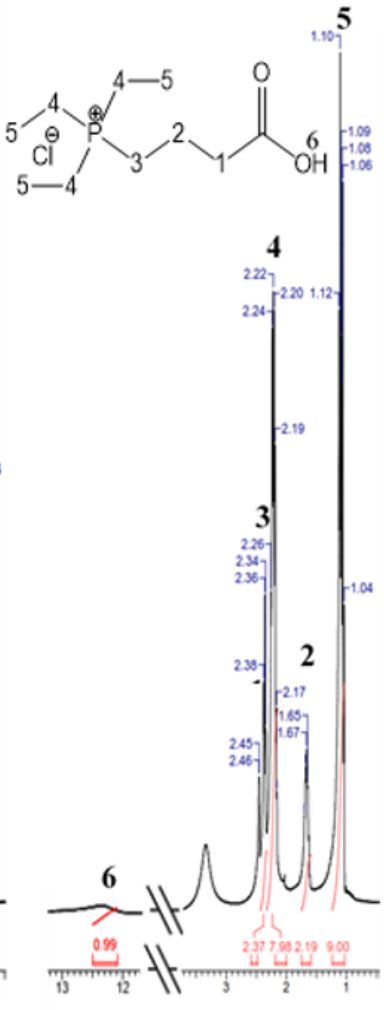

Figure 16. ^{1}H NMR spectrum of TEPB

Table 3. Table of synthesized ammonium chitosan derivatives with their abbreviations, yield (DS), and 1H NMR ppm assignments using D2O

Compound Name	**Abbreviation**	**DS**	**^{1}H NMR ppm D_2O**
2-(N-4-trimethylammonium) butanamide chitosan chloride	TMAB-CS	50.0%	4.45 (1H, **anomeric H**), 3.80-3.30 (6H, C_2-C_6 **H**'s), 3.21 (2H, -$CH_2C\mathbf{H}_2N^+(CH_3)$), 2.98 (9H, -$CH_2CH_2N^+(C\mathbf{H_3})_3$), 2.29 (2H, -$OC\mathbf{H}_2CH_2CH_2N^+(CH_3)$), 1.96 (2H, -$C\mathbf{H}_2CH_2N^+(CH_3)$.
2-(N-4-triethylammonium) butanamide chitosan chloride	TEAB-CS	43.0%	4.43 (1H, **anomeric H**), 4.0-3.25 (6H, C_2-C_6 **H**'s), 3.15 (6H, -$N^+(\mathbf{CH_2}CH3)_3$), 3.04 (2H, -$CH_2C\mathbf{H}_2N^+(CH_2CH3)_3$), 2.66 (1-2H, -2H-N**H**$COCH_2$-), 2.28 (2H, -$OC\mathbf{H}_2CH_2CH_2N^+$-, 1.84 (2H, -$C\mathbf{H}_2CH_2N^+(CH_2CH3)_3$, 1.11 (9H, -$CH_2CH_2N^+(CH_2\mathbf{CH3})_3$
2-(N-4-tripropylammonium) butanamide chitosan chloride	TPAB-CS	26.0%	4.48 (1H, C_1-Anomaric H), 4.0-3.25 (6H, C_2-C_6 **H**'s), 3.04 (6H, -$N^+(C\mathbf{H}_2CH_2CH_3)_3$), 2.74 (2H, -$C\mathbf{H}_2N^+(CH_2CH_2CH_3)_3$) , 2.26 (2H, -$C\mathbf{H}_2CH_2CH_2N^+$-), 1.85 (2H, -$C\mathbf{H}_2CH_2N^+$-), 1.55 (6H, -$N^+(CH_2C\mathbf{H}_2CH_3)_3$), 0.79 (9H, -$N^+(CH_2CH_2C\mathbf{H_3})_3$

Table 4. Table of synthesized phosphonium chitosan derivatives with their abbreviations, yield (DS), and 1H NMR ppm assignments using D2O

Compound Name	**Abbreviation**	**Yield**	**^{1}H NMR ppm D_2O**
2-(N-3-triethylphosphonium) propionamide chitosan chloride	TEPPr-CS	19.0%	4.48 (1H, **anomeric H**), 4.0-2.66 (6H, C_2-C_6 **H**'s,2H-N**H**), 2.55 (2H, -C**H**$_2$$CH_2N^+(CH_2CH_3)_3$), 2.38 (2H, -C**H**$_2N^+(CH_2CH_3)_3$) , 2.11 (6H, -$CH_2N^+(C$**H**$_2CH_3)_3$), 1.09 (9H, -$CH_2$ $N^+(CH_2C$**H**$_3)_3$
2-(N-4-triethylphosphonium) butanamide chitosan chloride	TEPB-CS	21.0%	4.82 (1H, **anomeric H**), 4.0-2.66 (6H, C_2-C_6 **H**'s ,2H-N**H**), 2.35 (2H, -OC**H**$_2CH_2CH_2N^+$ -), 2.07 (6H, -$N^+(C$**H**$_2CH_3)_3$) , 2.07 (2H, -C**H**$_2N^+(CH_2CH_3)_3$), 1.75 (2H, -C**H**$_2CH_2N^+(CH_2CH_3)_3$), 1.08 (9H, -$N^+(CH_2C$**H**$_3)_3$
2-(N-5-triphenylphosphonium) pentanamide chitosan chloride	TPPP-CS	42.0%	7.65-7.50 (15H, **P$^+$Ph**$_3$-CH_2CH_2-), 4.39 (1H, **anomeric H**), 4.0-2.66 (6H, C_2-C_6 **H**'s ,2H-N**H**), 3.13 (2H, P^+Ph_3-C**H**$_2CH_2$-), 2.16 (2H, P^+Ph_3-$CH_2CH_2CH_2C$**H**$_2$-), 1.60 (4H, P^+Ph_3-CH_2C**H**$_2C$**H**$_2$-)

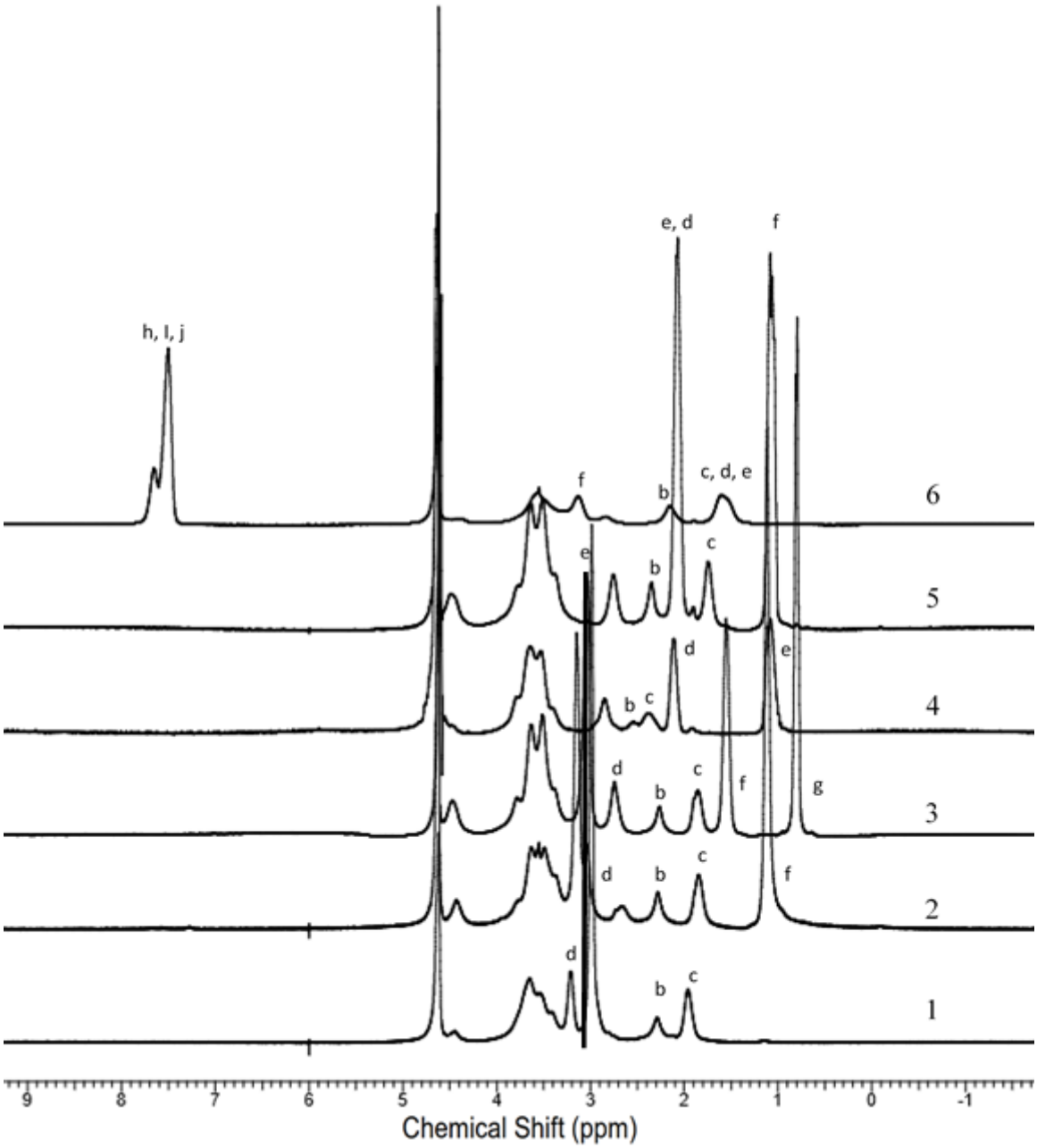

Figure 17. ^{1}H NMR spectra of 1) TMAB-CS, 2) TEAB-CS, 3) TPAB-CS, 4) TEPB-CS, 5) TEPPr-CS, and 6) TPPP-CS, using D2O.

the tripropyl group found on N^+ have chemical shift values of 3.04 ppm (6H), 1.55 ppm (6H), and 0.79 ppm (9H) and are labeled **e**, **f**, **and g**.

The phosphonium derivatives display similar chemical shift values compared to ammonium derivatives except for the -CH_2- located on the triethyl group attached to P^+. These -CH_2- protons experience far less deshielding from P^+ compared to N^+ and are observed having a 1.04 ppm difference in chemical shift value. As for TPPP-CS derivative, the ^{1}H NMR spectrum and ppm values are previously reported in scientific literature, can be seen in Table 2 and Figure 17.

For TEPPr-CS, the -CH_2- signals labeled **b**, and **c** are found between the amide and phosphonium group and have chemical shift values of 2.55 ppm (2H), and 2.38 ppm (2H), as shown in Figure 17. The proton signals for the triethyl group found on P^+ have chemical shift values of 2.11 ppm (6H) and 1.08 ppm (9H) and are labeled **d** and **e.**

For TEPB-CS, the -CH_2- signals, also labeled **b**, **c**, and **d,** are found between the amide and ammonium group and have chemical shift values of 2.35 ppm (2H), 1.75 ppm (2H), and 2.07 ppm (2H)), as shown in Figure 17 The proton signals for the triethyl group found on P^+ have chemical shift values of 2.07 ppm (6H) and 1.08 ppm (9H) and are labeled **e** and **f.**

3.1.3 PEGylated Ammonium, and Phosphonium, Chitosan Derivatives. Compound TEAB-CS, TEPB-CS, or TPPP-CS was reacted with mPEG-acid (MW: 5000), EDC, and HOBt to synthesis PEGylated chitosan derivatives. TEPB-CS and TEAB-CS were selected because they are direct analogs of each other and can provide a direct comparison between ammonium and phosphonium interaction before and after PEGylation. TPPP-CS already reported in scientific literature was found to be toxic to

mammalian cells by Quian et al.[37] and was selected to undergo PEGylation to evaluate PEGs ability to lower toxicity. All ^{1}H NMR spectra of PEGylated compounds have the same chemical shift values as their non-PEGylated derivatives, as shown in Table 5, except for PEG polymer chain located at 3.55 ppm (448H) and its methoxy at 3.20 ppm (3H). PEGylated ^{1}H NMR spectra can be seen in Figure 18.

3.1.4 Discussion. ^{1}H NMR was conducted for confirmation of successful ammonium/phosphonium carboxy ligand coupling to chitosan. EDC and HOBt were observed in ^{1}H NMR spectra until after the third wash cycle. Accurate integrations and spectra comparisons could be analyzed once EDC and HOBt were successfully removed. Integration values and peak assignments became more difficult to analyze after coupling due to the loss of resolution and peak broadening caused by the increased polydispersity and chitosan's long polymer backbone. All peak assignments are found in the experimental section, and in Appendix A. Ammonium carboxy ligands displayed a much higher deshielding effect than did phosphonium groups. In the case of triethylammonium carboxy ligands, the CH_2 associated with $N^+(\mathbf{CH_2}CH_3)_3$ was observed at 3.15 ppm; and displays more of an inductive effect from its neighboring N^+ than that of its P^+ analog. Comparing the same CH_2 found in $P^+(\mathbf{CH_2}CH_3)_3$, the chemical shift is more upfield at 2.0 ppm, displaying less of an inductive effect on neighboring carbons adjacent to P^+, and leading to a more localized cationic charge. The localization of cationic charge is expected to be more observable in future studies, including agarose gel electrophoresis. ^{1}H NMR was only conducted on ammonium/phosphonium propionic, butanoic, and pentanoic chitosan derivatives. Ammonium/phosphonium acetic acid chitosan derivatives proved to be unsuccessful in coupling to chitosan with EDC and HOBt. Although acetic

Table 5. Table of PEGylated ammonium, or phosphonium, chitosan derivatives with their abbreviations, yield (DS), and 1H NMR ppm assignments using D2O.

Compound Name	Abbreviation	DS	^{1}H NMR ppm D_2O
2-(N-4-triethylphosphonium) butanamide mPEG-*g*-chitosan chloride	TEPB-mPEG-CS	1.67%	4.82 (1H, **anomeric H**), 4.0-2.66 (6H, C_2-C_6 **H**'s ,2H-N**H**), 3.55 (mPEG backbone), 3.23 (3**H**, -OCH_3), 2.35 (2H, -$C\mathbf{H}_2CH_2CH_2P^+$-), 2.07 (6H, -$CH_2P^+(C\mathbf{H}_2CH_3)_3$) , 2.07 (2H, -$CH_2C\mathbf{H}_2P^+(CH_2CH_3)_3$), 1.75 (2H, -$C\mathbf{H}_2CH_2P^+(CH_2CH_3)_3$), 1.08 (9H, -$CH_2P^+(CH_2C\mathbf{H}_3)_3$
2-(N-4-triethylammonium) butanamide mPEG-*g*-chitosan chloride	TEAB-mPEG-CS	5.73%	4.43 (1H, **anomeric H**), 4.0-3.25 (6H, C_2-C_6 **H**'s), 3.55 (mPEG backbone), 3.23 (3**H**, -OCH_3) 3.15 (2H, -$N^+(\mathbf{CH_2}CH_3)_3$), 3.04 (6H, -$CH_2CH_2N^+(C\mathbf{H}_2CH_3)_3$), 2.66 (1-2H, -$CH_2C\mathbf{H}_2N^+(CH_2CH_3)_3$), 2.28 (2H, -$C\mathbf{H}_2CH_2CH_2N^+(CH_2CH_3)_3$, 1.84 (2H, -$C\mathbf{H}_2CH_2N^+(CH_2CH_3)_3$, 1.11 (9H, -$CH_2N^+(CH_2\mathbf{CH_3})_3$
2-(N-5-triphenylphosphonium) pentanamide mPEG-*g*-chitosan chloride	TPPP-mPEG-CS	2.76%	7.65-7.50 (15H, $\mathbf{P^+Ph}3$-$CH_2CH_2CH_2CH_2$-), 4.39 (1H, **anomeric H**), 4.0-2.66 (6H, C_2-C_6 **H**'s ,2H-N**H**), 3.55 (mPEG backbone), 3.23 (3**H**, -OCH_3), 3.13 (2H, P^+-$C\mathbf{H}_2CH_2CH_2CH_2$-), 2.16 (2H, Ph_3-$CH_2CH_2CH_2C\mathbf{H}_2$-), 1.60 (4H, Ph_3-$CH_2C\mathbf{H}_2C\mathbf{H}_2CH_2$-)

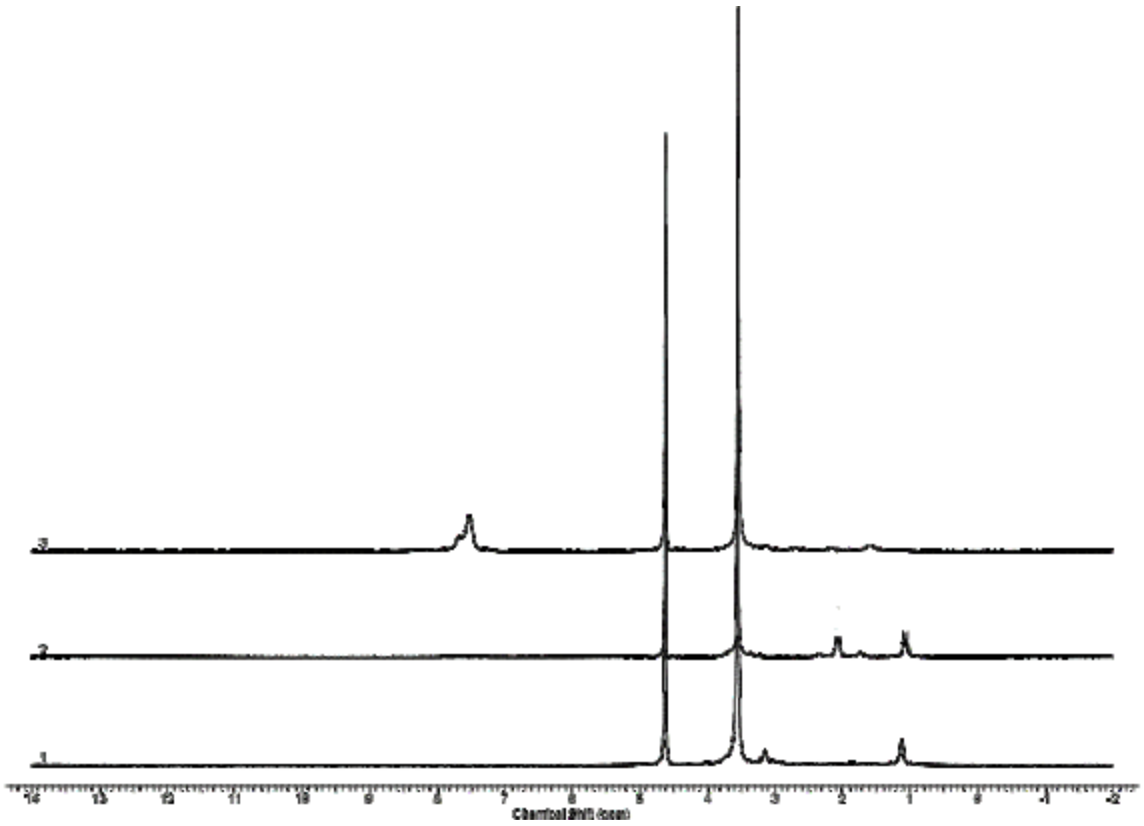

Figure 18. ^{1}H NMR spectra of 1) TEAB-mPEG-g-CS, 2) TEPB-mPEG-g-CS, and 3) TPPP-mPEG-g-CS, using D2O

acid ligands are small, the reactive carboxyl group is sterically hindered to a significant degree by the ammonium/phosphonium group directly adjacent. More efficient coupling was observed as the carbon chain increases on the carboxy ligand, as seen in Table 6. Variations in ammonium alkyl groups also displayed a correlation in degree of substitution. All substituion reactions contained same ratio of ligand to chitosan and reaction conditions. TMAB-CS had the highest coupling efficiency (DS=50%), compared to that of TEAB-CS and TPAB-CS, due to its long carbon chain and decreased steric hindrance from the trimethyl groups. Compared to TMAB-CS and TEAB-CS, TPAB-CS displayed the lowest coupling efficiency (DS=23%) as its bulky propyl substituents created increased steric hindrance.

Table 6. Calculated degree of substitution (DS) for all chitosan derivatives

Compound	Degree of Substitution
2-(N-3-triethylphosphonium) propionamide chitosan chloride (**TEPPr-CS**)	19% P^+
2-(N-4-triethylphosphonium) butanamide chitosan chloride (**TEPB-CS**)	21% P^+
2-(N-5-triphenylphosphonium) pentanamide chitosan chloride (**TPPP-CS**)	42% P^+
2-(N-4-trimethylammonium) butanamide chitosan chloride (**TMAB-CS**)	50% N^+
2-(N-4-triethylammonium) butanamide chitosan chloride (**TEAB-CS**)	43% N^+
2-(N-4-tripropylammonium) butanamide chitosan chloride (**TPAB-CS**)	26% N^+
2-(N-4-triethylphosphonium) butanamide mPEG-*g*-chitosan chloride **(TEPB-mPEG-CS)**	1.6% mPEG
2-(N-4-triethylammonium) butanamide mPEG-*g*-chitosan chloride **(TEAB-mPEG-CS)**	5.73% mPEG
2-(N-5-triphenylphosphonium) pentanamide mPEG-*g*-chitosan chloride **(TPPP-mPEG-CS)**	2.76% mPEG

3.2. FT-IR Analysis

FT-IR analysis was conducted on all ammonium and phosphonium chitosan derivatives to examine changes in spectra after cationic carboxyl substitution. Characteristic peaks corresponding to amide I and II formation observed near wavenumbers 1650 cm^{-1} and 1550 cm^{-1} were found for both ammonium and phosphonium derivatives as shown in Figure 19. C-N^+ stretching was observed in all ammonium derivatives near wavenumber 1480 cm^{-1} and was consistent with C-N^+ values found by Tan et al.[67] C-P^+ stretching was observed in all phosphonium derivatives between wavenumbers 1450 and 1410 cm^{-1} and was consistent with C-P^+ values found by Qian et al.[37] Characteristic wavenumbers for chitosan are observed at 3260 cm^{-1} and are assigned to the hydroxyl and amino groups found on carbons 3 and 6. C-H stretching was

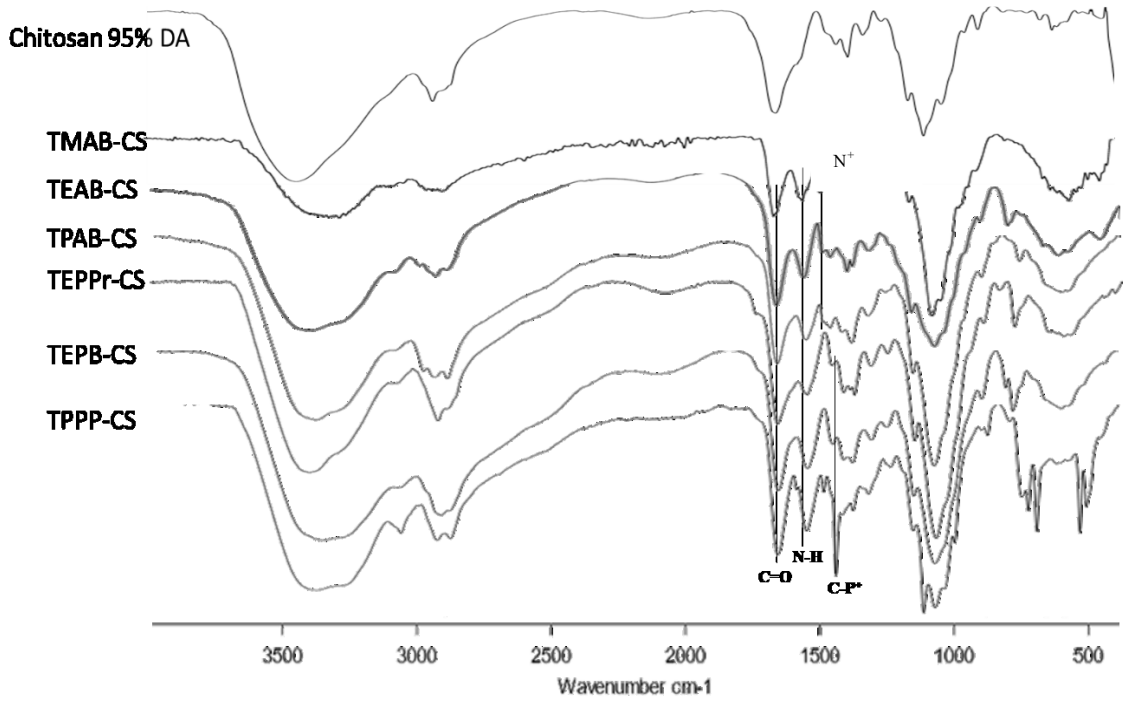

Figure 19. FT-IR spectra of TMAB-CS, TEAB-CS, TPAB-CS, TEPB-CS, TEPPr-CS, and TPPP-CS, showing C-P+ and C-N+ for synthesized chitosan derivatives.

observed near wavenumber 2880 cm^{-1} for all chitosan derivatives. For all chitosan derivatives, an amide I signal associated with C=O stretching vibration is observed near wavenumber 1650 cm^{-1}, while an amide II signal associated with N-H bending vibrations appears near wavenumber 1540 cm^{-1}.

Strong C-O stretching frequencies associated to carbons 1, 3, 4, 5, and 6 were observed near wavenumber 1060 cm^{-1}. PEGylated derivatives' additional C-H, and C-O stretching causes a dramatic increase in intensity near wavenumbers 2867 cm^{-1} and 1060 cm^{-1}, as shown in Apendix B. Characteristic chitosan derivative peaks were still observable after PEGylation indicating a low percentage of mPEG-acid substitution.

3.3. Degree of Substitution

Further characterization of chitosan and its derivatives relies on obtaining the degree of substitution (DS) of ammonium/phosphonium carboxy ligand and mPEG (MW: 5000) acid to chitosan. The degree to which these derivatives are substituted affects their overall interaction with biological molecules. Ammonium/phosphonium ligands promote higher electrostatic interactions due to their formally-charged nitrogen or phosphorous. Adapting DS calculation protocol from Jaidee et al.[44], ^{1}H NMR was used to obtain final DS values. Using ^{1}H NMR spectra, the degree of substitution can be obtained by comparing two independent integration values and the number of protons contributing to those values.[49] In Figure 20, we found the acetyl groups DS by comparing both chitosans, and acetyl groups, integral values to their associated protons. Dividing the acetyl group's integration value by the number of protons associated to that signal (3 protons), we obtain the integration value of 1 acetyl proton. Likewise, Dividing the chitosan polymer

$$DS = \frac{3.00 \div 3}{128.59 \div 6} \times 100 = 4.66\ \%\ \text{Acetylated}$$

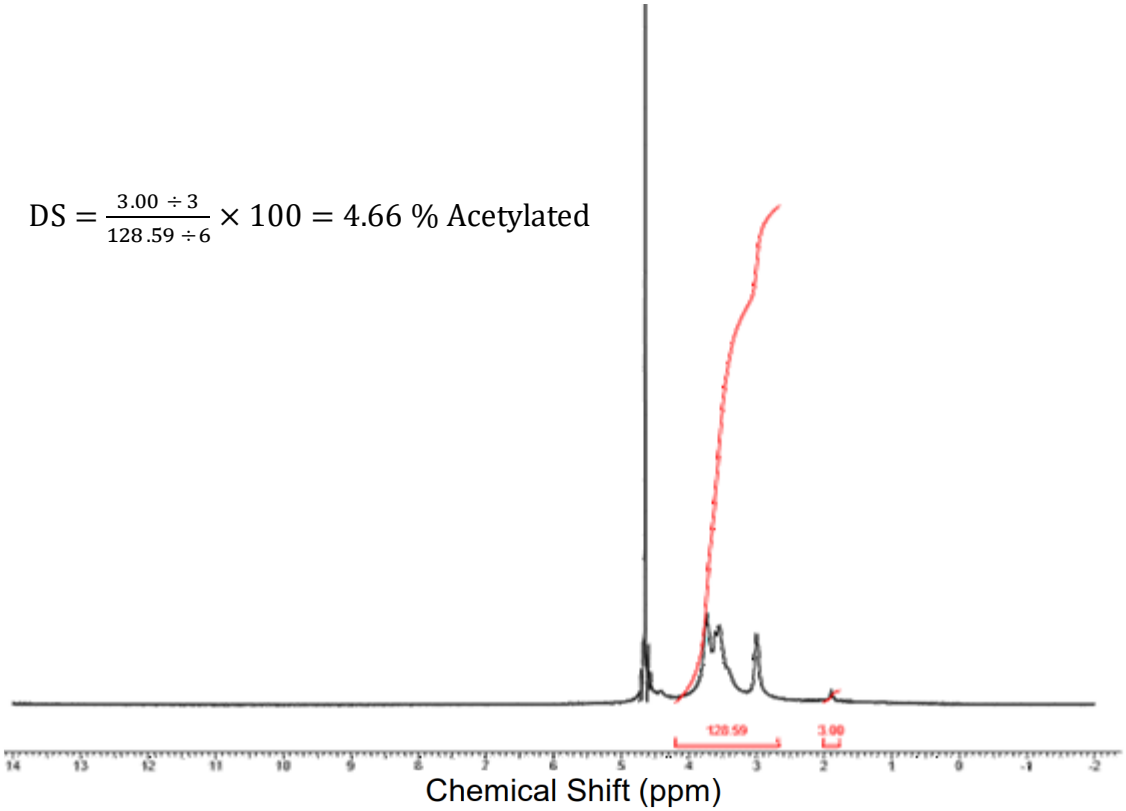

Figure 20. Calculation of degree of substitution (DS) using staring material 95% DA chitosan. Integral lines are in red and their values below the spectrum

integration value by the number of protons associated to that signal (6 protons, excluding the hydrogen attached to anomeric carbon), we obtain the integration value of 1 chitosan proton. Then dividing the 1 acetyl proton value by the 1 chitosan proton value and multiplying it by 100, gives us the degree of substitution of acetyl groups found on chitosan. Following the equation set forth above and also found in Figure 21, we obtained DS for our starting material. The acetyl integration value of 3.00 should be divided by 3, (for there are three protons found on acetyl groups) leaving a value of 1. Then chitosans integration value of 128.59 should be divided by 6, (for the sum of protons on carbons **C_2-C_6** is 6) leaving 21.43. Finally, dividing acetyls value of 1 by chitosans value of 21.43 and multiplying by 100, we obtain a DS=4.66%. The DS percent value represents the

percent of acetyl groups coupled to amino groups on chitosan. Thus, 4.66% of our starting material is acetylated. The chitosan shown in Figure 20 was purchased as 95% deacetylated chitosan from Bonding Chemical company.[66] Comparing these two values of acetylation from our calculations and Bonding Company analysis, we were able to obtain the same degree of accuracy of substitution up to (0.34%).[66]

mPEG DS was calculated following an altered mathematical procedure is shown in Figure 22. DS values of PEGylated chitosan derivatives needed to incorporate the DS of the previous reaction product before the DS of the mPEG could be evaluated. The equation given in Figure 21 can be rearranged to solve for chitosans integration value using the previously calculated DS for that particular ammonium/phosphonium derivative, as seen in Figure 22. After calculating the integration value for chitosan, we can subtract this value from the overlapping integration values, of mPEG and chitosan, to isolate mPEG's integration value. This value can be plugged in the equation found in Figure 21 to determine the DS of PEGyalted derivatives.

$$DS = \frac{I_s \div H_s}{\sum I_{chitosan\ (2.6\text{-}4.0\ ppm)} \div 6}$$

Figure 21. Equation used for calculating degree of substitution where I_s is, integrated signal value for substituted ligand, Hs is number of protons associated to substituted ligand, and $I_{chitosan}$ is the integrated signal value for chitosan protons (C2-C6 and -CH_2OH)

The DS values obtained for both PEGylated and non-PEGylated derivatives were used in both CD and agarose gel electrophoresis. These DS values were used to calculate moles of positive charge for each chitosan derivative and their average molecular weight per unit after substitution reactions. Using these calculated values, we were able to obtain

$$\sum I_{\text{chitosan (2.6–4.0 ppm)}} = \frac{DS \times 6}{I_s \div Hs}$$

Figure 22. equation used for calculating degree of substitution of PEGylated derivatives, where Is is, integrated signal value for substituted ligand, H_s is number of protons associated to substituted ligand, and Ichitosan is the integrated signal value for chitosan. After finding $\sum I_{\text{chitosan (2.6-4.0 ppm)}}$ this value can be subtracted from the integration value for the PEGylated spectrum to isolate just the mPEGs integration value.

accurate charge to charge ratios for determining ammonium, and phosphonium, derivatives' affinity to Dickerson Drew Dodecamer (DDD) B-form DNA.

3.4. Agarose Gel Electrophoresis

Agarose gel electrophoresis was used to examine ammonium and phosphonium chitosan derivatives' ability to complex DDD B-form DNA. The concentration of DDD was calculated using the absorbance value from 260 nm collected by Varian Cary 50 UV-Vis spectrophotometer and its extinction coefficient of 1.11×10^5 $M^{-1}cm^{-1}$ at 25° C.Using 24-mer DDD B-form DNA (consisting of 24 negatively charged phosphate groups), we were able to evaluate interactions using ammonium/phosphonium chitosan derivatives. All ratios established for electrophoresis are a charge to charge ratio determined by DS of each chitosan derivative. These ratios are written in (n)X notation, were "n" is whole number multiplied by 1 to 1 ratio of positive to negative charge (+/-). For all DNA-ammonium chitosan derivative complexes exceeding a ratio of 2X, we were able to observe complete complexation of DNA, evidenced by the fluorescence staying in the starting wells. Moving from the 2X ratio towards 0.25, we can observe a signal for free, uncomplexed DNA. When comparing ammonium chitosan derivatives affinities at

2X charge ratio, we can observe clear differences in cationic interaction between the different ammonium groups. At a charge ratio of 2X, TPAB-CS displayed the least affinity to DDD DNA, compared to TMAB-CS and TEAB-CS. TEAB-CS appeared to have the most effective interactions with DNA as evidenced by complete complexation at a charge ratio of 2X compared to TMAB-CS and TPAB-CS charge ratios of 4X, as seen in Figure 23. Attention should be drawn to the florescence that remain in the wells after complete complexation at 4X, 8X, and 16X. In the case of TPAB-CS, the fully-complexed DNA in 4X charge ratio appeared to be pushed towards the front of the well, as seen in Figure 23. As for the wells containing charge ratios of 8X and 16X, the

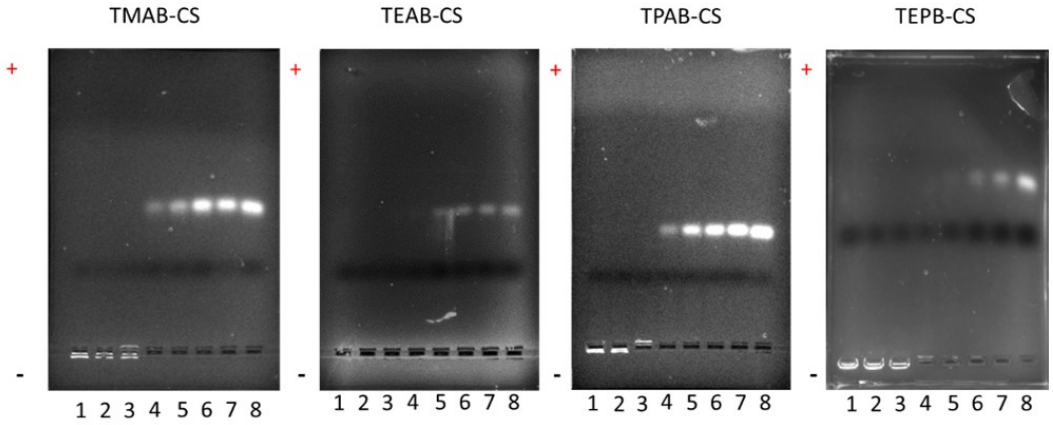

Figure 23. Agarose gel electrophoresis results of TMAB-CS, TEAB-CS, TPAB-CS, and TEPB-CS. Wells are in charge ratios of 1: 16x, 2: 8x, 3: 4x, 4: 2x, 5: 1x, 6: 0.5x, 7: 0.25x, 8: Control

florescence can be observed drawn toward the back of the well. Completely complexed DNA was observed in the starting wells having an over all complexation charge, as evidenced by their postion in the startings wells. In the case of phosphonium derivatives, there were not only differing results from the ammonium groups, but the phosphonium groups had different outcomes amongst themselves. TEPPr-CS appears less soluble compared to TEPB-CS leading to a dramatic loss of complexation of DDD DNA across

all charge ratios. Reaction conditions for TEPPr and chitosan coupling would have to be improved to increase solubility and the efficiency of DNA complexation at lower charge ratios. TPPP-CS displayed improved results when compared to ammonium derivatives; complete complexation occurs at a charge ratio of 2X; leaving little-to-no signal at concentration 1X. TEPB-CS had a more effective interaction than all other derivatives tested. Complete complexation using TEPB-CS occurred at a charge ratio of 1X. TEPB-CS had a higher affinity for DDD DNA at charge ratios 0.5 and 0.25X when compared to all other chitosan derivatives. Due to a more localized charge, TEPB-CS complexes DNA more efficiently. This increase in efficiency could make phosphonium chitosan derivatives viable candidates for gene therapy.

PEGylation of these compounds resulted in a severe loss of electrostatic interaction between chitosan derivatives and DNA, as seen in Figure 24. After PEGylation, TPPP-mPEG-g-CS and TEAB-mPEG-g-CS suffered a drastic loss in interaction with DDD compared to their previous un-PEGylated derivatives. The large size of mPEG-5000 increases steric hindrance to the already-bulky trialkyl chitosan derivatives. However, PEGylation of TEPB-CS resulted in only a slight loss of interaction with DDD. The DS for TEPB-CS was half that of TEAB-CS, and yet PEGylated TEPB-CS maintained high complexation of DDD DNA compared to PEGylated TEAB-CS. Although the PEGylated ammonium derivatives lack the same efficiency of un-PEGylated derivatives, electrostatic interaction leading to complete complexation can still be observed.

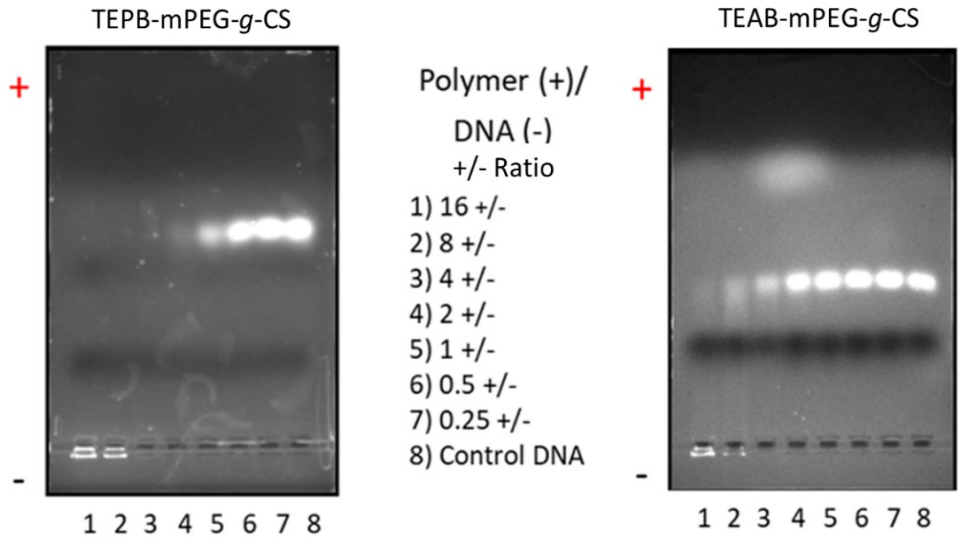

Figure 24. Agarose gel electrophoresis results of TEAB-mPEG-g-CS and TEPB-mPEG-g-CS. Wells are in charge ratios of 1: 16x, 2: 8x, 3: 4x, 4: 2x, 5: 1x, 6: 0.5x, 7: 0.25x, 8: Control

3.5. Turbidity

Chitosan derivatives were analyzed for pH-dependent solubility using a Varian Cary 50 UV-Vis spectrophotometer at 600 nm. Values of %T were collected over an increasing pH range from 3-13. The data points for each study were plotted on a graph and can be seen in Figure 25. Turbidity results are used to determine the potential viability of chitosan derivatives that can remain soluble long-term *in vivo*. During the analysis, TPPP-mPEG-*g*-CS was the only derivative with a noticeable decrease in %T after pH 7. Although the decrease was gradual, the derivative did not aggregate or fall out of solution. TEPPr-CS exhibited a steady overall %T that was lower than all other derivatives tested, which may be correlated to the poor interaction with DDD during agarose gel electrophoresis. The turbidity analysis displayed a lack of pH-dependent

solubility in the chitosan derivatives, ensuring that our products are not just protonated chitosan species.

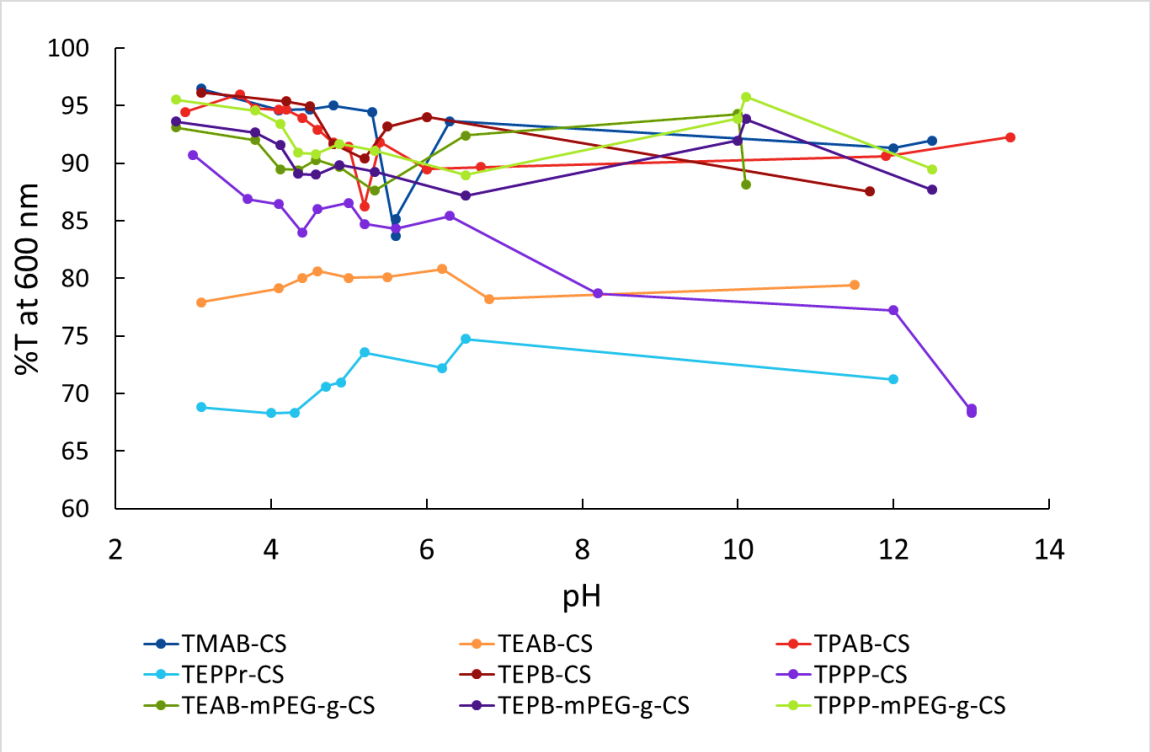

Figure 25. Turbidity analysis of all synthesized chitosan derivatives evaluated using %T at 600 nm. With an initial pH of 3, 0.1 M NaOH was added to increase pH till a value of 13 was obtained

3.6. Thermogravimetric analysis (TGA) and Differential Thermogravimetric (DTG)

It is known that intramolecular and intermolecular hydrogen bonding stabilizes fully acetylated chitin and 95% DA chitosan. most of these interactions are lost in carboxy substituted chitosan derivaitves.[66] It has been well established that chitosan derivatives with increasing DS exhibit lower intermolecular stability when compared to low DS derivatives.[66] Ammonium and phosphonium chitosan derivatives were analyzed using TGA, and their results displayed a clear correlation between increased DS and decreased thermal stability which were consistent with literature findings.[67]

Thermogravimetric analysis was conducted using a TA Instrument Q600 Thermogravimetric analyzer on all chitosan derivatives to evaluate thermal stability after ammonium, phosphonium, and mPEG (MW: 5000) substitutions. All samples were subjected to thermal degradation starting at room temperature and ending at 600 °C using a ramp rate of 20 °C/min. Although the stability is lower due to the loss of hydrogen bonding interactions, the degradation process takes on new phases as different ligands are coupled to chitosan. Unmodified chitosan TGA displayed initial degradation beginning at 265 °C, followed by a smooth decline until no further degradation phases were observed. The degradation phases for ammonium and phosphonium chitosan derivatives were close together making separate phases harder to distinguish. The TGA results for chitosan and its derivatives were converted to differential thermogravimetric (DTG) (%/°C) for more accurate comparisons.

Changes in chitosan derivatives' stability due to altered substituents is readily observed using DTG rather than unmodified TGA. DTG peaks indicate a high loss in weight % at a particular temperature. Using DTG, single- or multi-phase degradation is more easily observed compared to the cluttered signal of TGA, as seen in Figures 26 and 27. All DTG results display an initial phase between 25-100 °C due to loss of water adsorbed to the starting material, which is not considered to be a degradation phase. Chitosan follows a single-phase degradation process displaying no secondary stabilization structure. TEAB-CS displayed a degradation process similar like that of chitosan where only one phase is observed. However, TEAB-CS's degradation begins at

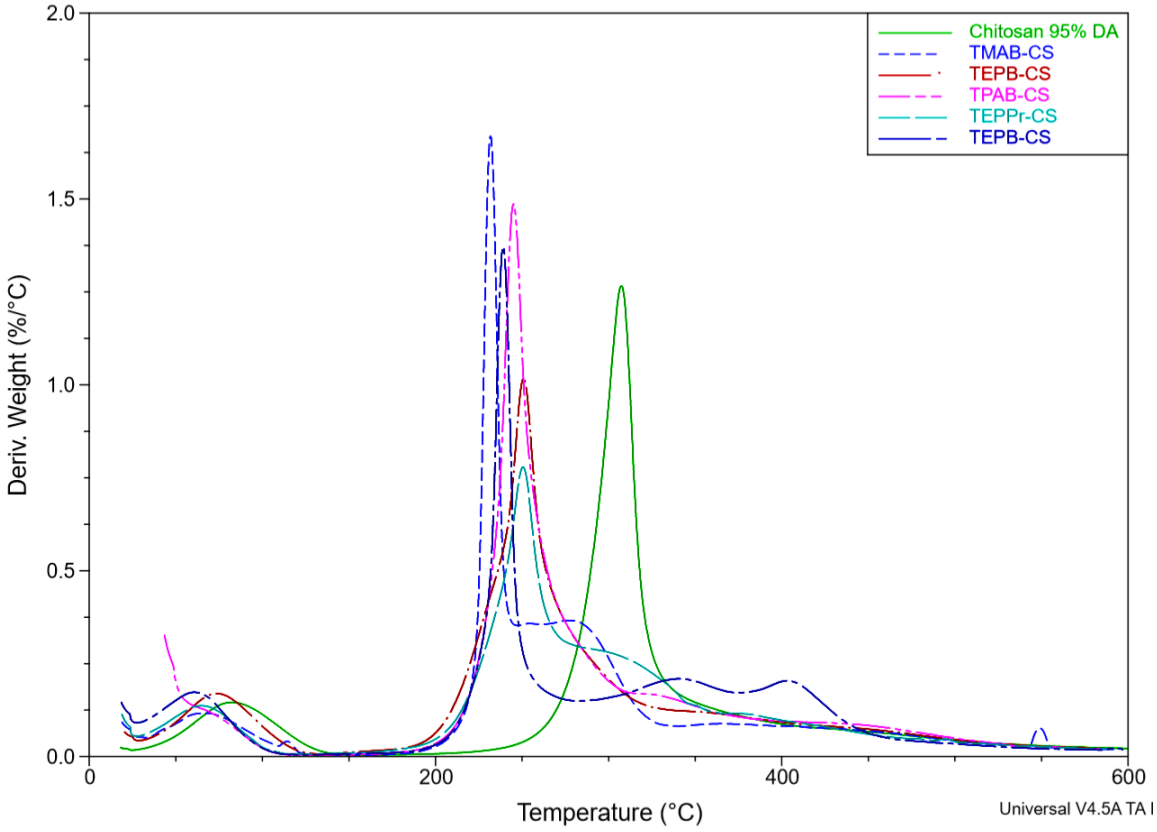

Figure 26. DTG of non-PEGylated ammonium, and phosphonium, chitosan derivatives was used to examine change in stability of chitosan's polymer chain after carboxylic coupling reaction

223 °C, which is 42 °C less than unmodified chitosan; indicating loss of intermolecular stabilization. Both TMAB-CS and TPAB-CS displayed a two-phase degradation process. Their first phases begin at 227 °C and 216 °C, indicating a loss of stabilization when compared to unsubstituted chitosan. Their second phases began at 239 °C and 259 °C and can be attributed to the ammonium ligands substitution. TEPB-CS displayed three phases of degradation and the lowest overall thermal stability. The first phase of TEPB-CS began at 205 °C which is significantly lower than that of unsubstituted chitosan beginning at 265 °C. TEAB-CS, TEPB-CS, and TPPP-CS were PEGylated to challenge the hypothesis of increased stability in mPEG *grafted* polymers.

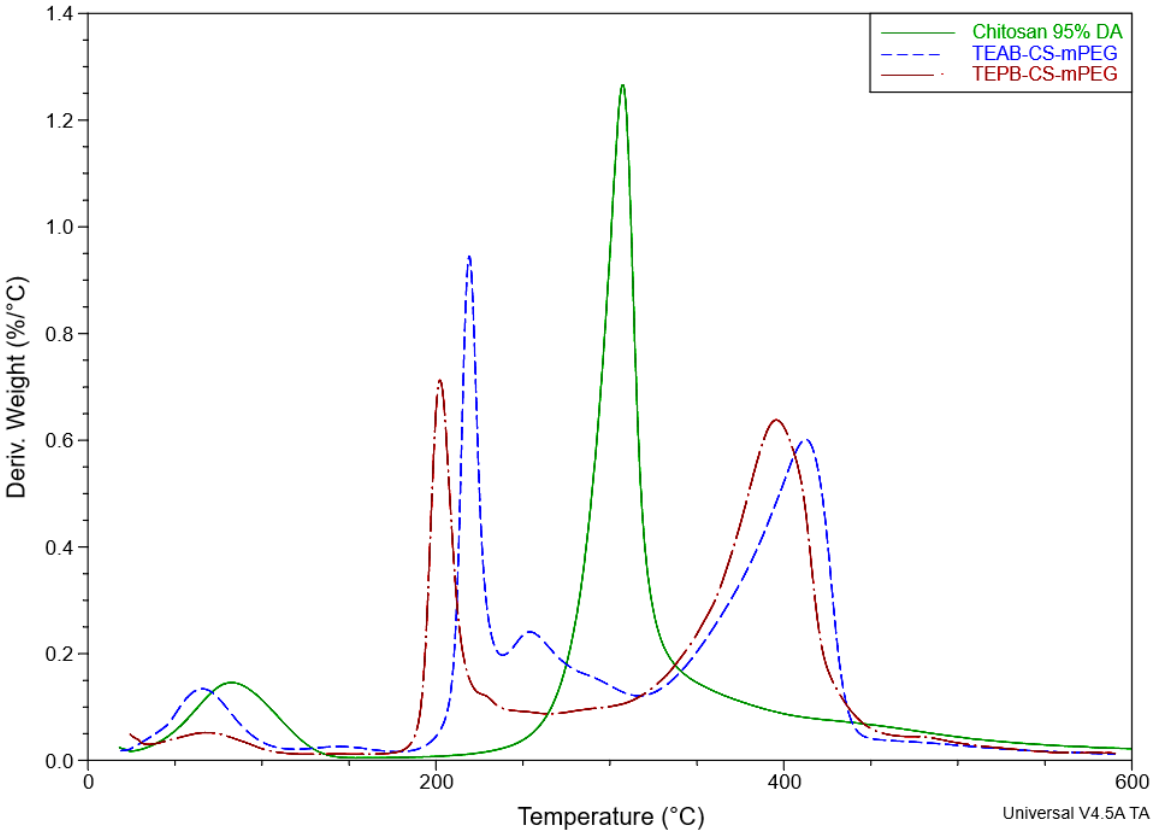

Figure 27. DTG of PEGylated TEAB-CS, and TEPB-CS, derivative used to examine the change in stability of chitosan's polymer chain after carboxylic and mPEG coupling reactions

There was an overall increase in stability, but not to the chitosan derivative' s main polymer chain. Phase 1 for compounds TEAB-CS, TEPB-CS, and TPPP-CS still had decreased degradation temperatures of 193 °C, 229 °C, and 208 °C, respectively. However, these PEGylated derivatives displayed an additional phase beginning at 344 °C, 310 °C, and 338 °C; which can be assigned to the degradation of the mPEG backbone. Although there was increased stability with more of the weight percent being preserved until higher temperature, this was due only to the addition of mPEG (MW: 5000), and not to the stability of chitosan derivatives. Ammonium and phosphonium chitosan derivatives were analyzed using TGA, and DTG, and their results of the first degradation phase demonstrates a correlation between increased DS and decreased thermal stability.[67]

3.7. Circular Dichroism (CD)

CD analysis was conducted to observe electrostatic interaction with the nucleotides found in DDD DNA and chitosan derivatives. Jasco J-815 CD spectrometer evaluated the effects of chitosan and its derivatives on DDD's secondary structure, B-form double-stranded DNA at 25 °C. The charge ratios used for CD analysis were prepared in the same manner as agarose gel electrophoresis. Unmodified chitosan and its derivatives do not produce a signal in the wavelengths being investigated. The positive and negative ellipticities of DDD are centered around 280 nm and 260 nm, and are in concordance with literature findings for B-form DNA.[68-70] In Figure 28, the chitosan derivatives were examined at a charge ratio of 4x. It is at this charge ratio we examined complete complexation of DNA in all derivatives. The greatest loss of B-form comformational normality was oberved with TPAB-CS. As charge ratios amongst the independent studies are increased, the loss of B-form conformational state is observed due to the complexation of chitosan derivative with DNA. Chitosan derivatives' interaction with DDD with increasing charge ratios are shown in Apendix E. As the +/- charge ratio is increased, the molar ellipticities of the DNA is suppressed; and the positive band near 280 nm is shifted. TPAB-CS displays the most significant increase in the signal of the negative band centered around 260 nm, and the most significant decrease of the positive band at 280 nm . All chitosan derivatives displayed interactions with DNA, as evidenced by the suppressed 260 nm (negative) signal and 280-290 nm (positive) signal.[69,70] Although changes in intensities were observed at 200-220 nm, their interpretations are unclear, and were not used for investigating chitosan derivatives

interaction with DNA.[69,70] Although there are no conclusive conformational changes from B to Z-form DNA, CD analysis did display an interaction between ammonium and phosphonium chitosan derivatives with DDD.

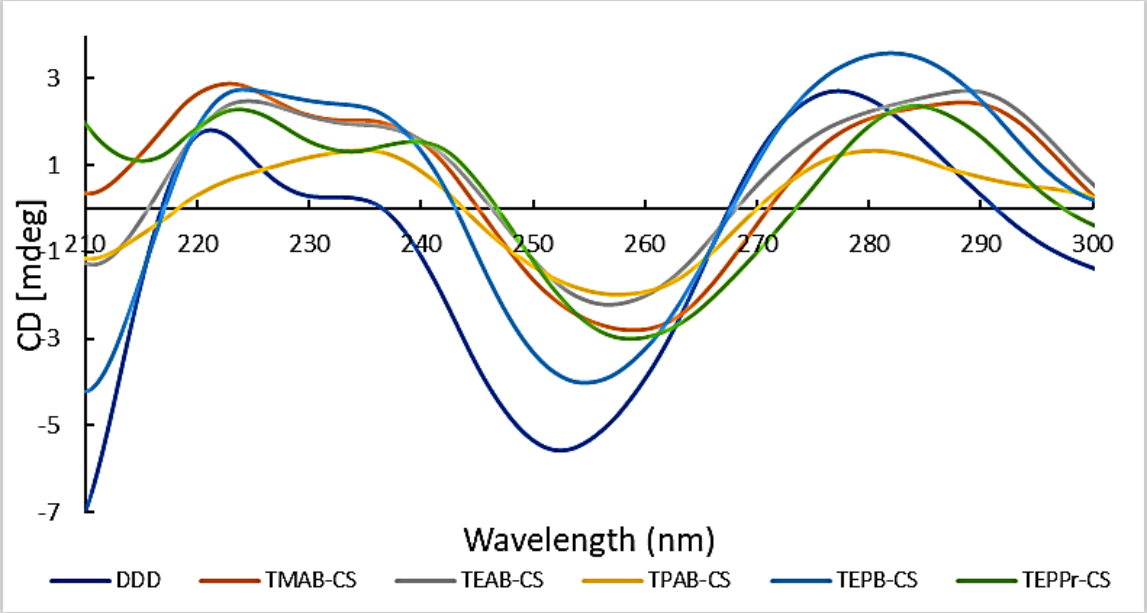

Figure 28. CD analysis was conducted to examine complexation/interaction of ammonium, and phosphonium, chitosan derivatives with DDD DNA using 1-42X charge ratios. The non-PEGylated chitosan derivatives above represent complete complexation at charge ratio 4X

3.8. Fluorescence Microscopy Studies

To evaluate if yeast cells would internalize ammonium or phosphonium derivatives, fluorescence microscopy studies were conducted using a 3i Lambda XL GFP 488 lamp for excitation of FITC, an Orca R2 wide-lens microscope for visualization of the cells, and Slidebook Image Capturing software for digitally capturing the images. The procedure used for preparing the cells with FITC tagged chitosan derivatives is outlined in section 2.1.9. In Figures 29 and 30, cells with FITC-tagged chitosan derivatives can be seen as a green hue. An intensity heat map was used to visualize the yeast cells

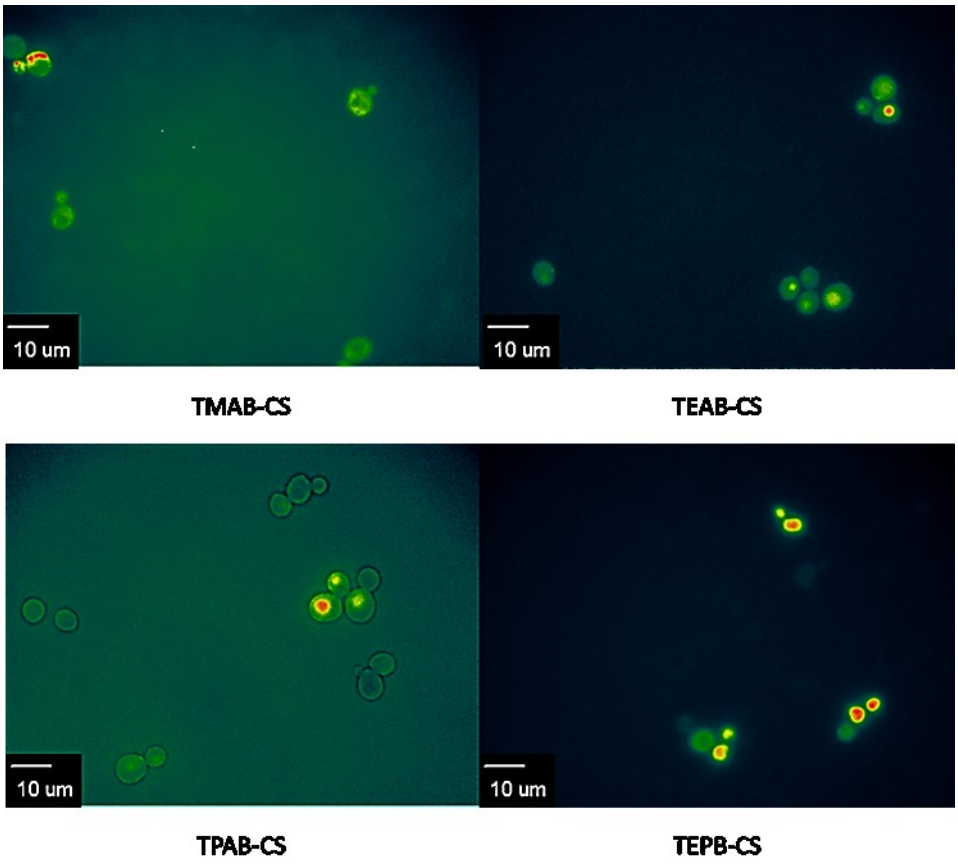

Figure 29. Fluorescence Microscopy results utilizing intensity heat mapping to vizualize FITC tagged derivatives TMAB-CS, TEAB-CS, TPAB-CS, and TEPB-CS

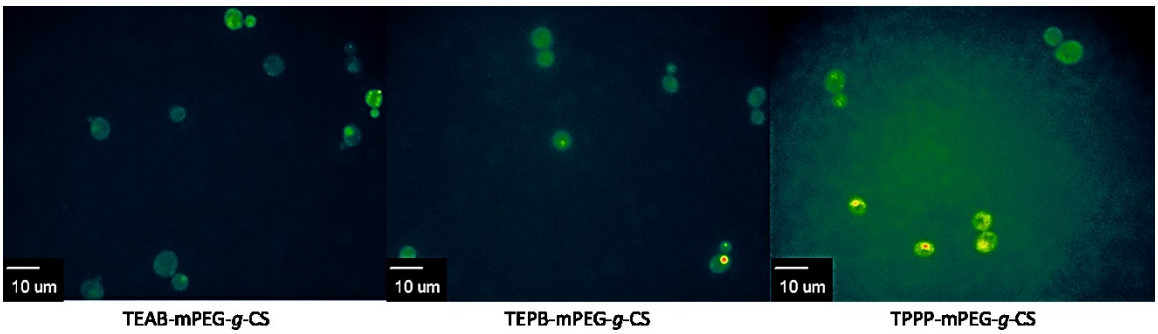

Figure 30. Fluorescence Microscopy results utilizing intensity heat mapping to vizualize FITC tagged derivatives TEAB-mPEG-g-CS, TEPB-mPEG-g-CS, and TPPP-mPEG-g-CS

containing FITC-tagged chitosan derivatives. A new preparation procedure and visualization protocol for the internalization of FITC-tagged chitosan derivatives is being implemented in future studies to improve the accuracy of the results. Further investigations are underway to investigate the internalization of FITC-tagged chitosan derivatives into mammalian cells. As for this study, the results can only conclude FITC tagged derivatives are adsorbed to the cell membrane or internalized. Neither result can be explicitly confirmed.

3.9. Yeast Growth Assays

The antifungal properties of ammonium and phosphonium chitosan derivatives were examined using a BioTek ELx808 microplate reader and freshly inoculated yeast cells. The preparation procedure for yeast growth assays is found in section 2.1.5. The data collected was normalized by taking the final OD reading for each concentration, dividing it by the final OD of the control, and multiplying by 100. The results of each study were compiled into a plot and can be seen in Appendix G. The normalization of the data was necessary for accurate comparisons to be made between each sample. Figure 31 displays a clear inhibition of yeast growth at just 5 μg/mL; while at 1 μg/mL, some samples increased growth. TEPB-CS displayed the greatest inhibition of yeast growth compared to TMAB-CS, TEAB-CS, and TPAB-CS. The promotion of yeast growth using TMAB-CS and TPAB-CS is currently unexplained and is being researched further. For all samples tested, no growth was observed at concentrations greater than 5 μg/mL. Future experiments will narrow the concentration between 1 and 5 μg/mL to discover an accurate inhibition cutoff.

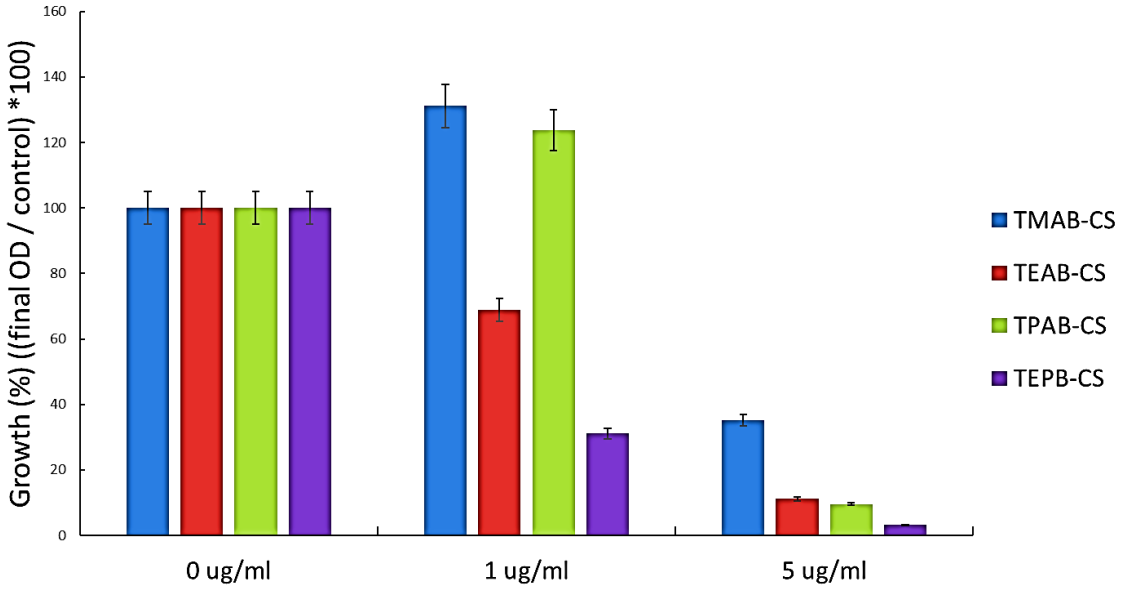

Figure 31. Yeast growth assay conducted using TMAB-CS, TEAB, TPAB-CS, and TEPB-CS derivatives with concentrations of 0, 1, and 5 µg/mL to analize antifungal properties

CHAPTER 4. CONCLUSION

In this work, ammonium and phosphonium chitosan derivatives (see page 16, Figure 4) have been synthesized and characterized by ^{1}H NMR, FT-IR, TGA, CD, agarose gel electrophoreses, confocal microscopy, and yeast growth assays. Although some ammonium derivatives have been reported in the literature, to the best of our knowledge the synthesis and characterization of the derivatives made in this work have not yet been reported in the literature.

TEPB-CS displayed the best interaction with Dickerson Drew Dodecamer DNA when compared against all ammonium derivatives synthesized. ^{1}H NMR was able to display the localization of positive charge found on phosphoniums derivatives; while FT-IR was able to display strong coupling of the cationic carboxy ligands to chitosan. Agarose gel electrophoreses observed that TEPB-CS was able to complex DDD at 1x concentration, compared to that of ammonium where complete complexation occurred at 2x, or higher. CD was able to observe that TMAB-CS had the most significant interaction with DDD when compared to the interactions of the chitosan derivatives. Finally, yeast growth assays were conclusive in determining that TEPB-CS was able to inhibit yeast growth better than ammonium compounds, and will be used in future studies with mammalian cells to observe their interaction.

Future work will examine the cytotoxicity of the compounds made in this work as well as the transfection efficiency with regard to mammalian cells.

REFERENCES

(1) Abbas, A. M. *Iowa Research Online*. **2010**, 1-365.

(2) Henrissat, B. *Chitin and Chitinases.* **1999**, 137–156.

(3) Kas, H. S. *J. of Microencapsulation.* **1997**, *14*, 689–711.

(4) Singla, A. K.; Chawla, M. *J. of Pharmacy and Pharmacology.* **2001**, *53*, 1047–1067.

(5) Argin-Soysal, S.; Kofinas, P.; Lo, Y. M. *Food Hydrocolloids.* **2009**, *23*, 202–209.

(6) Higashimura, T.; Sisido, M.; Fuyama, H. *Polymer.* **1977**, *18*, 291–294.

(7) Vårum, K. M.; Antohonsen, M. W.; Grasdalen, H.; Smidsrød, O. *Carbohydrate Research.* **1991**, *211*, 17–23.

(8) Porter, C. *Suicide Gene Therapy.* **2009,** 91–106.

(9) Fukazawa, K. *International J. of Molecular Medicine.* **2009**, *25* (01).

(10) Chung, T. W.; Lu, Y. F.; Wang, H. Y.; Chen, W. P.; Wang, S. S.; Lin, Y. S.; Chu, S. H. *Artificial Organs.* **2003**, *27*, 155–161.

(11) Kim, S. H.; Robbins, P. D. *Lysosomal Storage Disorders.* **2007**, 53–67.

(12) Aiba, S. I. *International J. of Biological Macromolecules.* **1992**, *14*, 225–228.

(13) Lee, K. Y.; Ha, W. S.; Park, W. H. *Biomaterials.* **1995**, *16*, 1211–1216.

(14) Hirano, S. *Biotechnology Annual Review.* **1996**, 237–258.

(15) Plance K. *Material Science of Chitin and Chitosan.* **2001,** 165–190.

(16) Lamarque, G.; Lucas, J. M.; Viton, C.; Domard, A. *Biomacromolecules.* **2005**, *6*, 131–142.

(17) Ottey, M. *Carbohydrate Polymers.* **1996**, *29*, 17–24.

(18) Huang, M.; Khor, E.; Lim, L. Y. *Pharmaceutical Research.* **2004**, *21*, 344–353.

(19) Allan, G.; Peyron, M. *Carbohydrate Research.* **1995**, *277*, 257–272.

(20) Tokura, S.; Ueno, K.; Miyazaki, S.; Nishi, N. *Macromolecular Symposia.* **1997**, *120*, 1–9.

(21) Kiang, T.; Wen, J.; Lim, H. W.; Leong, K. W. *Biomaterials.* **2004**, *25*, 5293–5301.

(22) Köping-Höggård, M.; Melnikova, Y. S.; Vårum, K. M.; Lindman, B.; Artursson,

P. *The J. of Gene Medicine.* **2002**, *5*(2), 130–141.

(23) Margolis, H. *Nature.* **1998**, *392*, 857–857.

(24) Templeton, N.S.; *Gene and Cell Therapy.* **2015**, 1271–1310.

(25) Scanlon, K.J.; *Cancer Gene Therapy.* **2004**, *11*, 841–841.

(26) Flotte, T. R.; *J of Cellular Physiology.* **2007**, *213*, 301–305.

(27) Boulaiz, H.; *Cancer Gene Therapy by Viral and Non-viral Vectors.* **2014**, i-xii.

(28) Lavertu, M.; Méthot, S.; Tran-Khanh, N.; Buschmann, M. D. *Biomaterials.* **2006**, *27*, 4815–4824.

(29) Tan, W.; Zhang, J.; Luan, F.; Wei, L.; Chen, Y.; Dong, F.; Li, Q.; Guo, Z. *International J. of Biological Macromolecules.* **2017**, *102*, 704–711.

(30) Qian, C.; Xu, X.; Shen, Y.; Li, Y.; Guo, S. *Carbohydrate Polymers.* **2013**, *97*, 676–683.

(31) Kim, Y. H.; Gihm, S. H.; Park, C. R.; Lee, K. Y.; Kim, T. W.; Kwon, I. C.; Chung, H.; Jeong, S. Y. *Bioconjugate Chemistry.* **2001**, *12*, 932–938.

(32) Kim, K.; Kwon, S.; Park, J. H.; Chung, H.; Jeong, S. Y.; Kwon, I. C.; Kim, I.-S. *Biomacromolecules.* **2005**, *6*, 1154–1158.

(33) Dou, Xiaozheng; Missouri State University, **2015**.

(34) Jiang, X.; Dai, H.; Leong, K. W.; Goh, S.-H.; Mao, H.-Q.; Yang, Y.-Y. *The J. of Gene Medicine.* **2006**, *8*, 477–487.

(35) Dhulipala, V.; Maddali, K.; Welshons, W.; Reddy, C. *Birth Defects Research Part B: Developmental and Reproductive Toxicology.* **2005**, *74*, 233–242.

(36) Weber, P. C.; Wendoloski, J. J.; Pantoliano, M. W.; Salemme, F. R. *J. of the American Chemical Society.* **1992**, *114*, 3197–3200.

(37) Nakajima, N.; Ikada, Y. *Bioconjugate Chem*. **1995**, 6, 123–130

(38) Tang, Y.; Cummins, J.; Huard, J.; Wang, B. *Expert Opinion on Biological Therapy.* **2010**, *10*, 395–408.

(39) Yeomans, D. C.; Wilson, S. P. *Gene Therapy.* **2009**, *16*, 502–508.

(40) Chalikonda, S.; Bartlett, D. L. *Cancer Drug Discovery and Development Gene Therapy for Cancer.* **2004**, 73–85.

(41) Lu, Y.; Madu, C. O. *Expert Opinion on Drug Delivery.* **2009**, *7*, 19–35.

(42) Schmidt-Wolf, G. D.; Schmidt-Wolf, I. G. *Trends in Molecular Medicine.* **2003**, *9*, 67–72.

(43) Gao, X.; Kim, K.-S.; Liu, D. *The AAPS J.* **2007**, *9*.

(44) Jaidee, A.; Rachtanapun, P.; Luangkamin, S. *Advanced Materials Research.* **2012**, *506*, 158–161.

(45) Köping-Höggård, M.; Vårum, K.; Issa, M.; Danielsen, S.; Christensen, B.; Stokke, B.; Artursson, P. *Gene Therapy.* **2004**, *11*, 1441–1452.

(46) Boussif, O.; Lezoualch, F.; Zanta, M. A.; Mergny, M. D.; Scherman, D.; Demeneix, B.; Behr, J. P. *Proceedings of the National Academy of Sciences.* **1995**, *92*, 7297–7301.

(47) Bragonzi, A.; Dina, G.; Villa, A.; Calori, G.; Biffi, A.; Bordignon, C.; Assael, B. M.; Conese, M. *Gene Therapy.* **2000**, *7*, 1753–1760.

(48) Tang, M. X.; Redemann, C. T.; Szoka, F. C. *Bioconjugate Chemistry.* **1996**, *7*, 703–714.

(49) Turunen, M. P.; Hiltunen, M. O.; Ruponen, M.; Virkamäki, L.; Jr, F. S.; Urtti, A.; Ylä-Herttuala, S. *Gene Therapy.* **1999**, *6*, 6–11.

(50) Gebhart, C. L.; Kabanov, A. V. *J of Controlled Release.* **2001**, *73*, 401–416.

(51) Luo, D.; Saltzman, W. M. *Nature Biotechnology.* **2000**, *18*, 33–37.

(52) Godbey, W.; Wu, K. K.; Mikos, A. G. *Biomaterials.* **2001**, *22*, 471–480.

(53) Putnam, D.; Gentry, C. A.; Pack, D. W.; Langer, R. *Proceedings of the National Academy of Sciences.* **2001**, *98*, 1200–1205.

(54) Regnström, K.; Ragnarsson, E. G. E.; Köping-Höggård, M.; Torstensson, E.; Nyblom, H.; Artursson, P. *Gene Therapy.* **2003**, *10*, 1575–1583.

(55) Kunath, K. *J of Controlled Release.* **2003**, *89*, 113–125.

(56) Kulikov, S. N.; Lisovskaya, S. A.; Zelenikhin, P. V.; Bezrodnykh, E. A.; Shakirova, D. R.; Blagodatskikh, I. V.; Tikhonov, V. E. *European J of Medicinal Chemistry.* **2014**, *74*, 169–178.

(57) Negishi, E.; Wang, G. *1,3-Dienes.* **2009**, 1.

(58) Maschmeyer, G. *International J of Antimicrobial Agents.* **2006**, *27*, 3–6.

(59) Cowen, L. E.; Anderson, J. B.; Kohn, L. M. *Annual Review of Microbiology.* **2002**, *56*, 139–165.

(60) Tan, W.; Li, Q.; Dong, F.; Chen, Q.; Guo, Z. *Molecules.* **2017**, *22*, 1438.

(61) Vorlfckova, M.; Sagi, J. *Nucleic Acids Research.* **1991**, *19*, 2343–2347.

(62) Nelson, H.; Finch, J.; Luisi, B.; Klug, A. **1992**.

(63) Alexeev, D. G.; Lipanov, A. A.; Skuratovskii, I. Y. *Nature.* **1987**, *325*, 821–823.

(64) Trantírek Lukáš; Štefl, R.; Vorlíčková Michaela; Koča, J.; Sklenářář Vladimír; Kypr, J. *J. of Molecular Biology.* **2000**, *297*, 907–922.

(65) Studdert, D. S.; Patroni, M.; Davis, R. C. *Biopolymers.* **1972**, *11*, 761–779.

(66) Shi, B.; Shen, Z.; Zhang, H.; Bi, J.; Dai, S. *Biomacromolecules.* **2011**, *13*, 146–153.

(67) Tan W., Zhang J., Luan F., Wei L., Chen Y., Dong F.; *International J of Science and Research (IJSR).* **2016**, *5*, 606–608.

(68) Wang, L.; Xu, X.; Guo, S.; Peng, Z.; Tang, T. *International J of Biological Macromolecules.* **2011**, *48*, 375–380

(69) Layek, B.; Haldar, M. K.; Sharma, G.; Lipp, L.; Mallik, S.; Singh, J. *Molecular Pharmaceutics.* **2014**, *11*, 982–994.

(70) Lin, W. J.; Hsu, W. Y. *Carbohydrate Polymers.* **2015**, *120*, 7–14.

(71) Casettari, L.; Vllasaliu, D.; Mantovani, G.; Howdle, S. M.; Stolnik, S.; Illum, L. *Biomacromolecules.* **2010**, *11*, 2854–2865.

(72) Ornelas-Megiatto, C.; Wich, P. R.; Fréchet, J. M. J. *J. of the American Chemical Society.* **2012**, *134*, 1902–1905.

(73) Ono, Y.; Shikata, T. *The J. of Physical Chemistry B.* **2006**, *110*, 9426–9433.

(74) Camplo, M.; Wathier, M.; Chow, J.; Grinstaff, M. W. *Chem. Commun.* **2011**, *47*, 2128–2130.

APPENDICES

Appendix A. NMR

The ^{1}H NMR Spectra was collected using a Varian 400 MHz NMR spectrometer and plotted using Varian VNMRJ software. All the spectra presented in this appendix displays a ppm range of -2-14 to display the isolation of each compound free of starting materials or impurities. The red lines indicate the range of which integration occurred and their values presented in red under the spectra. Thee ppm values of all signals are indicated in blue are located above the spectra.

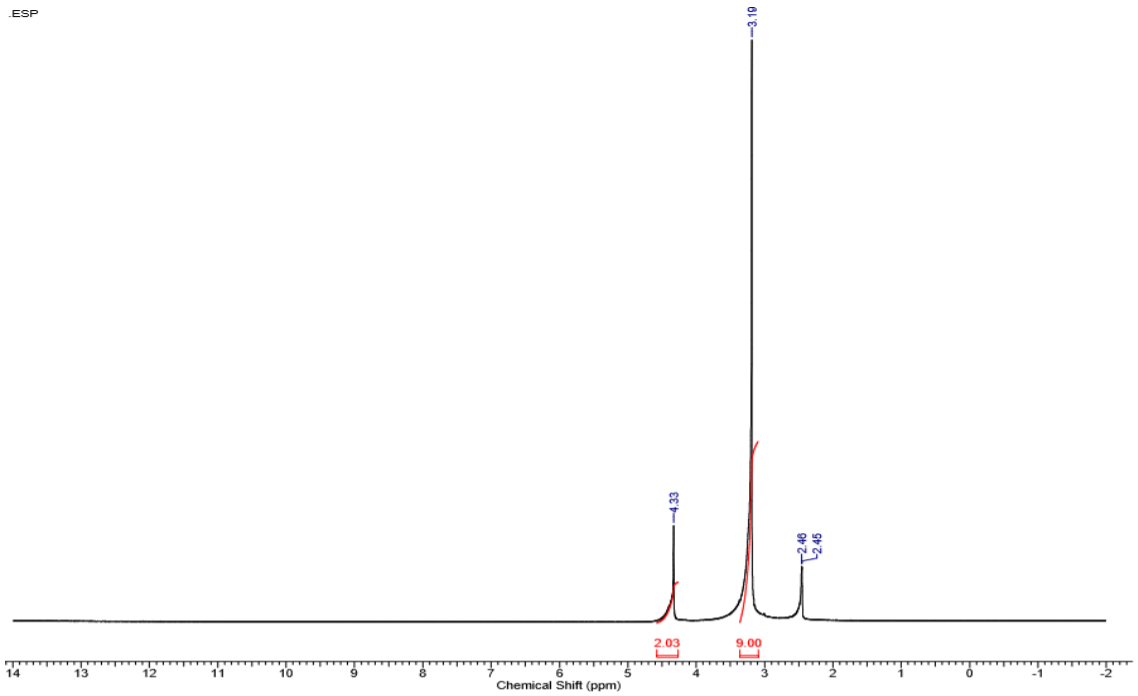

Appendix A-1. ^{1}H NMR spectrum of (1-Carboxymethyl) trimethylammonium chloride. 4.33 (2H, -C**H**$_2$N$^+$(CH$_3$)$_3$), 3.19 (9H, -N$^+$(C**H**$_3$)$_3$), DMSO$_{d6}$

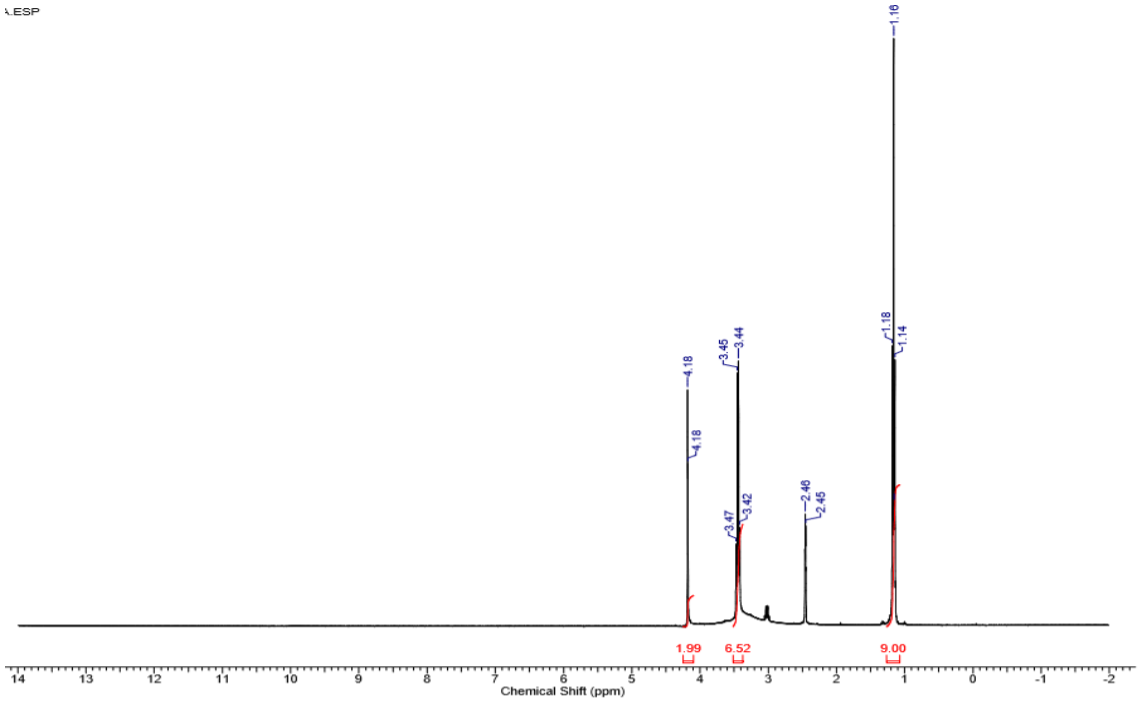

Appendix A-2. ^{1}H NMR spectrum of (1-Carboxymethyl) triethylammonium chloride. $DMSO_{d6}$: 4.18 (2H, -C**H**$_2$N$^+$(CH$_2$CH$_3$)$_3$), 3.44 (6H, -N$^+$(C**H**$_2$CH$_3$)$_3$), 1.16 (9H, -N$^+$(CH$_2$C**H**$_3$)$_3$.

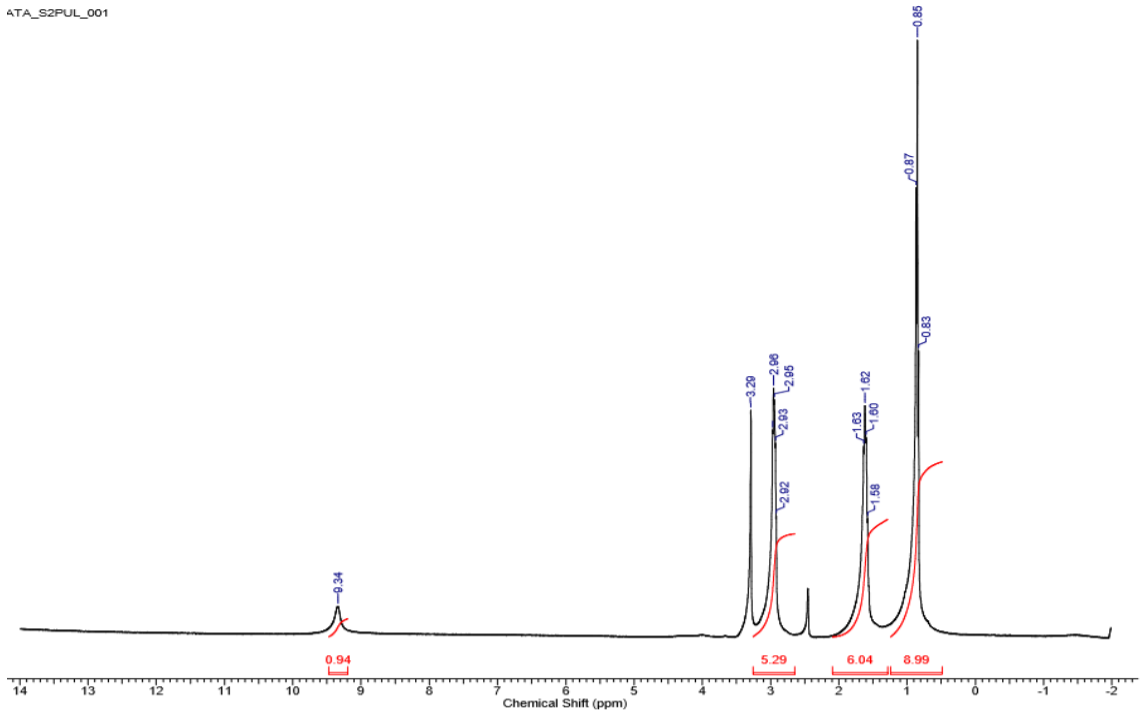

Appendix A-3. ^{1}H NMR spectrum of (1-Carboxymethyl) tripropylammonium chloride. $DMSO_{d6}$: 3.29 (2H, HO$_2$CC**H**$_2$-), 2.96 (6H, -N$^+$(C**H**$_2$CH$_2$CH$_3$)$_3$), 1.62 (6H, -N$^+$(CH$_2$C**H**$_2$CH$_3$)$_3$), 0.85 (9H, -N$^+$(CH$_2$CH$_2$C**H**$_3$)$_3$

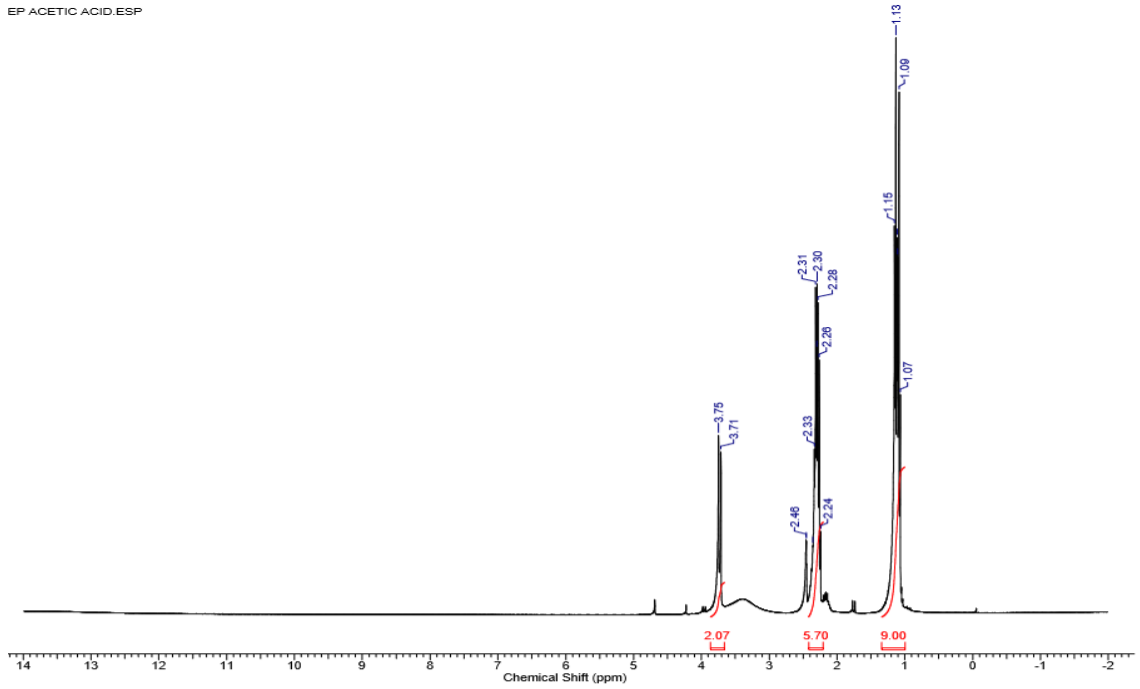

Appendix A-4. ^{1}H NMR spectrum of (1-Carboxymethyl) triethylphosphonium chloride. 3.75 (2H, -$\mathbf{H}_2$P$^+$($CH_2CH3)_3$), 2.30 (6H, HO_2CCH_2 P$^+$($C\mathbf{H}_2CH3)_3$), 1.10 (9H, -P$^+$($CH_2C\mathbf{H}3)_3$

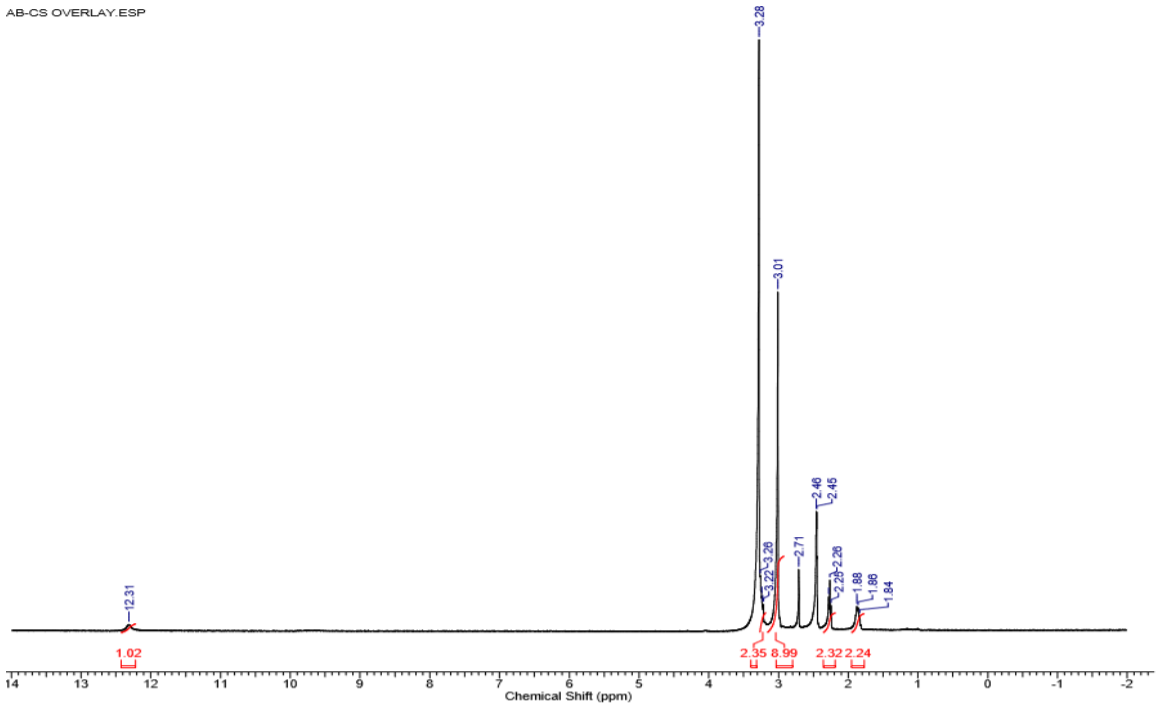

Appendix A-5. ^{1}H NMR spectrum of (3-Carboxypropyl) trimethylammonium chloride. 12.31 (1H, $\mathbf{H}O_2CCH_2$-), 3.01 (9H, -$CH_2CH_2CH_2N(C\mathbf{H}_3)_3$), 2.71 (2H, -$C\mathbf{H}_2CH_2CH_2N^+(CH_3)_3$), 2.26 (2H, -$CH_2CH_2C\mathbf{H}_2N^+(CH_3)_3$), 1.88 (2H, -$CH_2C\mathbf{H}_2CH_2N^+(CH_3)_3$

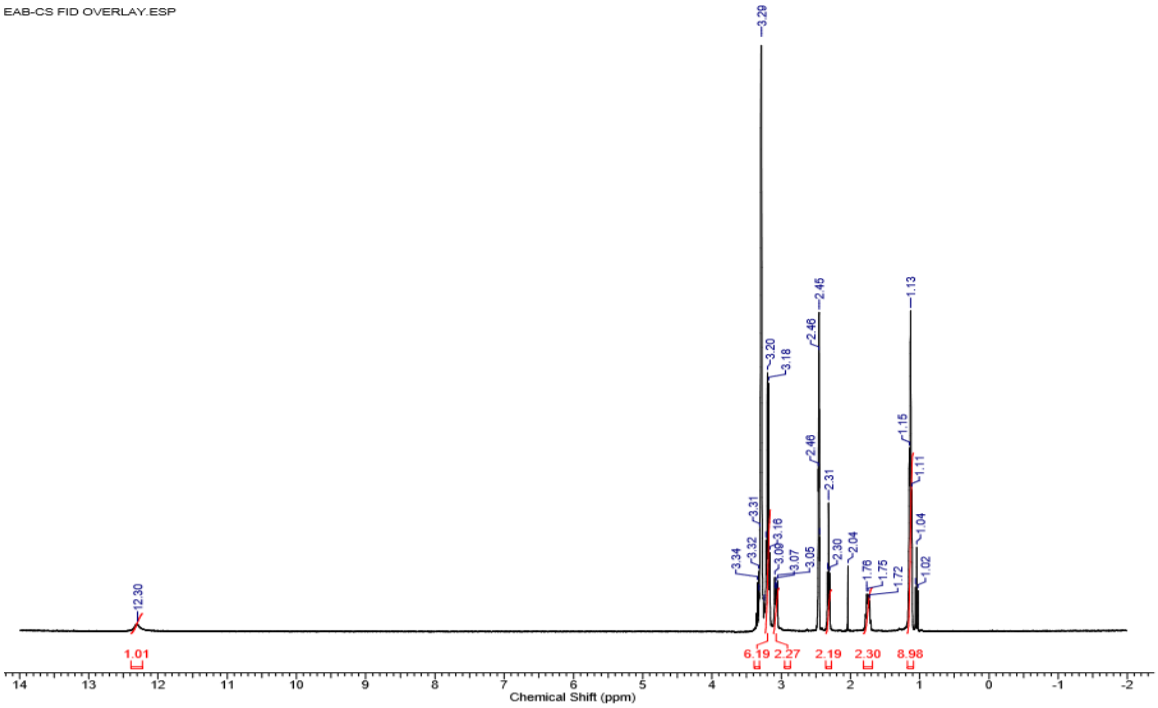

Appendix A-6. ^{1}H NMR spectrum of (3-Carboxypropyl) triethylammonium chloride. 12.31 (1H, **H**O_2CCH_2-), 3.20 (9H, -N^+(C**H**$_2CH_3)_3$), 3.07 (2H, -C**H**$_2N^+$($CH_2CH_3)_3$), 2.31 (2H, -C**H**$_2CH_2CH_2N^+$-), 1.75 (2H, -CH_2C**H**$_2CH_2N^+$-), 1.13 (2H, -N^+(CH_2C**H**$_2)_3$

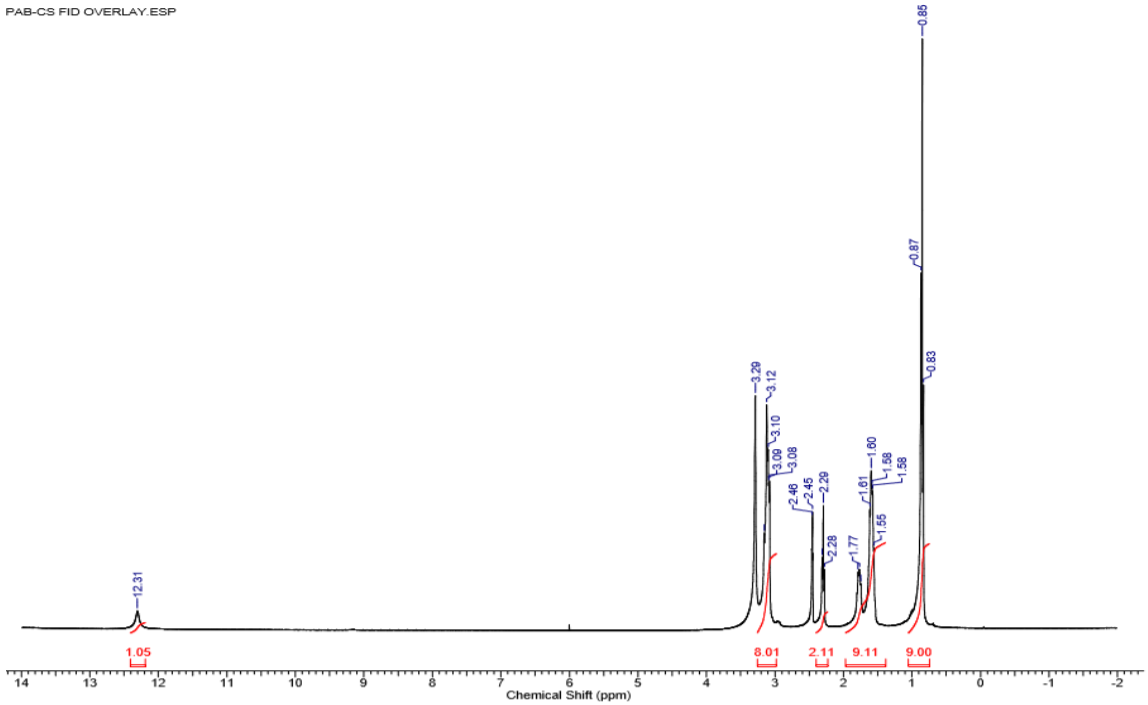

Appendix A-7. ^{1}H NMR spectrum of (3-Carboxypropyl) tripropylammonium chloride. 12.31 (1H, **H**O_2CCH_2-), 3.20 (9H, -N^+(C**H**$_2CH_2CH_3)_3$), 3.07 (2H, -C**H**$_2N^+$($CH_2CH_2CH_3)_3$), 2.31 (2H, -C**H**$_2CH_2CH_2N^+$-), 1.75 (2H, -CH_2C**H**$_2CH_2N^+$-), 1.13 (2H, -N^+(CH_2CH_2C**H**$_3$)

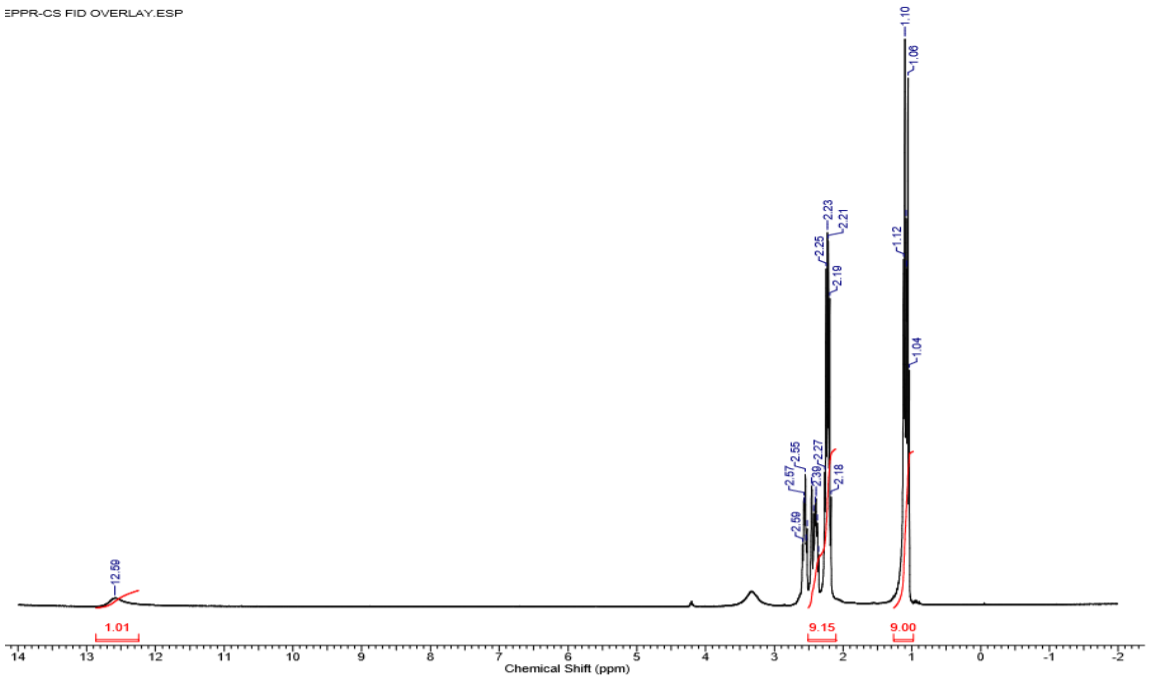

Appendix A-8. ^{1}H NMR spectrum of (2-Carboxyethyl) triethylphosphonium chloride. 12.58 (1H, **H**O_2CCH_2-), 2.55 (2H, -C**H**$_2CH_2P^+$-), 2.39 (2H, -C**H**$_2$ $P^+(CH_2CH_3)_3$), 2.23 (6H, -$P^+(CH_2CH_3)_3$), 1.08 (9H, -$P^+(CH_2CH_3)_3$

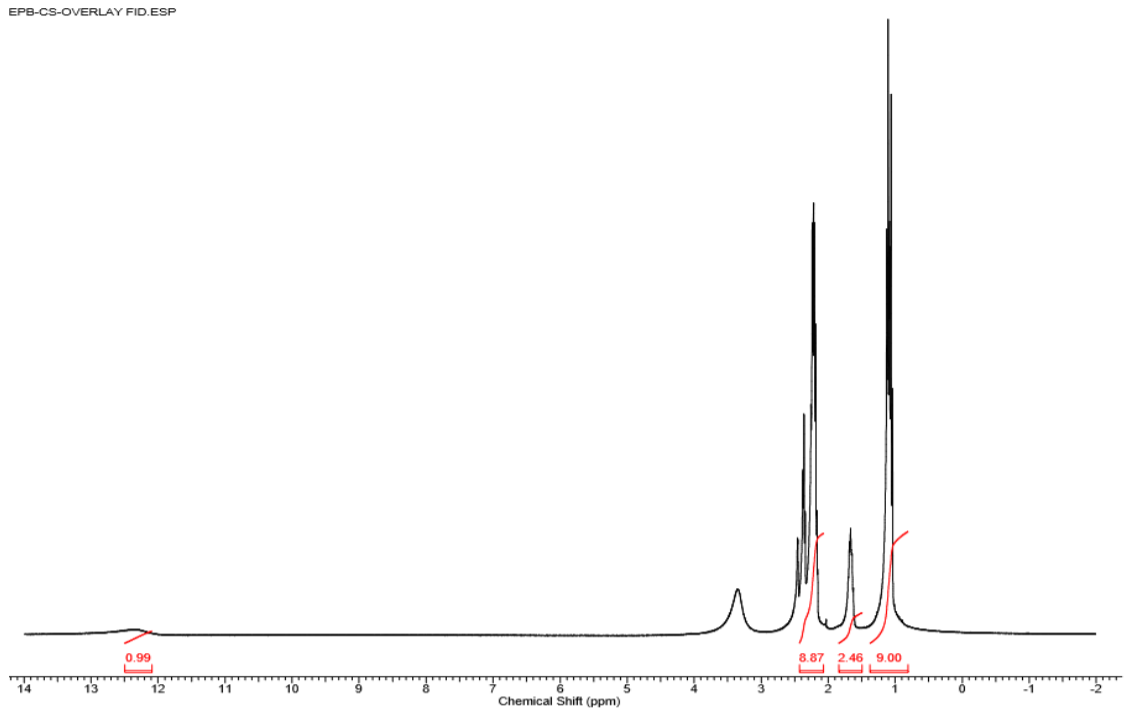

Appendix A-9. ^{1}H NMR spectrum of (3-Carboxypropyl) triethylphosphonium chloride. 12.16 (1H, **H**$O_2CCH_2CH_2$-), 2.36 (2H, $HO_2CCH_2CH_2CH_2$-), 2.26 (2H, -C**H**$_2$ $P^+(CH_2CH_3)_3$), 2.22 (6H, -$P^+(CH_2CH_3)_3$), 1.67 (2H, -C**H**$_2CH_2P^+(CH_2CH_3)_3$), 1.08 (9H, -$P^+(CH_2CH_3)_3$

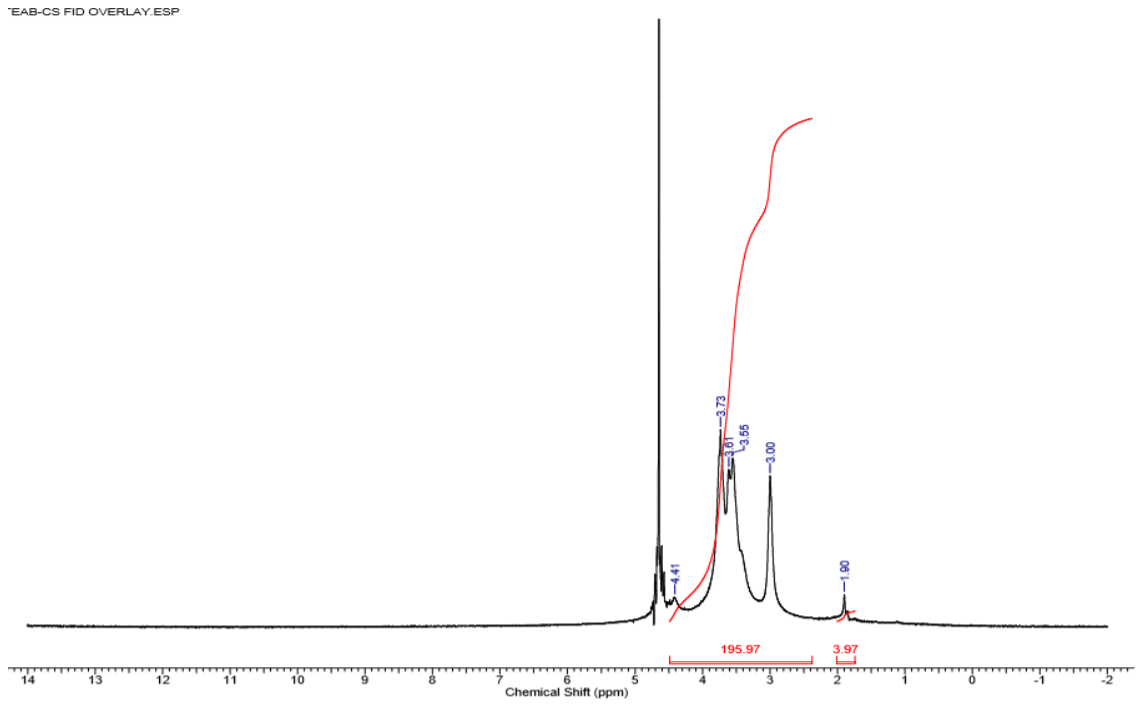

Appendix A-10. ^{1}H NMR spectrum of 95% Chitosan. 4.45 (1H, **anomeric H**), 3.80-3.30 (6H, C_2-C_6 **H**'s).

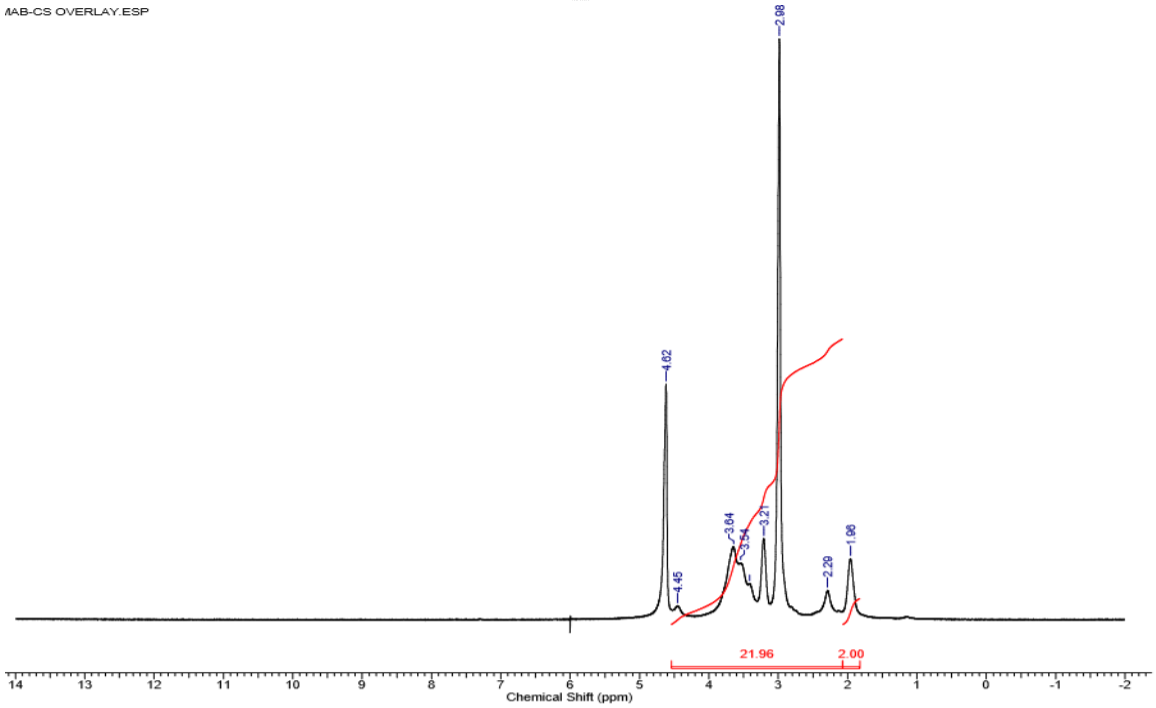

Appendix A-11. ^{1}H NMR spectrum of 2-(N-4-trimethylammonium chloride) butanamide chitosan. 4.45 (1H, **anomeric H**), 3.80-3.30 (6H, C_2-C_6 **H**'s), 3.21 (2H, -$CH_2C\mathbf{H}_2N^+(CH_3)$), 2.98 (9H, -$CH_2CH_2N^+(C\mathbf{H}_3)$), 2.29 (2H, -$OC\mathbf{H}_2CH_2CH_2N^+(CH_3)$), 1.96 (2H, -$C\mathbf{H}_2CH_2N^+(CH_3)$.

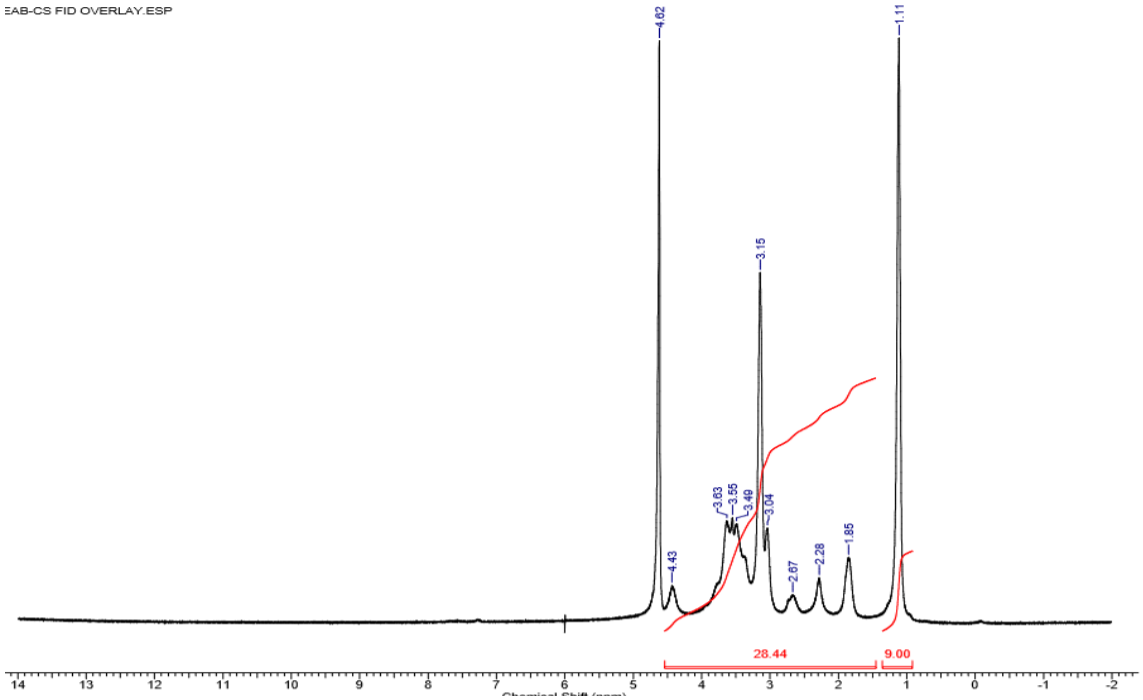

Appendix A-12. ^{1}H NMR spectrum of 2-(N-4-triethylammonium chloride) butanamide chitosan. 4.43 (1H, **anomeric H**), 4.0-3.25 (6H, C_2-C_6 **H**'s), 3.15 (2H, -N^+(**CH_2**$CH3)_3$), 3.04 (9H, -CH_2C**H**$_2N^+(CH_2CH3)_3$), 2.66 (1-2H, -2H-N**H**$COCH_2$-), 2.28 (2H, -OC**H**$_2CH_2CH_2N^+$-, 1.84 (2H, -C**H**$_2CH_2N^+(CH_2CH3)_3$, 1.11 (2H, -$CH_2CH_2N^+(CH_2$**CH3**$)_3$

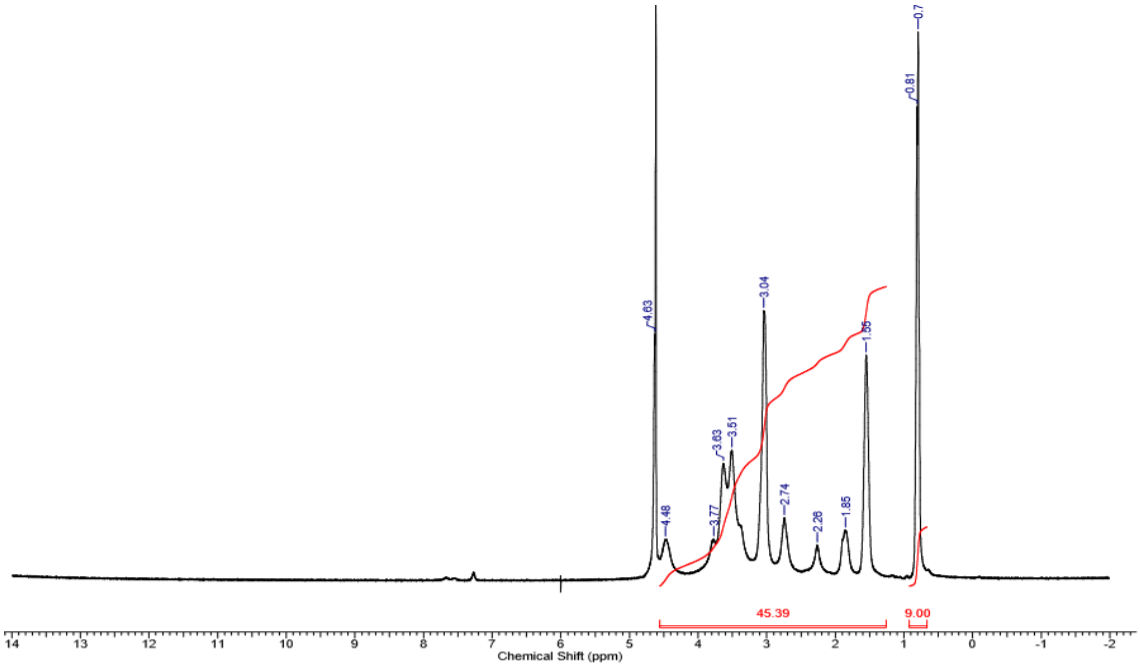

Appendix A-13. ^{1}H NMR spectrum of 2-(N-4-tripropylammonium chloride) butanamide chitosan. 4.48 (1H, C_1-Anomaric H), 4.0-3.25 (6H, C_2-C_6 **H**'s), 3.04 (6H, -N^+(C**H**$_2CH_2CH_3)_3$), 2.74 (2H, -C**H**$_2N^+(CH_2CH_2CH_3)_3$) , 2.26 (2H, -C**H**$_2CH_2CH_2N^+$-), 1.85 (2H, -C**H**$_2CH_2N^+$-), 1.55 (6H, -$N^+(CH_2C$**H**$_2CH_3)_3$), 0.79 (9H, -$N^+(CH_2CH_2C$**H**$_3)_3$

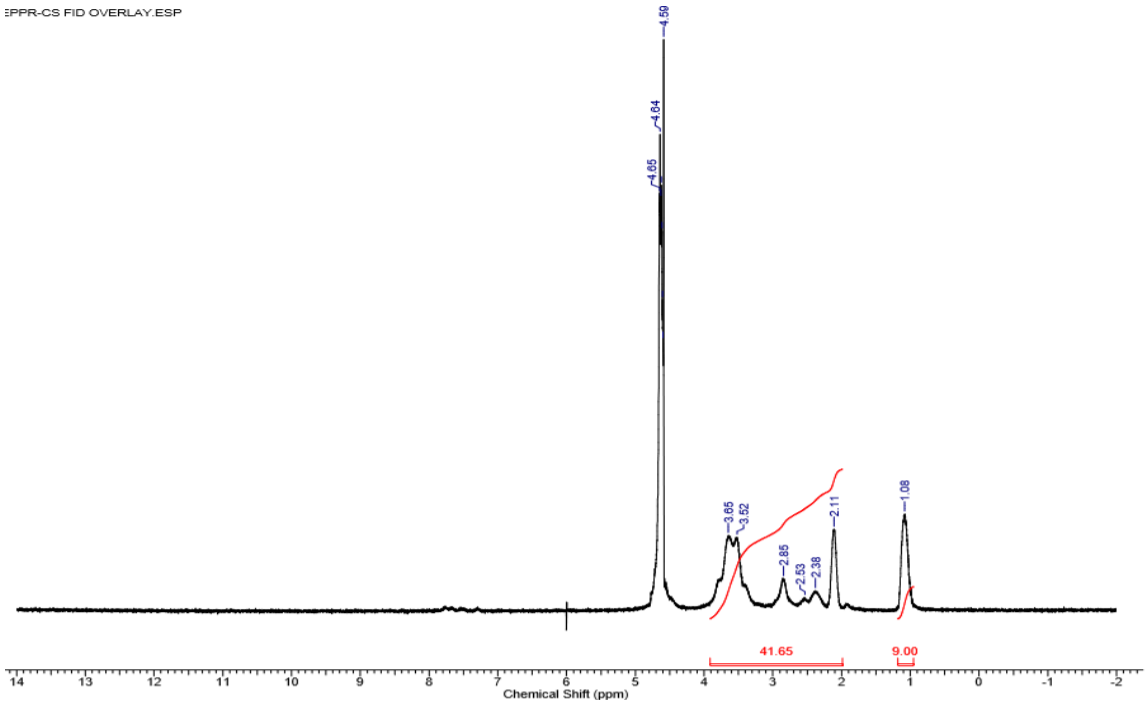

Appendix A-14. ^{1}H NMR spectrum of 2-(N-3-triethylphosphonium chloride) propionamide chitosan. 4.48 (1H, **anomeric H**), 4.0-2.66 (6H, C_2-C_6 **H**'s,2H-N**H**), 2.55 (2H, -C**H**$_2$CH$_2$N$^+$(CH$_2$CH$_3$)$_3$), 2.38 (2H, -C**H**$_2$N$^+$(CH$_2$CH$_3$)$_3$) , 2.11 (6H, -CH$_2$N$^+$(C**H**$_2$CH$_3$)$_3$), 1.09 (9H, -CH$_2$ N$^+$(CH$_2$C**H**$_3$)$_3$

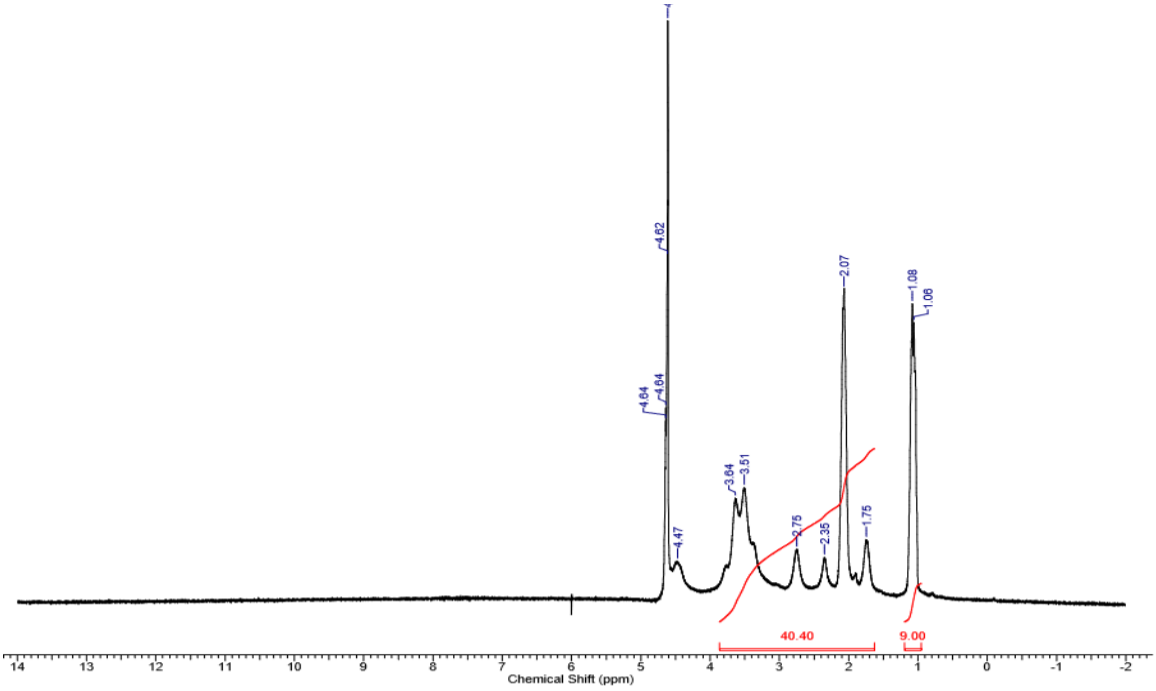

Appendix A-15. ^{1}H NMR spectrum of 2-(N-4-triethylphosphonium chloride) butanamide chitosan. 4.82 (1H, **anomeric H**), 4.0-2.66 (6H, C_2-C_6 **H**'s ,2H-N**H**), 2.35 (2H, -OC**H**$_2$CH$_2$CH$_2$N$^+$ -), 2.07 (6H, -N$^+$(C**H**$_2$CH$_3$)$_3$) , 2.07 (2H, -C**H**$_2$N$^+$(CH$_2$CH$_3$)$_3$), 1.75 (2H, -C**H**$_2$CH$_2$N$^+$(CH$_2$CH$_3$)$_3$), 1.08 (9H, - N$^+$(CH$_2$C**H**$_3$)$_3$

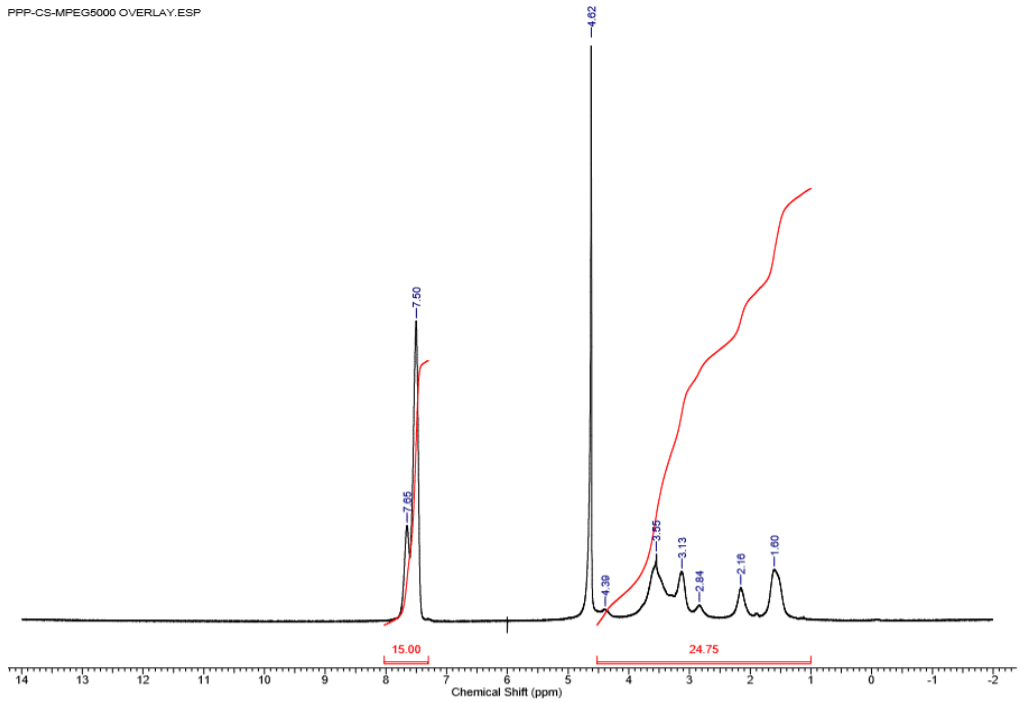

Appendix A-16. ^{1}H NMR spectrum of 2-(N-5-triphenylphosphonium chloride) pentanamide chitosan. 7.65-7.50 (15H, **$P^{+}Ph_3$**-CH_2CH_2-), 4.39 (1H, **anomeric H**), 4.0-2.66 (6H, C_2-C_6 **H**'s ,2H-N**H**), 3.13 (2H, $P^{+}Ph_3$-C**H_2**CH_2-), 2.16 (2H, $P^{+}Ph_3$-$CH_2CH_2CH_2C$**H_2**-), 1.60 (4H, $P^{+}Ph_3$-CH_2C**H_2C****H_2**-)

Appendix B. IR

The IR Spectra was collected using a Bruker Vertex 70 FT-IR spectrometer and plotted using Bruker OPUS 7.5 software. All the spectra presented in this appendix displays a wavenumber (cm^{-1}) range of 400-4000 to display the amide I, amide II, C-O, N-H, C-H, C-N^+, and C-P^+ stretch peaks found on coupled chitosan derivatives. The wavenumber (cm^{-1}) values of all signals are indicated in black are located below the spectra.

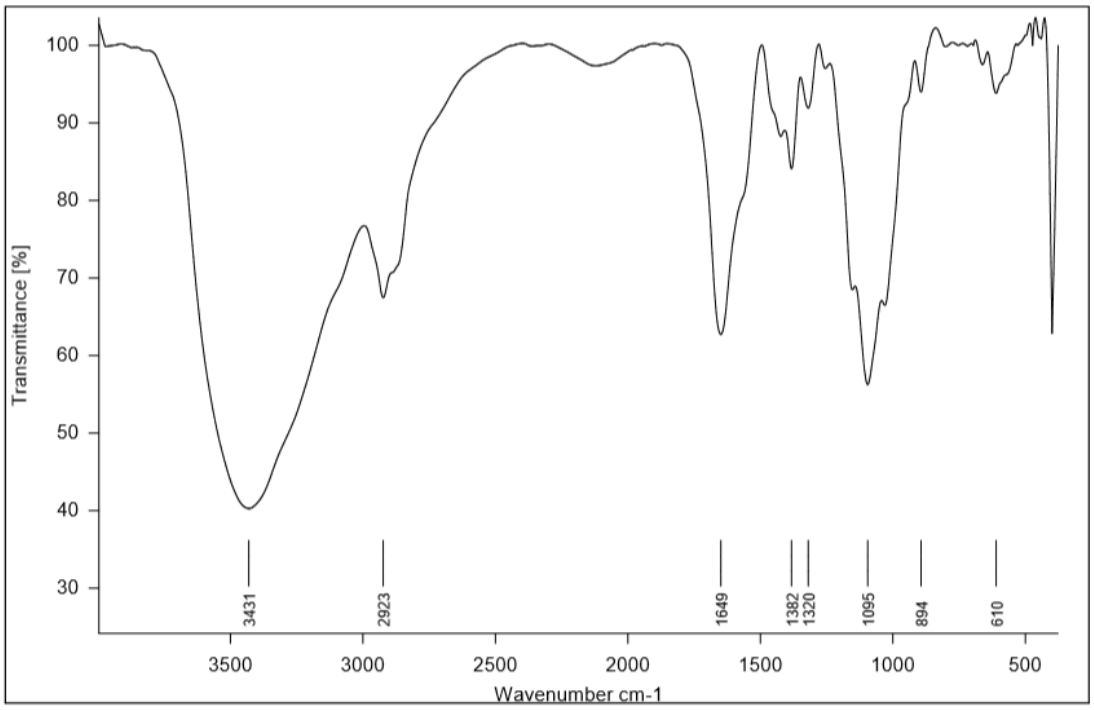

Appendix B-1. IR spectrum of 95% DA Chitosan

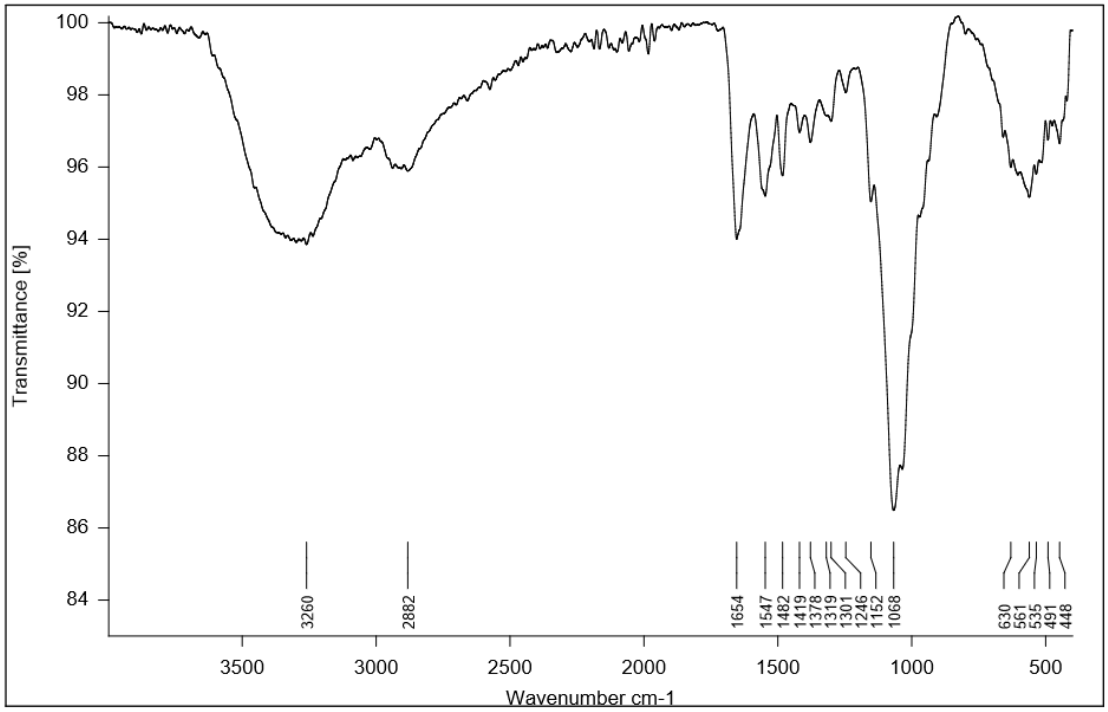

Appendix B-2. IR spectrum of 2-(N-4-trimethylammonium chloride) butanamide chitosan.

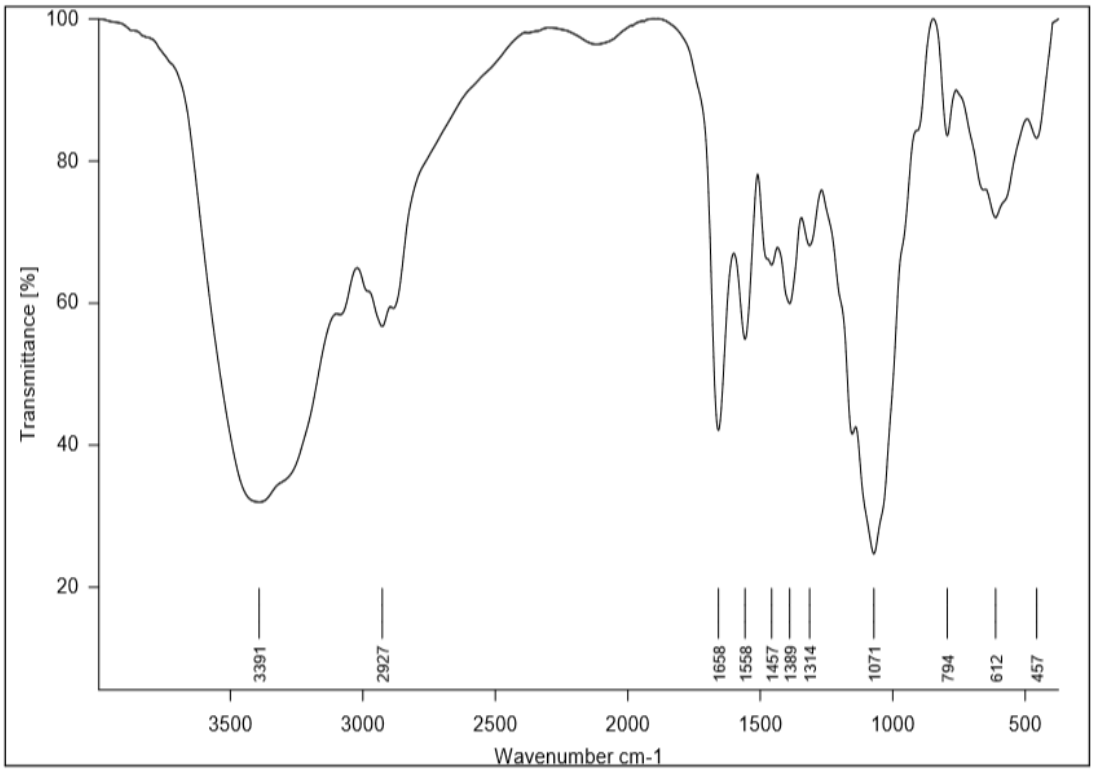

Appendix B-3. IR spectrum of 2-(N-4-triethylammonium chloride) butanamide chitosan.

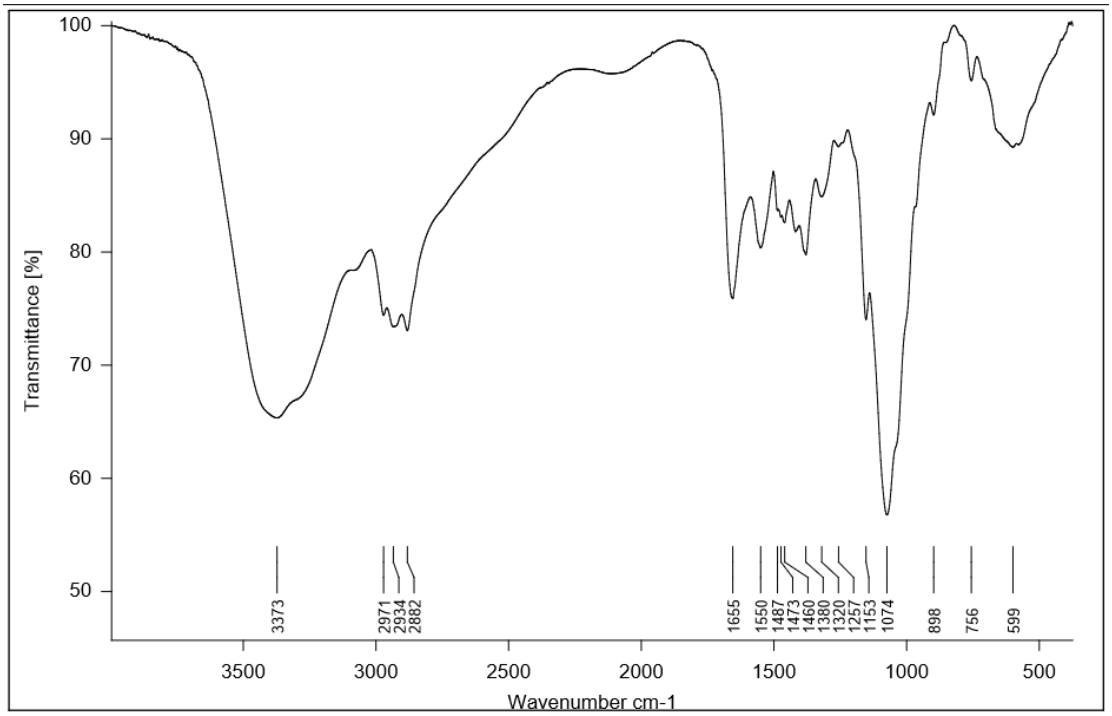

Appendix B-4. IR spectrum of 2-(N-4-tripropylammonium chloride) butanamide chitosan.

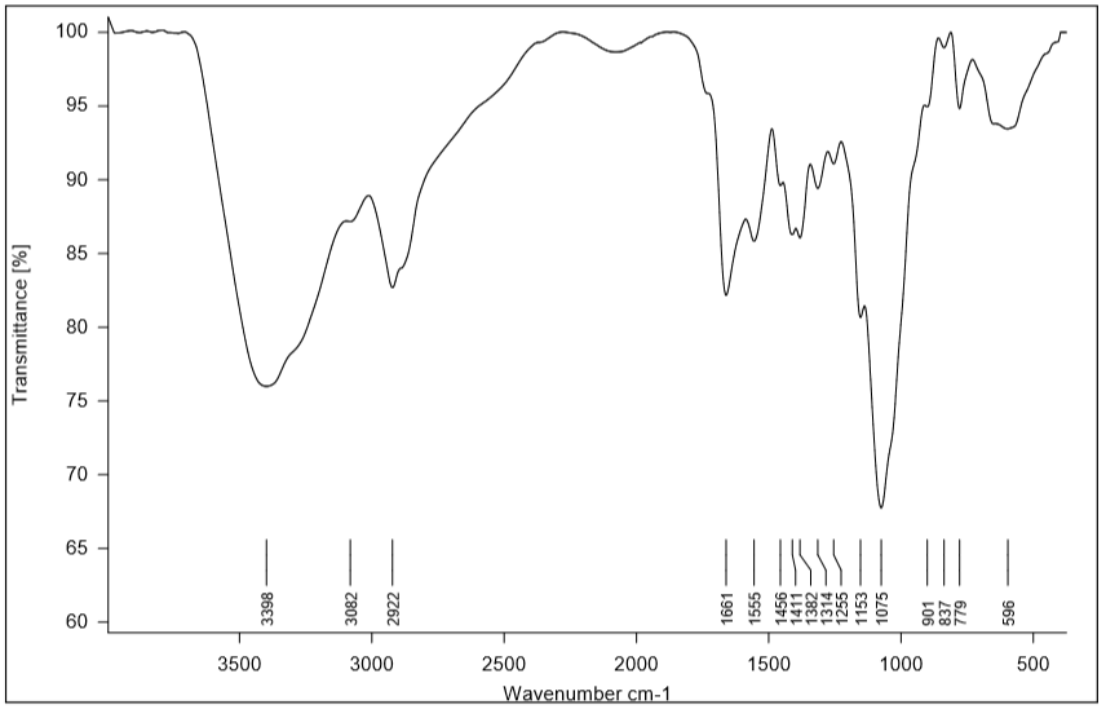

Appendix B-5. IR spectrum of 2-(N-3-triethylphosphonium chloride) propionamide chitosan

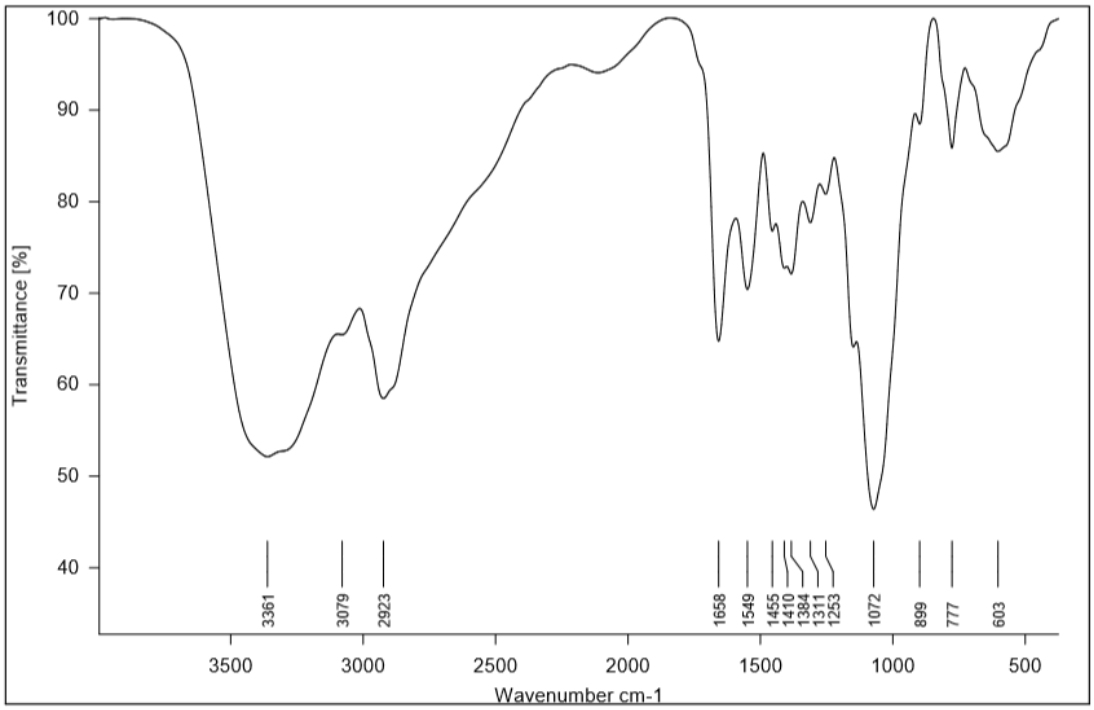

Appendix B-6. IR spectrum of 2-(N-4-triethylphosphonium chloride) butanamide chitosan

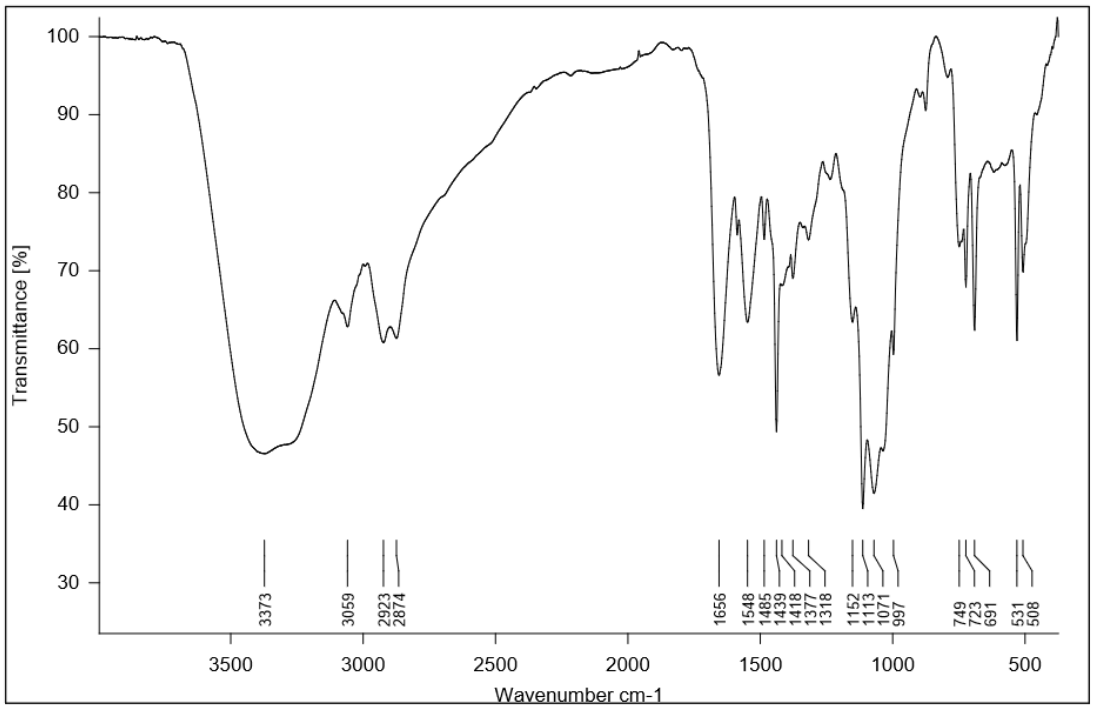

Appendix B-7. IR spectrum of 2-(N-5-triphenylphosphonium chloride) pentanamide chitosan

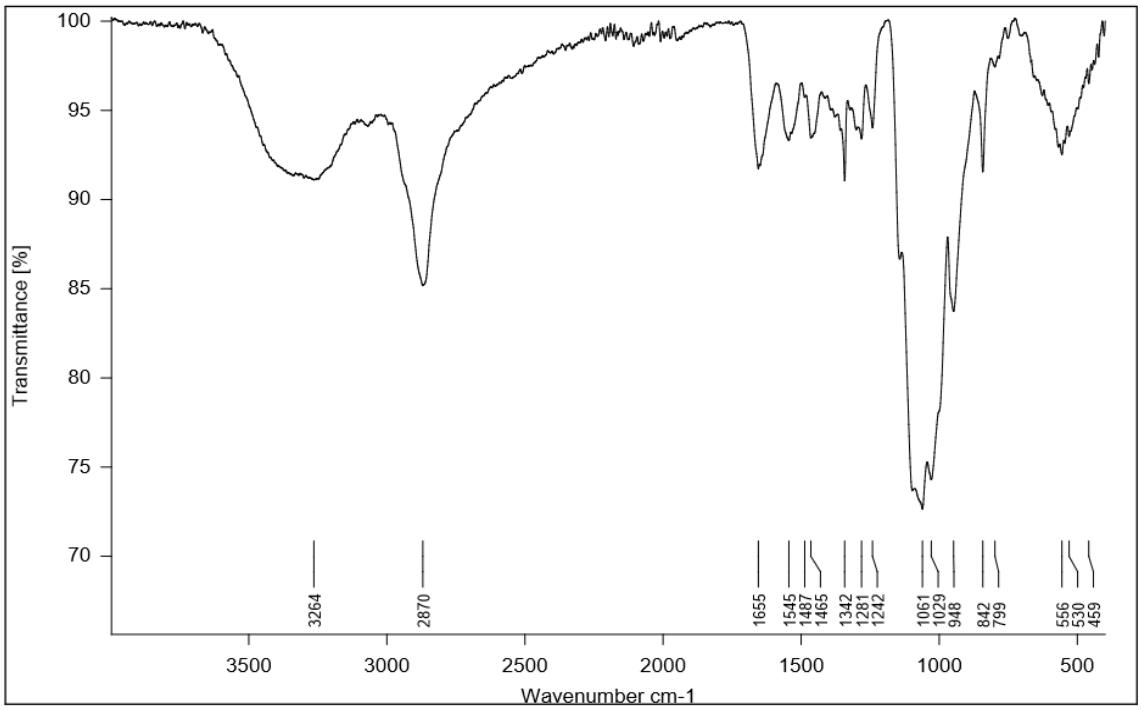

Appendix B-8. IR spectrum of 2-(N-4-triethylphosphonium chloride) butanamide mPEG-*g*-chitosan

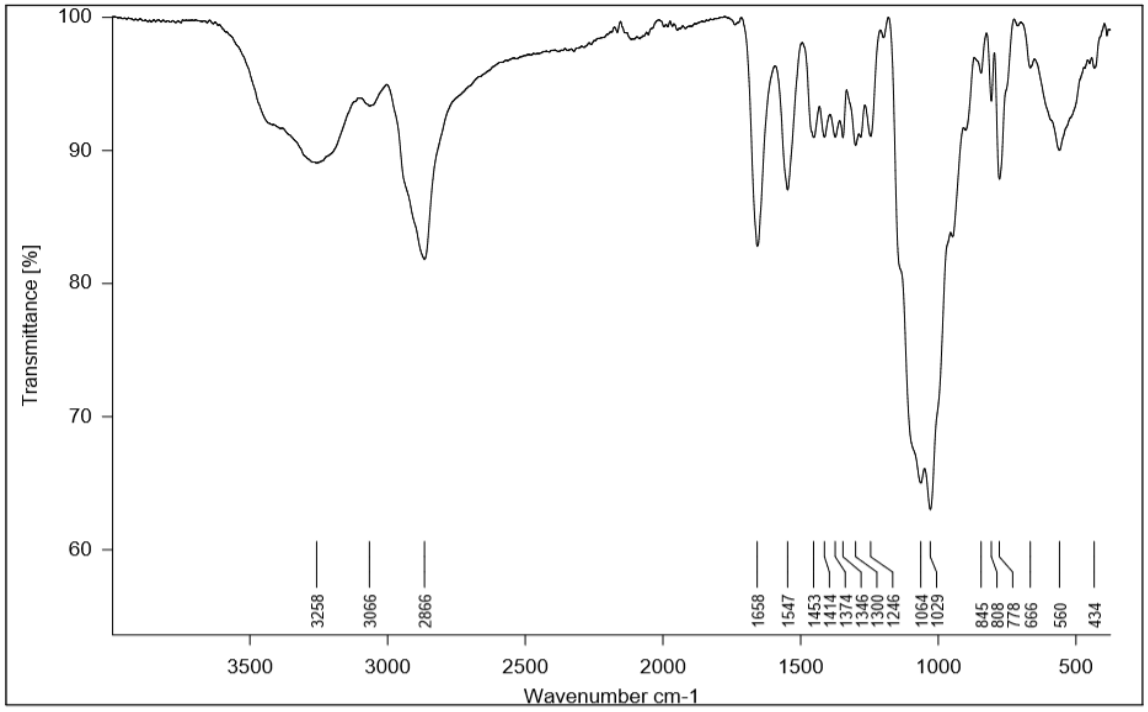

Appendix B-9. IR spectrum of 2-(N-4-triethylphosphonium chloride) butanamide chitosan

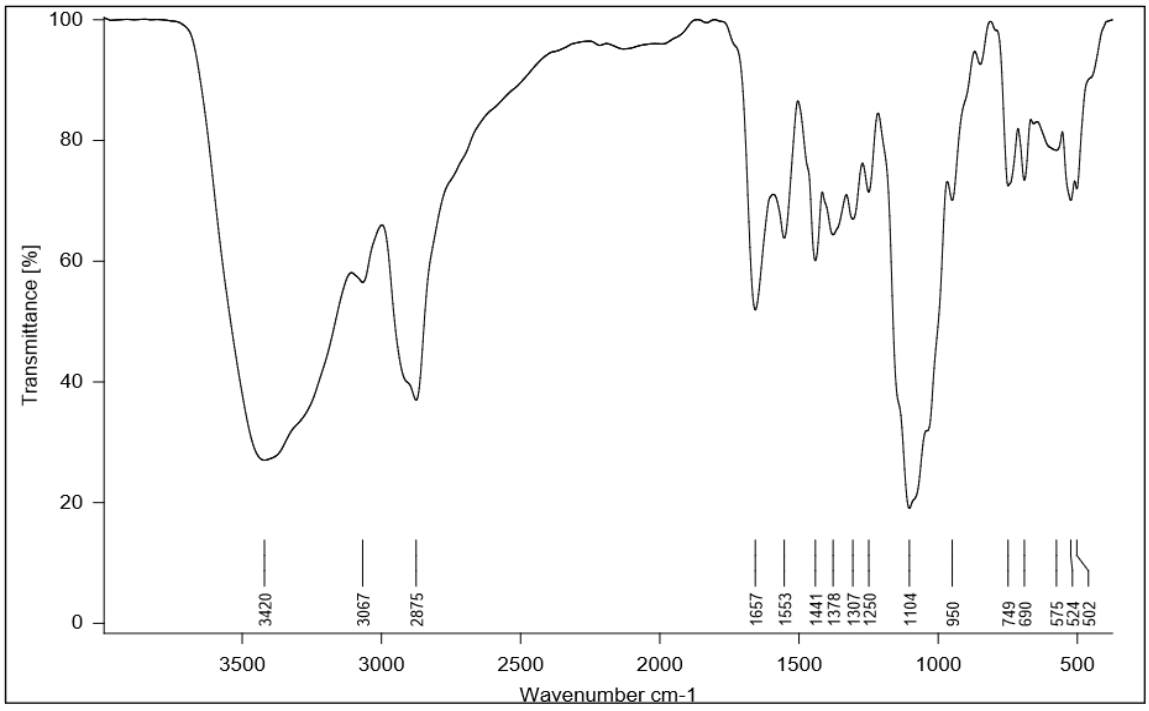

Appendix B-10. IR spectrum of 2-(N-5-triphenylphosphonium chloride) pentanamide chitosan

Appendix C. TGA and DTG

TGA (green) and DTG (blue) was conducted to examine the change in stability of chitosan's polymer chain after coupling of carboxy ligands. The TGA and DTG Spectra were collected using a TA Instrument Q600 Thermogravimetric Analyzer and plotted using TA Universal Analyzer software. All the spectra presented in this appendix displays weight % (green), and 1st Derivative weight % (blue) of all chitosan derivatives. The beginning and end of each degradation phase are marked along the TGA (green) spectra.

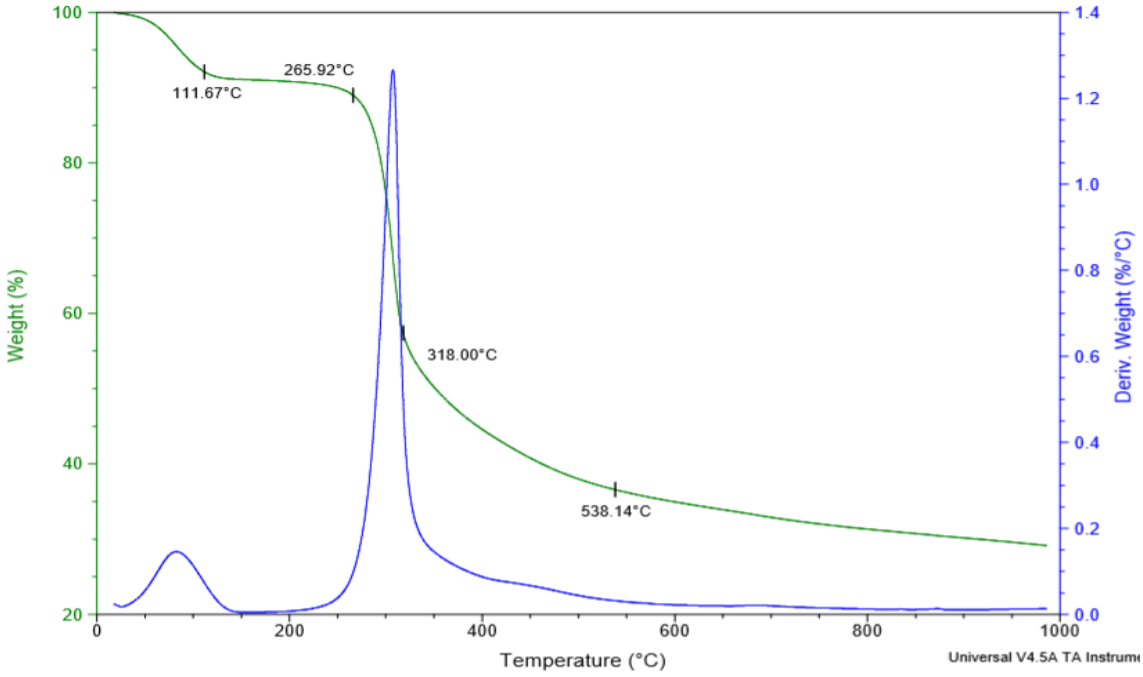

Appendix C-1. TGA and DTG analysis of 95% DA Chitosan

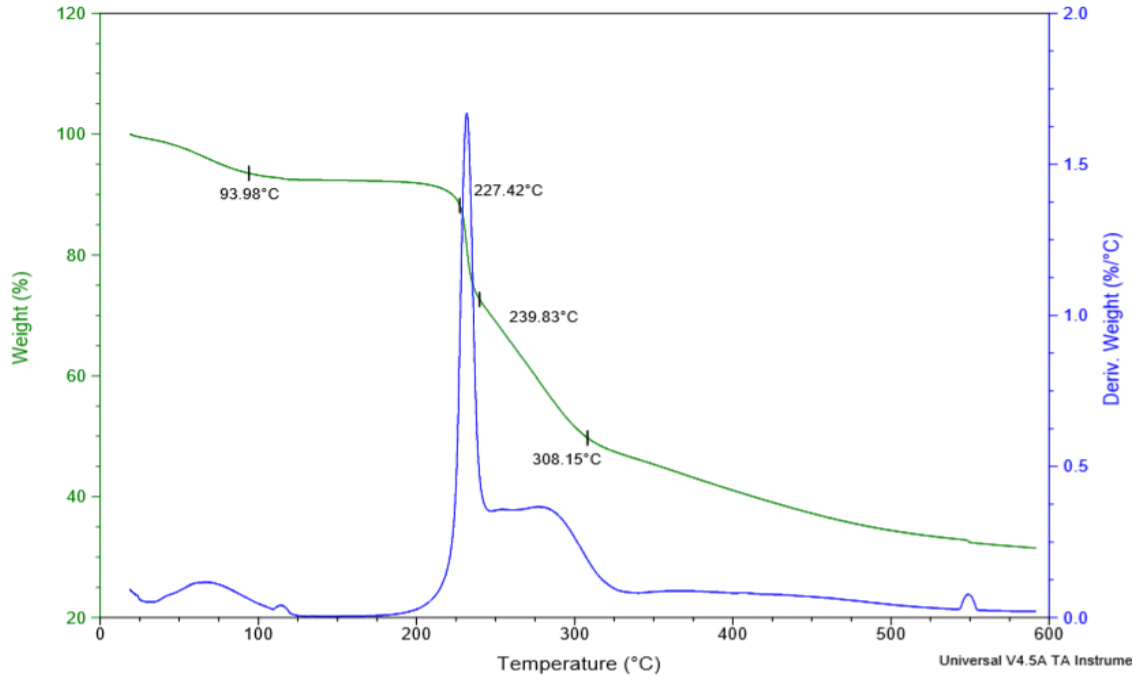

Appendix C-2. TGA-DTG 2-(N-4-trimethylammonium chloride) butanamide chitosan

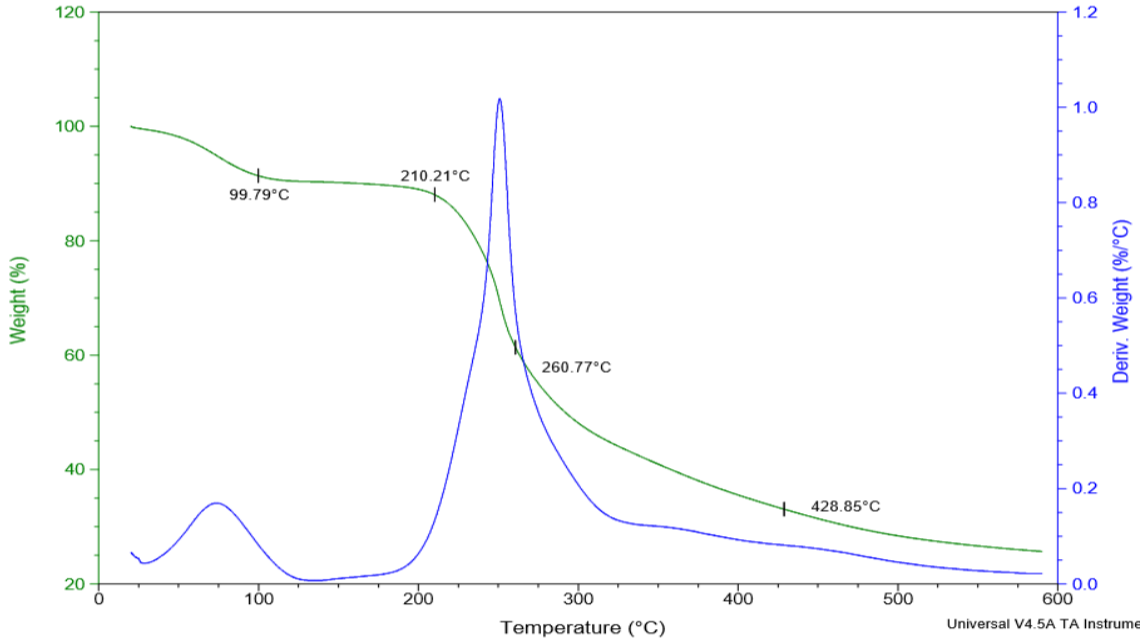

Appendix C-3. TGA-DTG analysis of 2-(N-4-triethylammonium chloride) butanamide chitosan

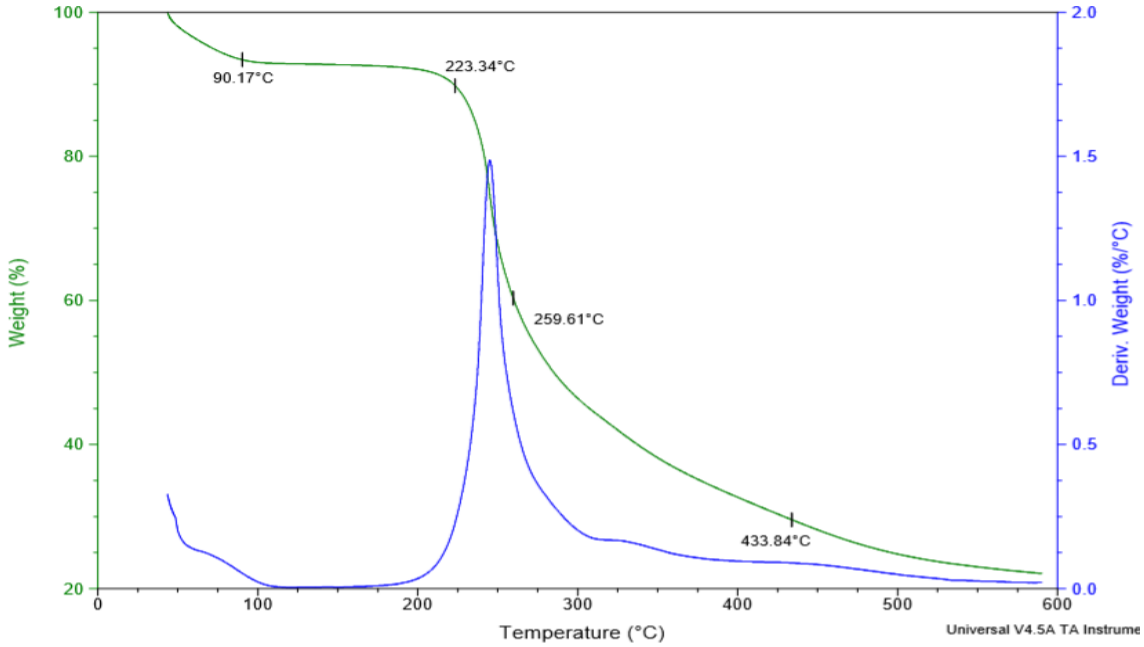

Appendix C-4. TGA-DTG analysis of 2-(N-4-tripropylammonium chloride) butanamide chitosan

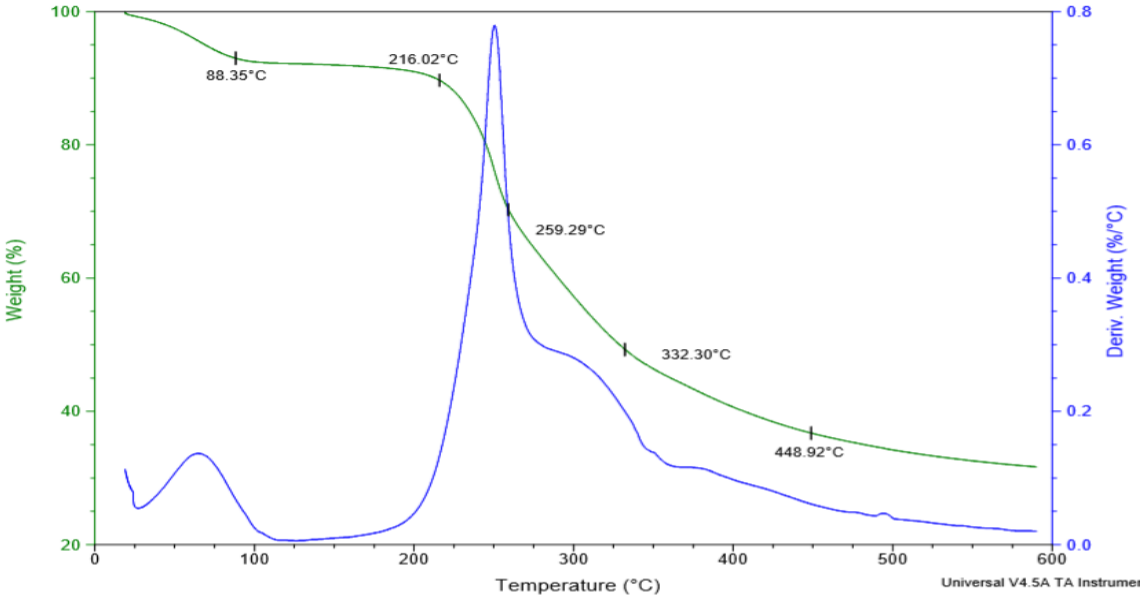

Appendix C-5. TGA-DTG analysis of 2-(N-3-triethylphosphonium chloride) propionamide chitosan

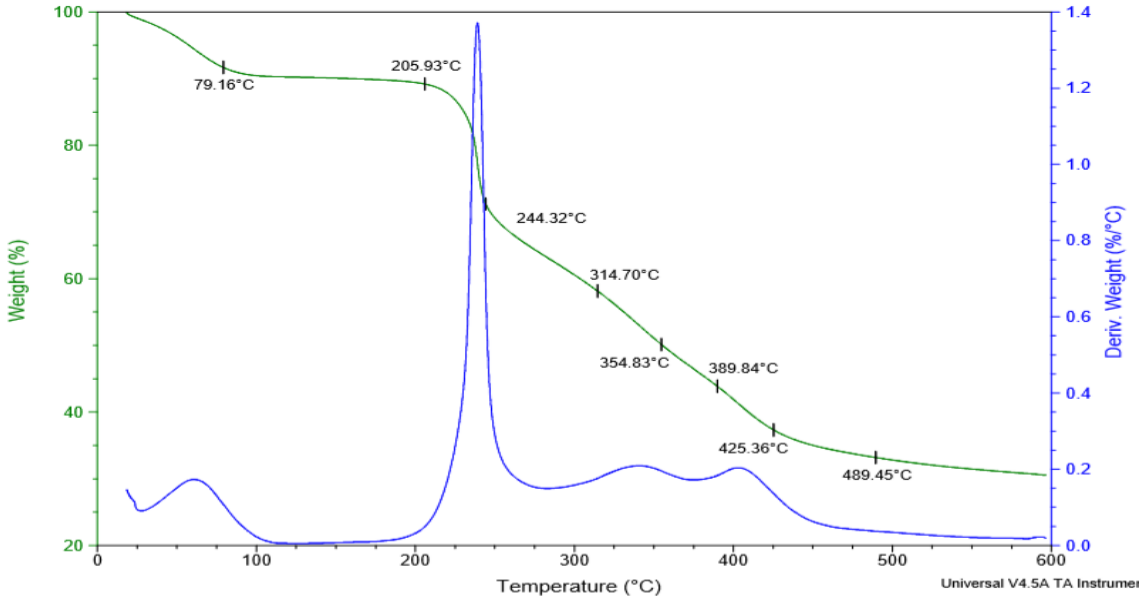

Appendix C-6. TGA-DTG analysis of 2-(N-4-triethylphosphonium chloride) butanamide chitosan

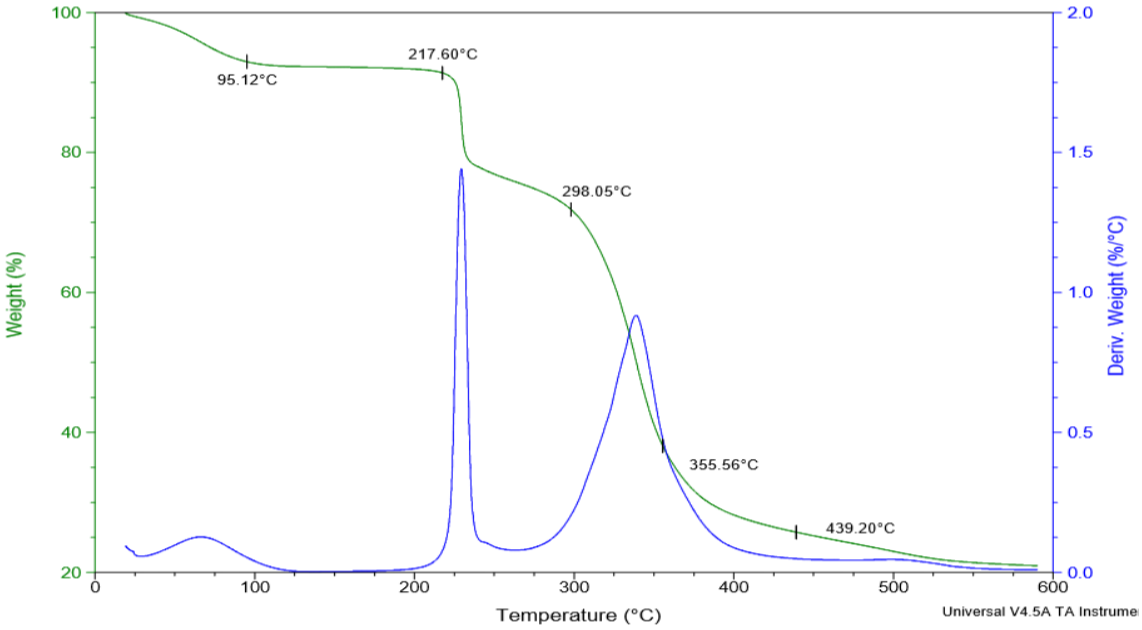

Appendix C-7. TGA-DTG analysis of 2-(N-5-triphenylphosphonium chloride) pentanamide chitosan

Appendix D. Agarose Gel Electrophoresis

Agarose gel electrophoresis was conducted to examine complexation affinity of all cationic chitosan derivatives. The images were visualized using ethidium bromide, short-wave UV light, and Microsoft Windows image capturing software. All chitosan derivatives examined with Drew Dickerson Dodecamer DNA are shown in this appendix using 2% agarose gel. Wells are in charge ratios of 1) 16x, 2) 8x, 3) 4x, 4) 2x, 5) 1x, 6) 0.5x, 7) 0.25x, 8) Control

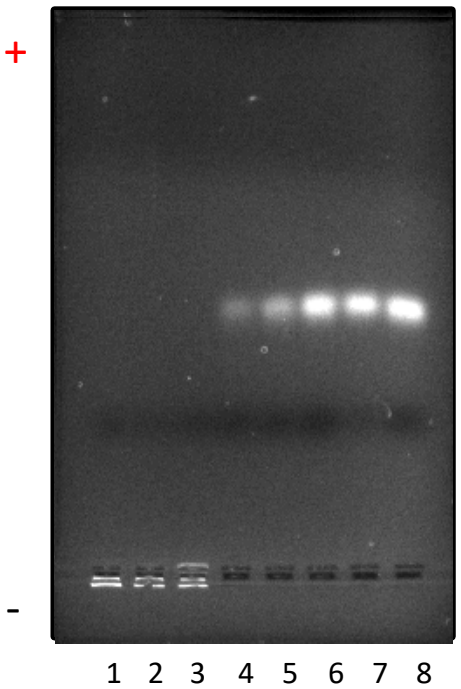

Appendix D-1. Agarose gel electrophoresis result of TMAB-CS. Wells are in charge ratios of 1) 16, 2) 8, 3) 4, 4) 2, 5) 1, 6) 0.5, 7) 0.25, 8) Control

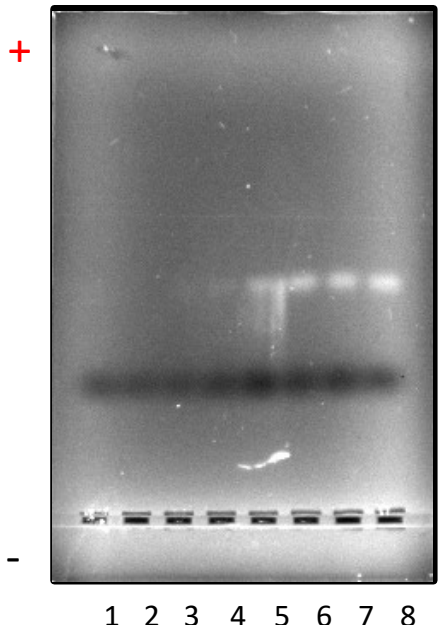

Appendix D-2. Agarose gel electrophoresis result of TEAB-CS. Wells are in charge ratios of 1) 16, 2) 8, 3) 4, 4) 2, 5) 1, 6) 0.5, 7) 0.25, 8) Control

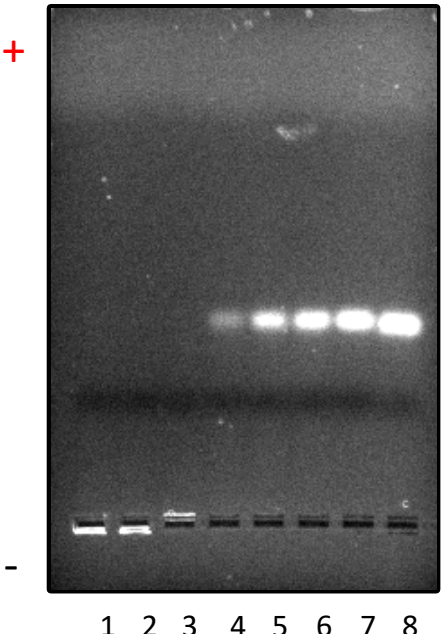

Appendix D-3. Agarose gel electrophoresis result of TPAB-CS. Wells are in charge ratios of 1) 16, 2) 8, 3) 4, 4) 2, 5) 1, 6) 0.5, 7) 0.25, 8) Control

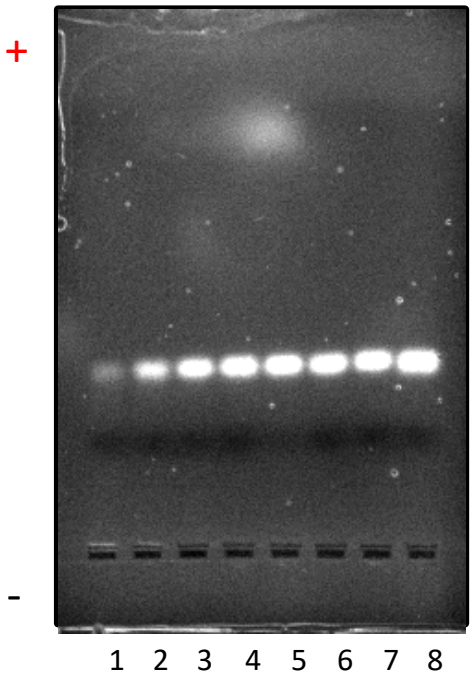

Appendix D-4 Agarose Gel of Agarose gel electrophoresis result of TEPPr-CS. Wells are in charge ratios of 1) 16, 2) 8, 3) 4, 4) 2, 5) 1, 6) 0.5, 7) 0.25, 8) Control

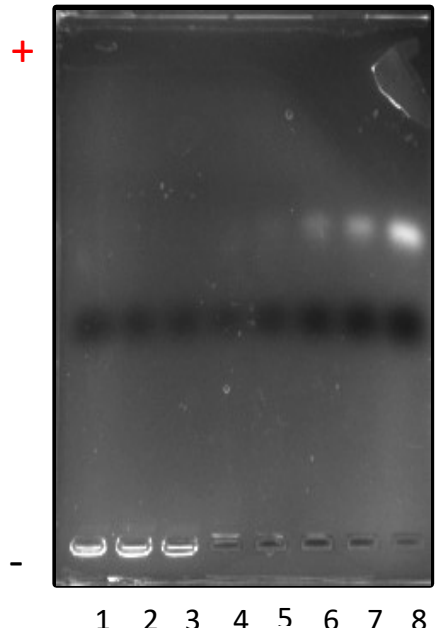

Appendix D-5. Agarose Gel of Agarose gel electrophoresis result of TEPB-CS. Wells are in charge ratios of 1) 16, 2) 8, 3) 4, 4) 2, 5) 1, 6) 0.5, 7) 0.25, 8) Control

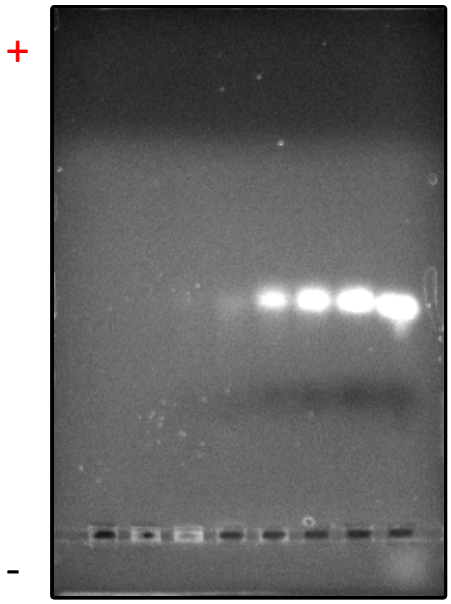

Appendix D-6. Agarose Gel of Agarose gel electrophoresis result of TPPP-CS. Wells are in charge ratios of 1) 16, 2) 8, 3) 4, 4) 2, 5) 1, 6) 0.5, 7) 0.25, 8) Control

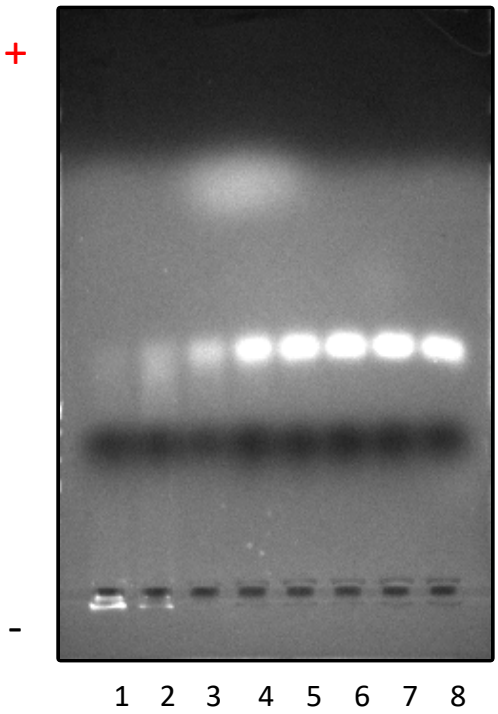

Appendix D-7. Agarose Gel of Agarose gel electrophoresis result of TEAB-mPEG-CS. Wells are in charge ratios of 1) 16, 2) 8, 3) 4, 4) 2, 5) 1, 6) 0.5, 7) 0.25, 8) Control

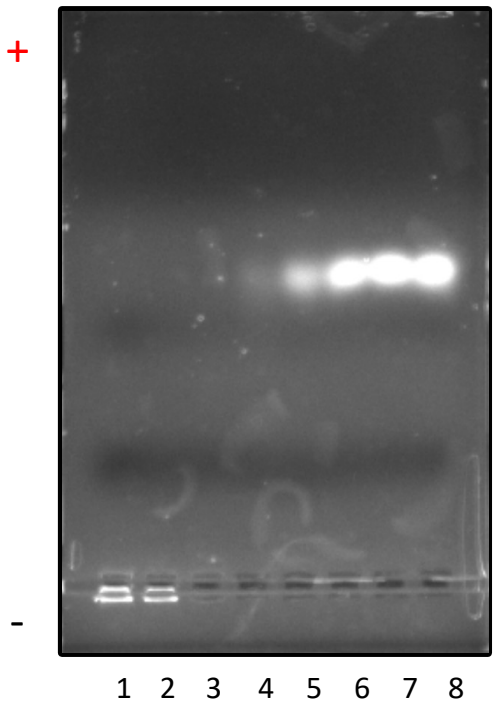

Appendix D-8. Agarose Gel of Agarose gel electrophoresis result of TEPB-mPEG-CS. Wells are in charge ratios of 1) 16, 2) 8, 3) 4, 4) 2, 5) 1, 6) 0.5, 7) 0.25, 8) Control

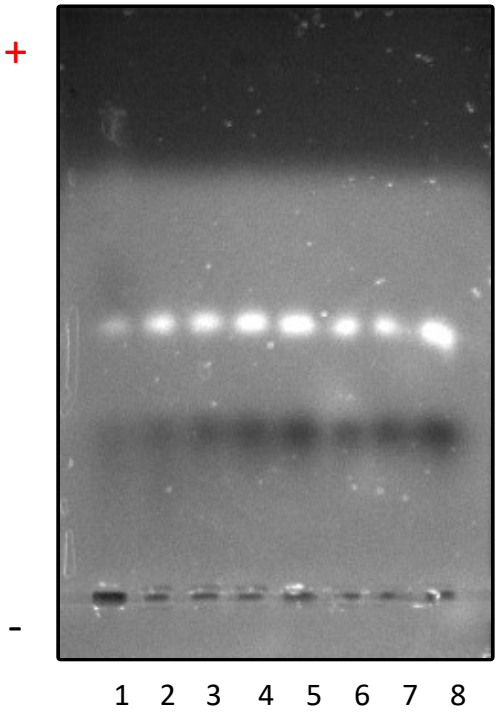

Appendix D-9. Agarose Gel of Agarose gel electrophoresis result of TEPB-mPEG-CS. Wells are in charge ratios of 1) 16, 2) 8, 3) 4, 4) 2, 5) 1, 6) 0.5, 7) 0.25, 8) Control

Appendix E. Circular Dichroism (CD)

Circular Dichroism was conducted to examine changes in conformational states and complexation affinity of all cationic chitosan derivatives using DDD DNA. CD spectra were obtained using Jasco J-815 spectrometer coupled with PFD-425s Single Position Peltier. All spectra in this appendix were gathered using cationic chitosan derivatives with B-form DNA and evaluated between 210-300 nm.

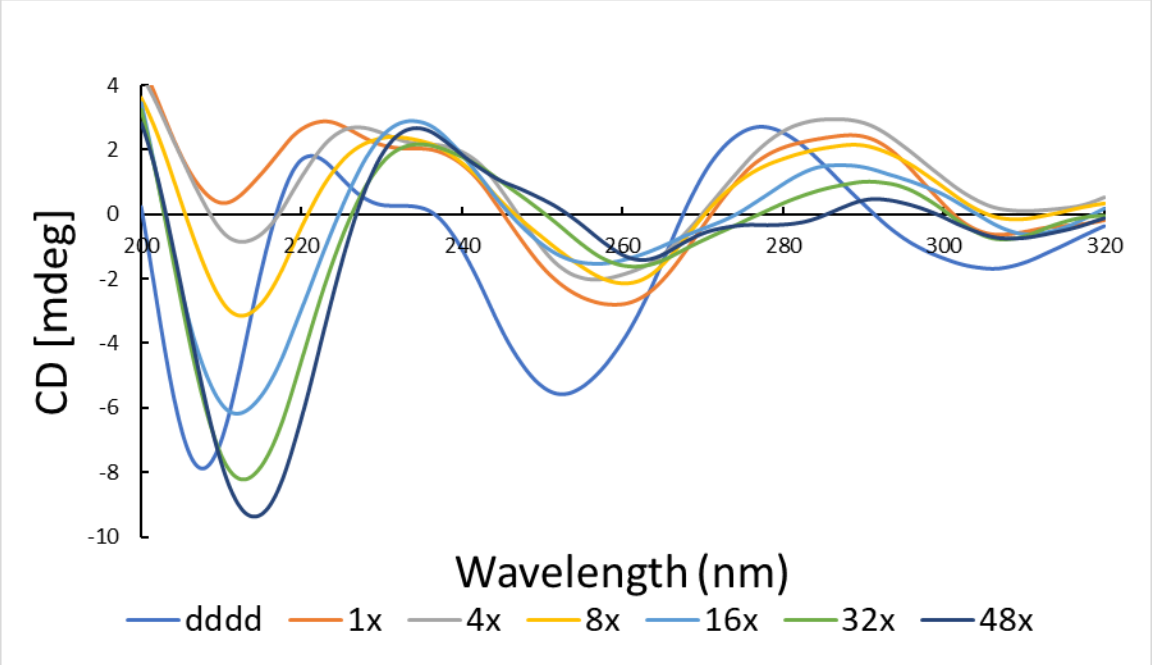

Appendix E-1. CD spectrum of 2-(N-4-trimethylammonium chloride) butanamide chitosan was examine using charge ratios of 1x, 2x, 4x, 8x, 16x, 32x, 42x.

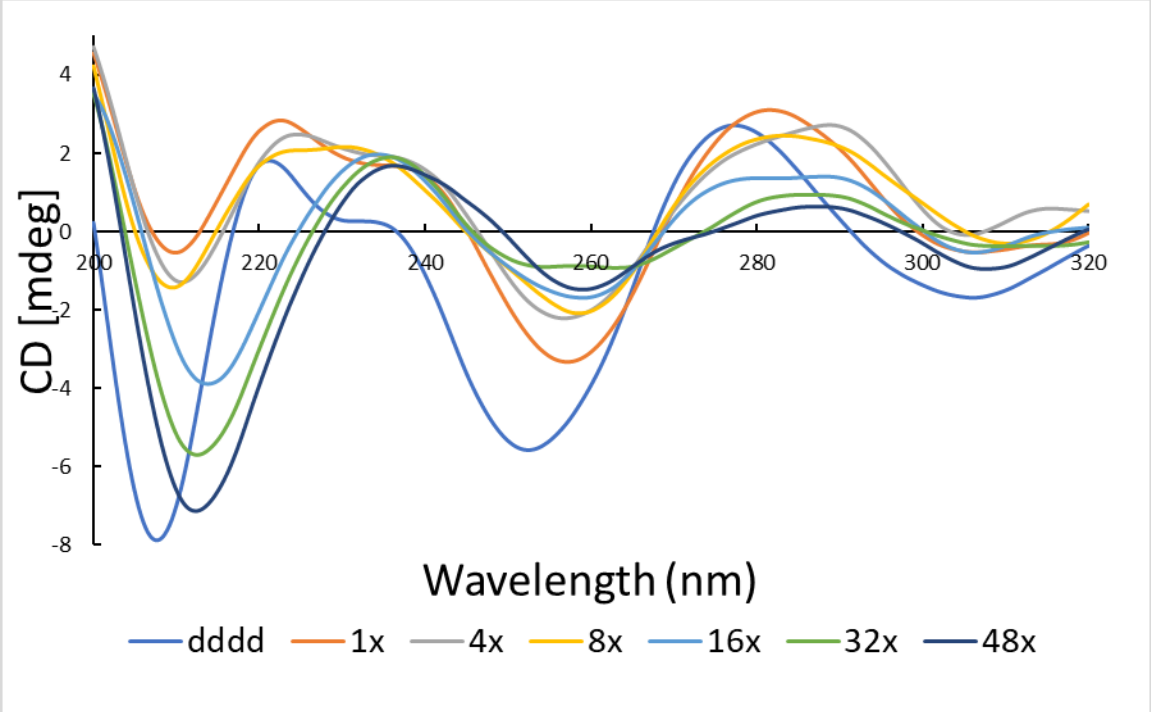

Appendix E-2. CD spectrum of 2-(N-4-triethylammonium chloride) butanamide chitosan was examine using charge ratios of 1x, 2x, 4x, 8x, 16x, 32x, 42x.

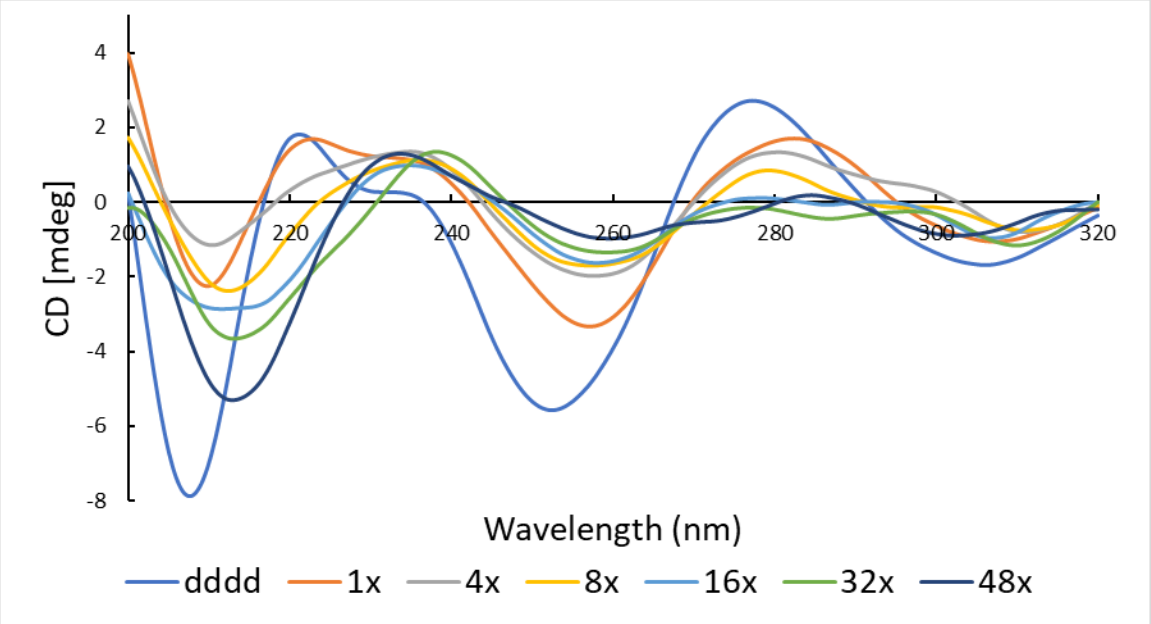

Appendix E-3. CD spectrum of 2-(N-4-propylammonium chloride) butanamide chitosan was examine using charge ratios of 1x, 2x, 4x, 8x, 16x, 32x, 42x.

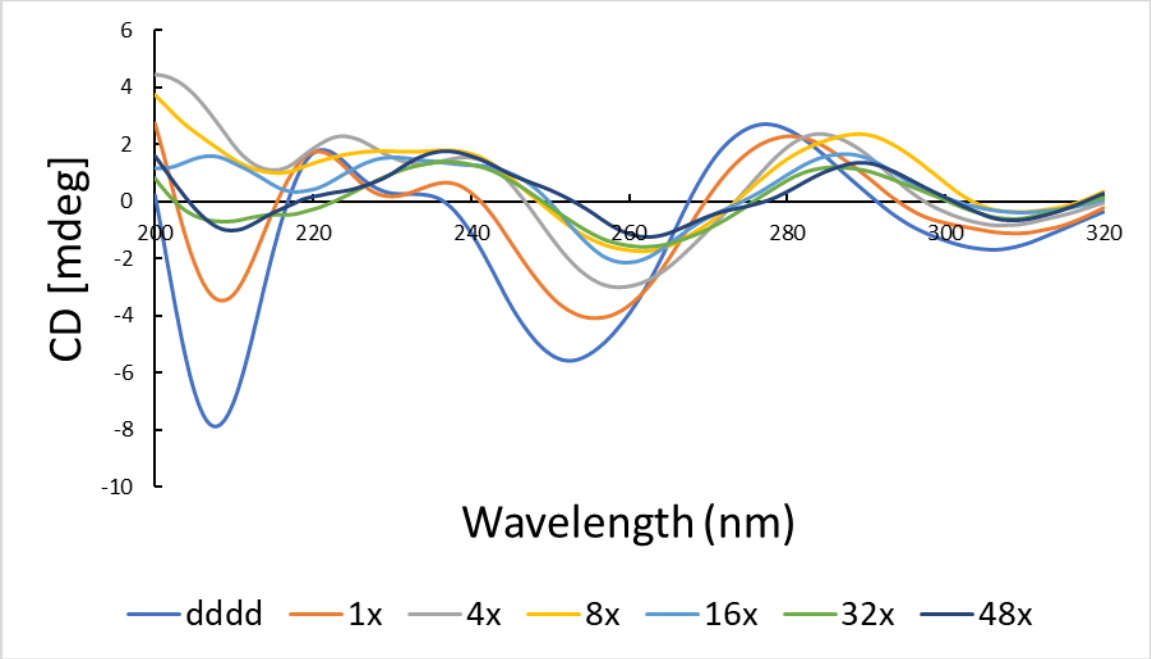

Appendix E-4. CD spectrum of 2-(N-3-triethylphosphonium chloride) propionamide chitosan was examine using charge ratios of 1x, 2x, 4x, 8x, 16x, 32x, 42x.

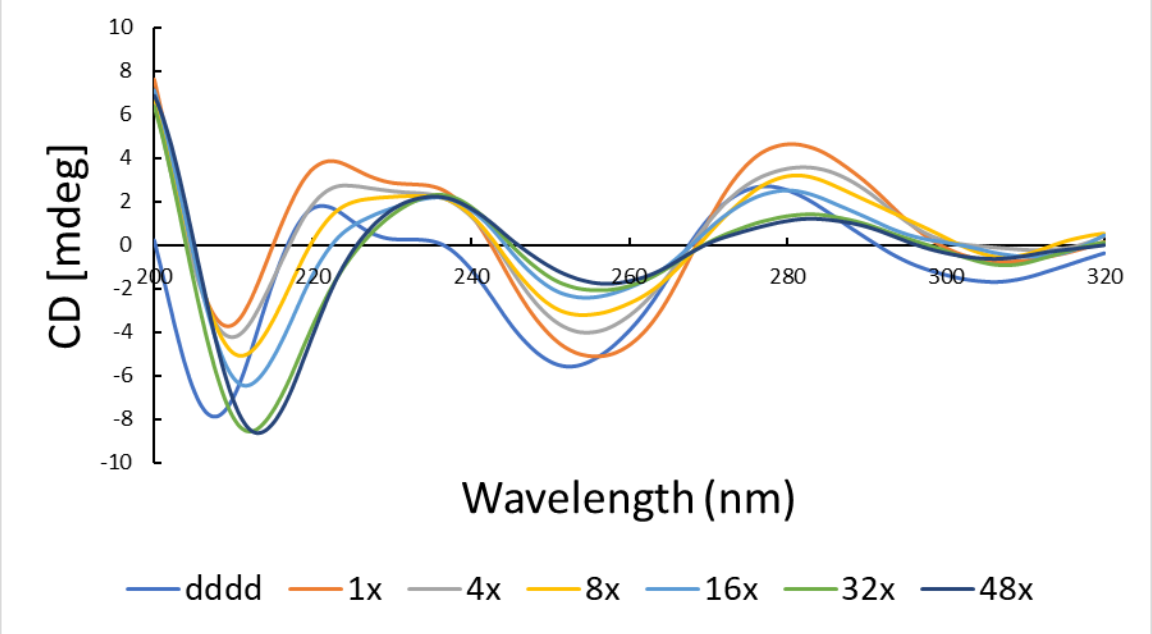

Appendix E-5. CD spectrum of 2-(N-4-triethylphosphonium chloride) butanamide chitosan was examine using charge ratios of 1x, 2x, 4x, 8x, 16x, 32x, 42x.

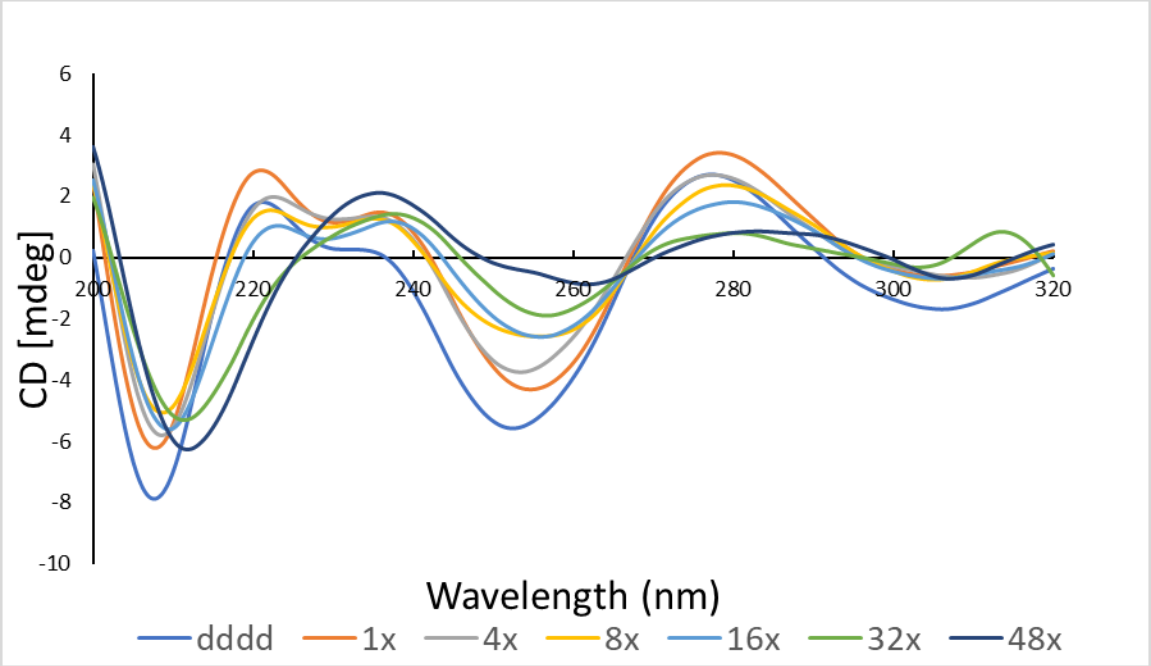

Appendix E-6. CD spectrum 2-(N-4-triethylammonium chloride) butanamide mPEG-*g*-chitosan was examine using charge ratios of 1x, 2x, 4x, 8x, 16x, 32x, 42x.

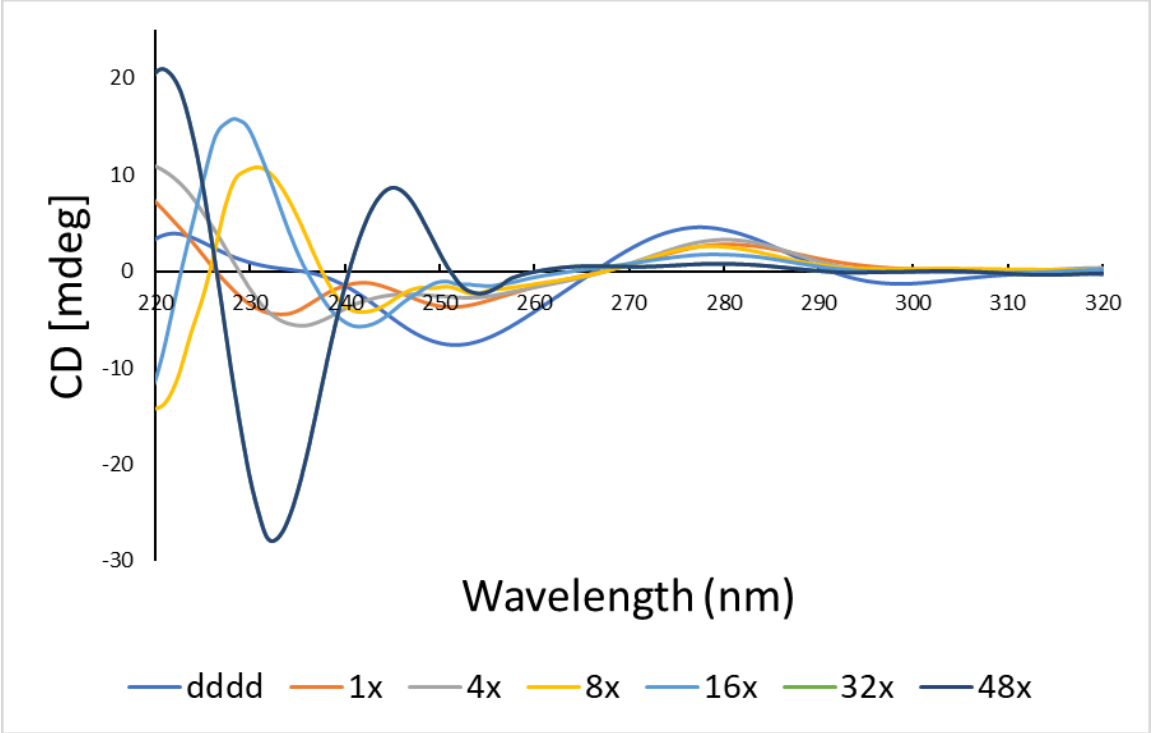

Appendix E-7. CD spectrum 2-(N-4-triethylphosphonium chloride) butanamide mPEG-*g*-chitosan was examine using charge ratios of 1x, 2x, 4x, 8x, 16x, 32x, 42x.

Appendix F. Fluorescence Microscopy

To evaluate chitosan derivatives ability to be internalized by yeast they were examined using fluorescence microscopy studies. Chitosan derivatives were tagged with FITC, incubated with yeast cells, then washed and placed on a slide and examined. All chitosan derivative images obtained were digitally colored using intensity heat mapping and are displayed in this appendix.

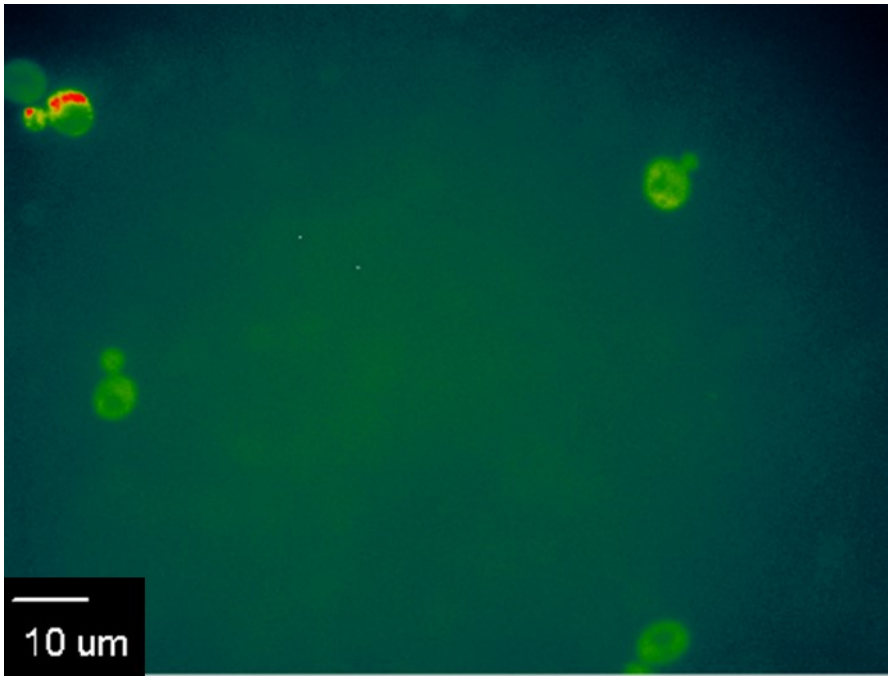

Appendix F-1. Fluorescence microscopy image of FITC tagged 2-(N-4-trimethylammonium chloride) butanamide chitosan with yeast cells

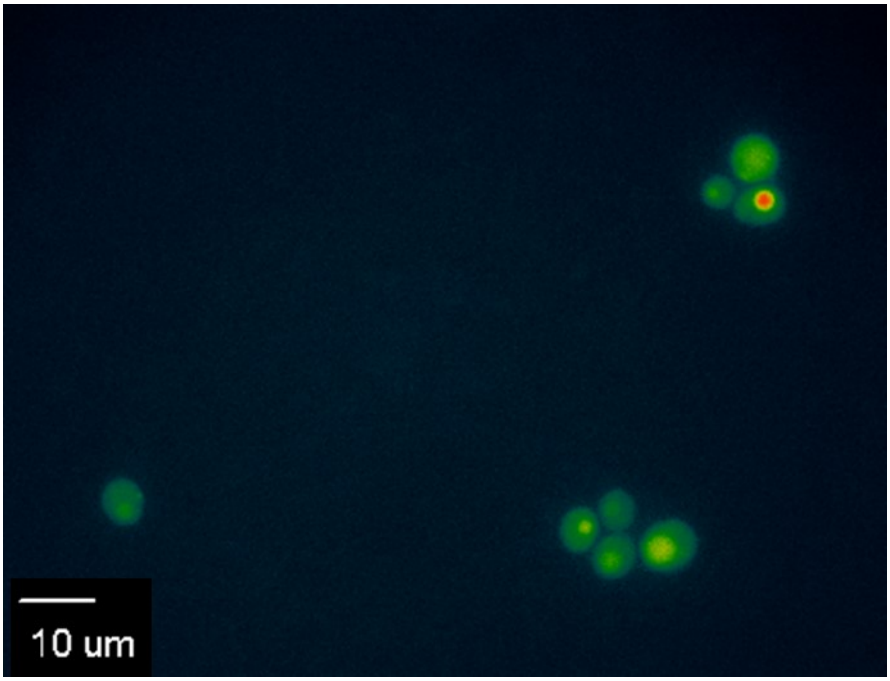

Appendix F-2. Fluorescence microscopy image of FITC tagged 2-(N-4-triethylammonium chloride) butanamide chitosan with yeast cells

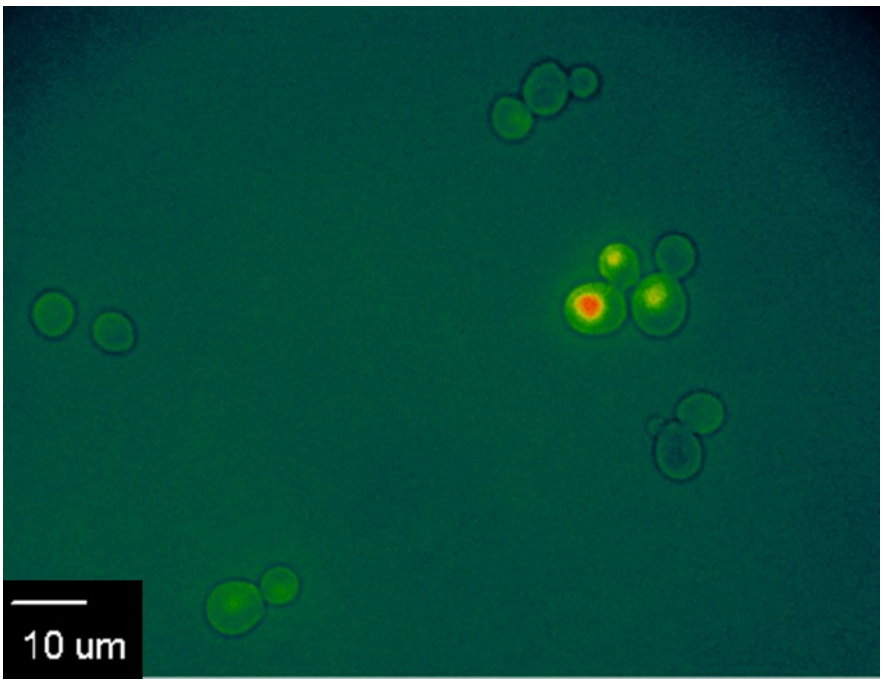

Appendix F-3. Fluorescence microscopy image of FITC tagged 2-(N-4-tripropylammonium chloride) butanamide chitosan with yeast cells

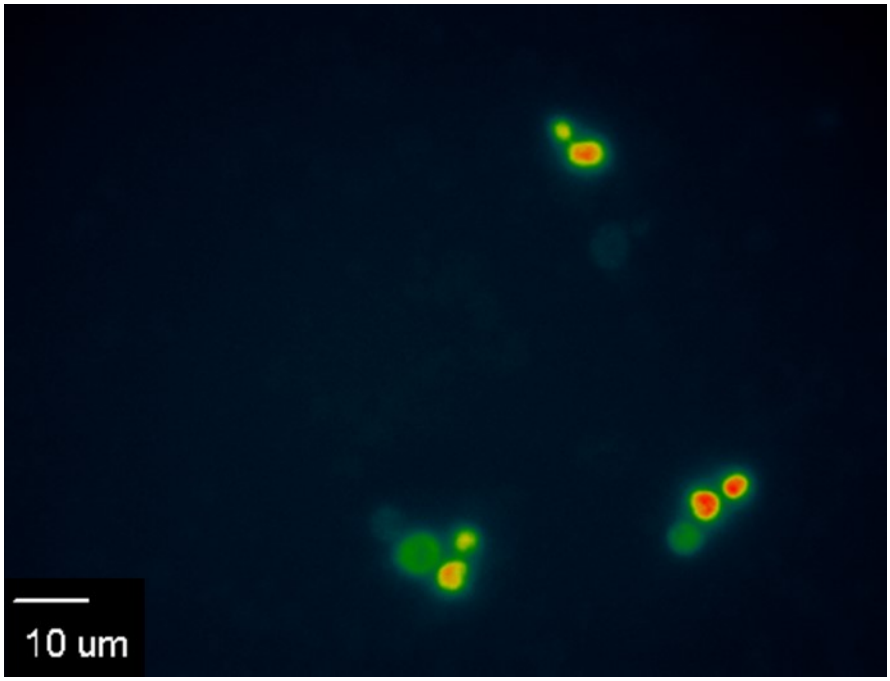

Appendix F-4. Fluorescence microscopy image of FITC tagged 2-(N-4-triethylphosphonium chloride) butanamide chitosan with yeast cells

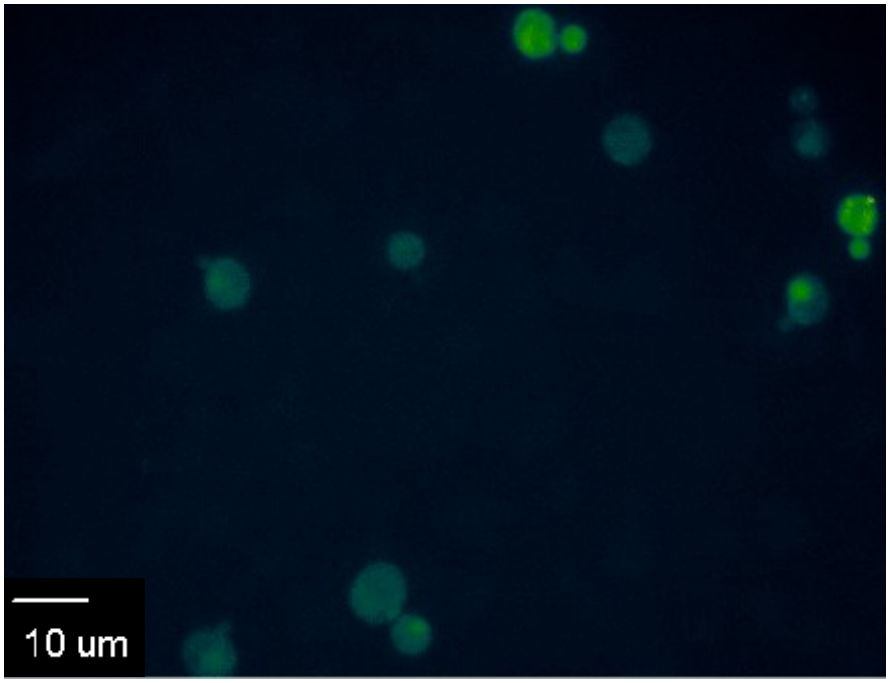

Appendix F-5. Fluorescence microscopy image of FITC 2-(N-4-triethylammonium chloride) butanamide mPEG-*g*-chitosan with yeast cells

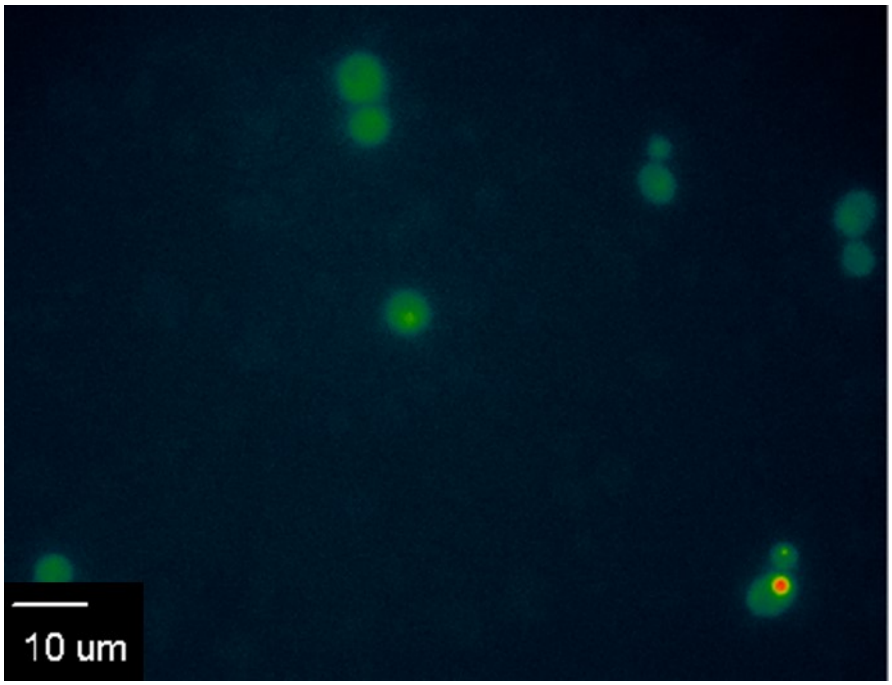

Appendix F-6. Fluorescence microscopy image of FITC 2-(N-4-triethylphosphonium chloride) butanamide mPEG-*g*-chitosan with yeast cells.

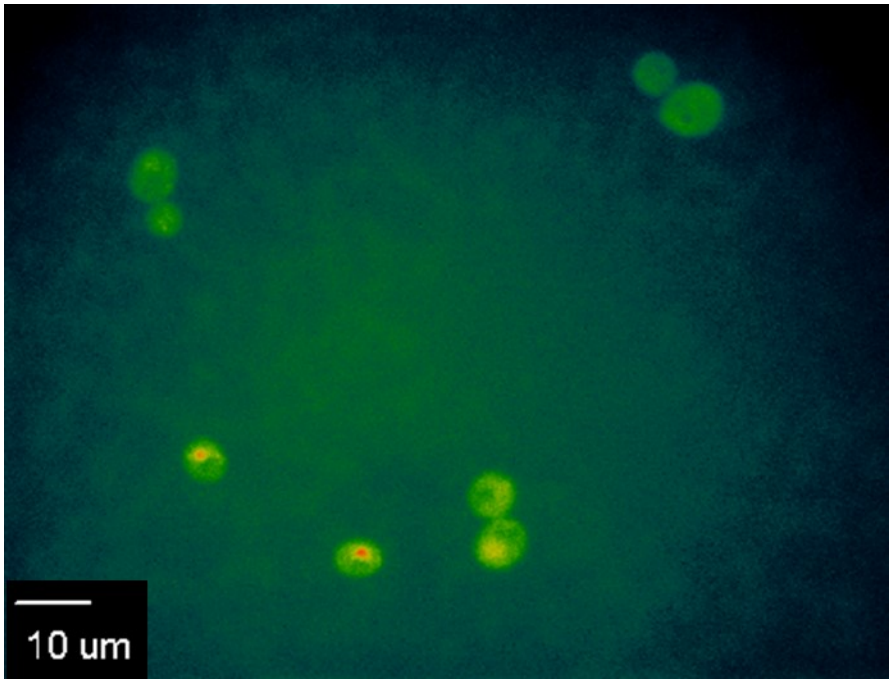

Appendix F-7. Fluorescence microscopy image of 2-(N-5-triphenylphosphonium chloride) pentanamide mPEG-*g*-chitosan with yeast cells

Appendix G. Yeast Growth Assays

Chitosan derivatives antifungal properties were evaluated using freshly inoculated yeast cells to test for potential growth inhibition. All cells were placed into a 96 well plate with various concentration of chitosan derivatives ranging from 0.1-1000 µg/mL and examined over 24 hours with their OD read every 10 minutes. The spectra shown in this appendix has concentrations of 0, 0.1, and 5 µg/mL, all other concertation's completely inhibited growth.

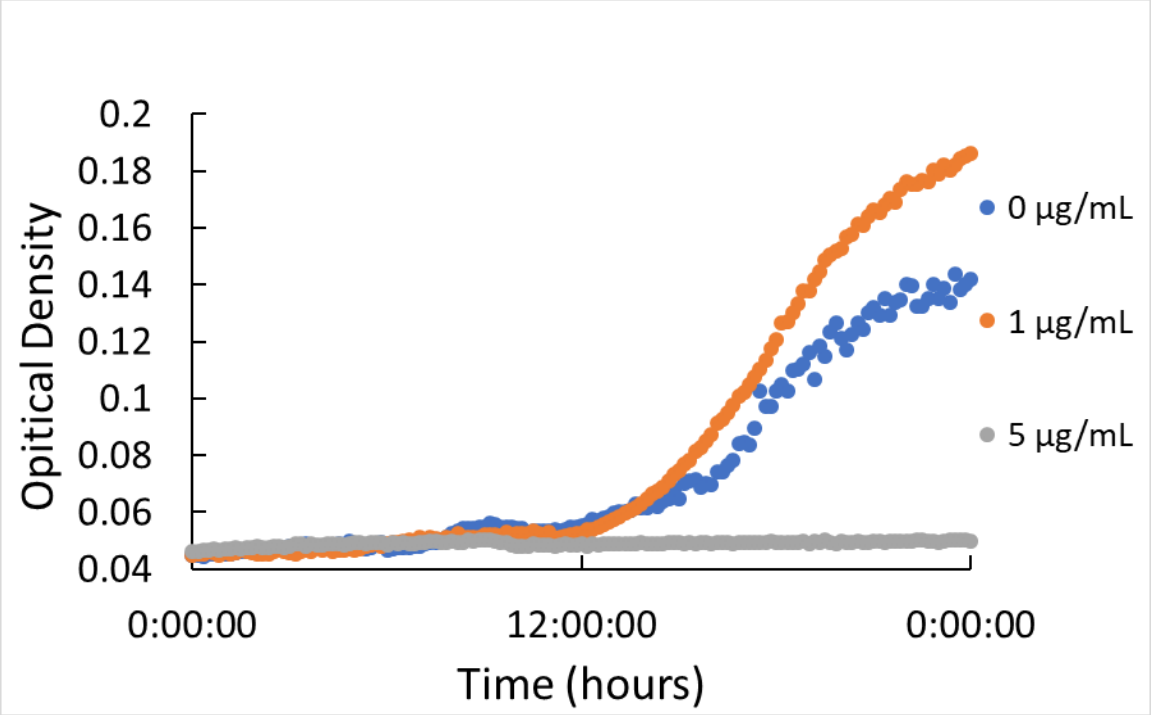

Appendix G-1. 2-(N-4-trimethylammonium chloride) butanamide chitosan's Yeast Growth Assay over the period of 24 hours

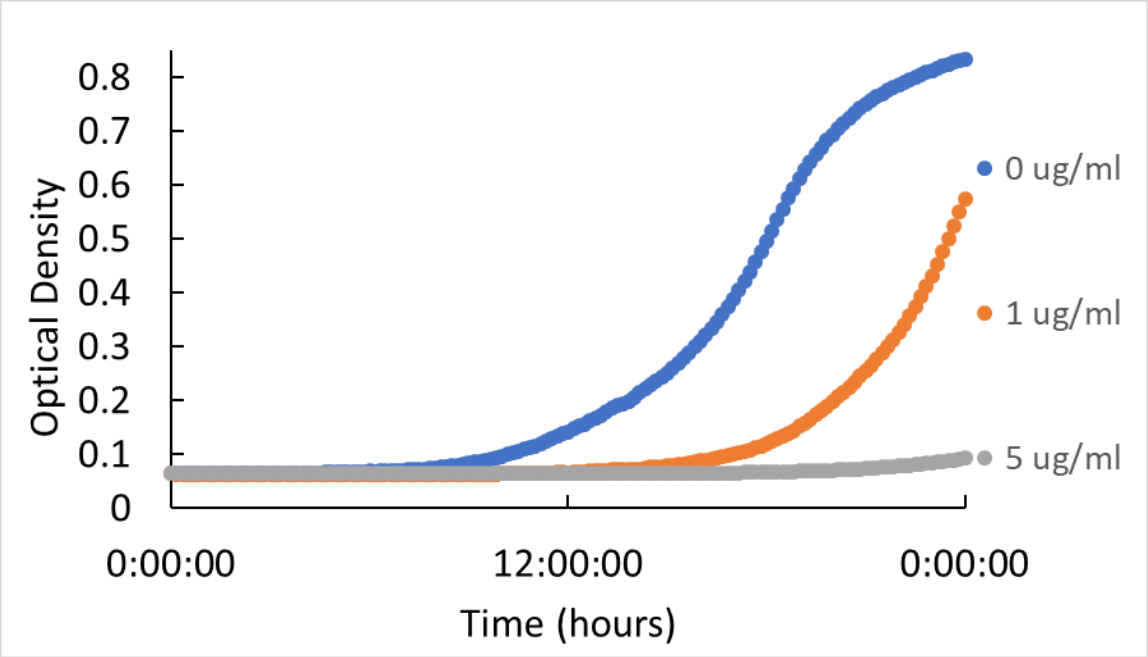

Appendix G-2. 2-(N-4-triethylammonium chloride) butanamide chitosan's Yeast Growth Assay over the period of 24 hours

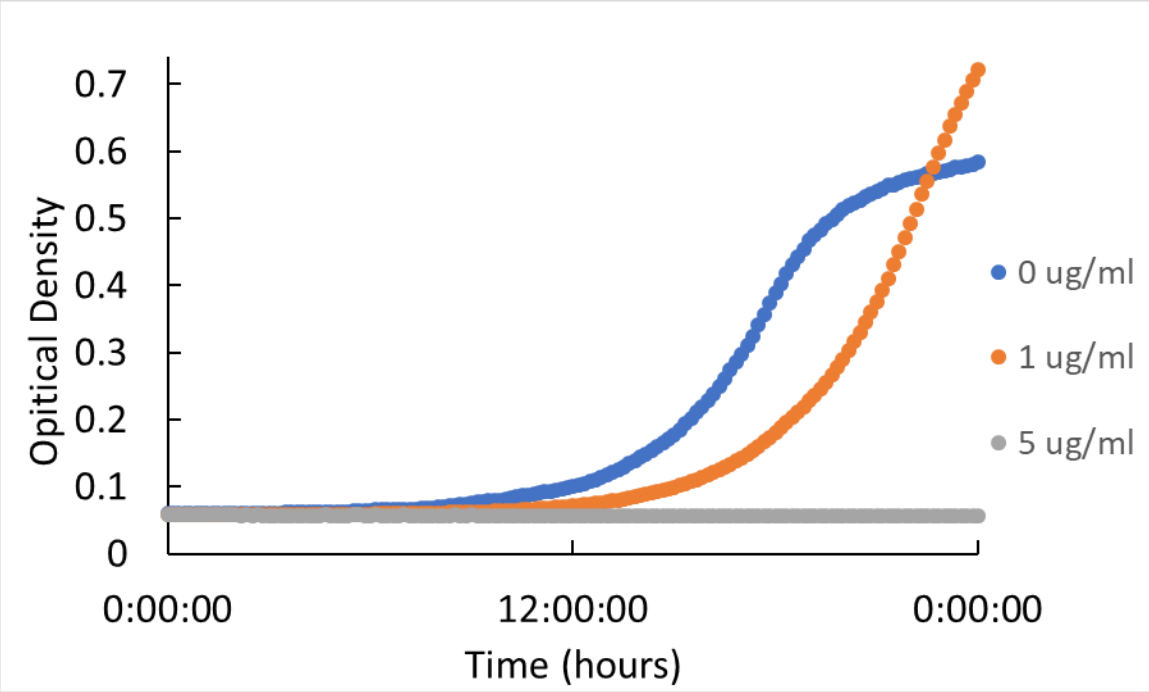

Appendix G-3. 2-(N-4-tripropylammonium chloride) butanamide chitosan's Yeast Growth Assay over the period of 24 hours

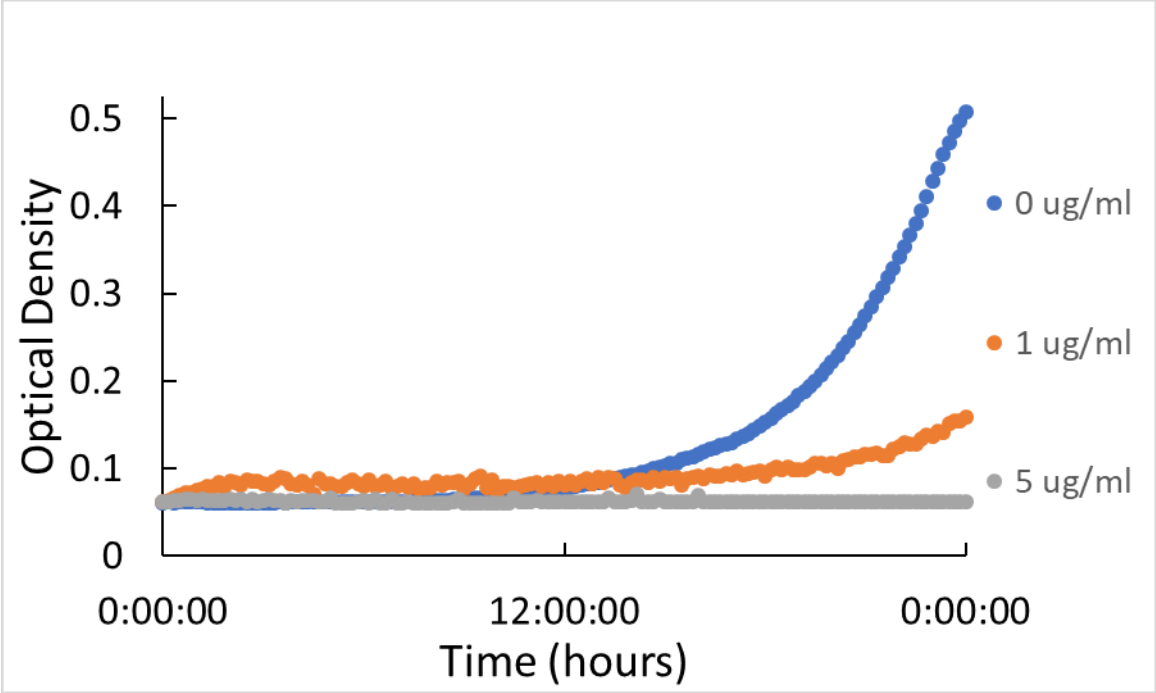

Appendix G-4. 2-(N-4-triethylphosphonium chloride) butanamide chitosan's Yeast Growth Assay over the period of 24 hours